공학박사 학위논문

Spatial Manipulation of Model Membranes for Lipid Raft Formation and Protein Localization

지질 래프트 형성과 단백질 고정화를 위한 모델 지질막의 공간적 분포 연구

2013 년 8 월

서울대학교 대학원

공과대학 전기컴퓨터공학부

유용상

Spatial Manipulation of Model Membranes for Lipid Raft Formation and Protein Localization

지도교수 이 신 두

이 논문을 공학박사 학위논문으로 제출함

2013 년 8 월

서울대학교 대학원

공과대학 전기 · 정보공학부

유 용 상

유용상의 박사 학위논문을 인준함

2013 년 6 월

위 원 장 ____________________ (인)

부위원장 ____________________ (인)

위 원 ____________________ (인)

위 원 ____________________ (인)

위 원 ____________________ (인)

Abstract

Spatial Manipulation of Model Membranes for Lipid Raft Formation and Protein Localization

Yong-Sang Ryu
Department of Electrical and Computer Engineering
The Graduate School
Seoul National University

In cell membranes, reorganization and distribution of membrane components such as lipids and protein has attracted great attention because of its scientific importance in cell biology including immunology in terms of signal trafficking. Especially, dynamic nature of lipids plays an important role in controlling the concentration profiles of membrane components and those associated molecules for understanding of membrane deformation, vesicle budding, and signal transduction. In an effort to understand those processes systematically, a lipid bilayer system reconstituted on solid supportshas been a primary route to quantitative analysis on lipid dynamics.

In this thesis, viable approaches to spatial manipulation of model membrane components into micro-scaled distinct domains on the solid supports by controlling interfacial interactions, which are investigated from the view point of fundamental physics and potential applications. The intrinsic properties such as adhesion force, interfacial energy, elasticity, spontaneous curvature, electric field, are manipulated by surface micro-templates to organize the membrane components, and colloidal particles in a site selective manner for broad applications of the materials at easy.

As one of model systems of soft matters on solid supports in vitro, fluid lipid bilayers are manipulated to grow in a micrometer-scale, array format through a vesicle adsorption and rupture process according to the surface characters of solid supports. The formation of lipid bilayers on various substrates, so–called supported lipid bilayers (SLBs), has been a primary route to the fundamental studies of membrane activities as well as the development of membranes-based biocompatible devices. As a one of the interesting topics of membrane physics, lipid rafts have been tried to reconstituted *in vitro* due to not only their roles on the biological activities, but their distinct physical characters in the plasma membrane in living cells. Lipid rafts are sphingolipid- and cholesterol-rich domains of plasma membrane which contain a variety of signaling and transport proteins. The importance of lipid raft signaling in the pathogenesis of a variety of conditions, such as Alzheimer’s, Parkinson’s, prion and cardiovascular disease, systemic lupus erythematosus and HIV, has been elucidated over recent years and makes these specific membrane domains an interesting target for pharmacological approaches in the cure and prevention of these diseases,. As mentioned above, special type of membrane components, that is, lipid rafts, are known to deeply related to the vital roles for cardiovascular disease, immune system, apoptosis and carcinogenesis, and neurological disease. Although their crucial roles in pathogenesis of a variety of disease, definite roles and even the formative principles of rafts have not been demonstrate yet.

In the line with elasticity-based approach to the patterned growth of the raft assembly into spatial regions, geometrically patterned structure induce loop-like raft domain for the first time in model membrane system. Molecular shapes of raft domain prefer to locate at the curved surface for release elastic energy of a patch of membrane which provides lateral diffusions of lipid molecules without any disruption. Another example of approach to organization of patterned assemblies of raft on the solid supports is surface energy-driven construction of raft domains. Author shows binary membrane morphology, appositional formation of lipid monolayer and bilayer maintaining fluidity and continuity within a membrane. Stamping the dry polydimethylsiloxane (S-PDMS) mold on the hydroxylated glass offers sufficient hydrophobicity for generating lipid monolayer morphologies surrounded by unstamped lipid bilayer morphologies without any disruptions and lipid-free regions and consequent introduction of raft component-involved vesicle lead phase separation into liquid ordered domains on stamped regions. This morphological character due to continuity of membrane between monolayer and bilayer regions provides the robust platforms to solve the fundamental question of lipid rafts. That is, how the raft domain generate within the membrane. S-PDMS transfer method and additional injection of secondary vesicle was used for formation of heterogeneous membrane which involves sphingo lipids and cholesterol at each region. Furthermore, by reconstructing heterogeneous membrane which force to phase-separating the L_O domain at expected space, we could observed kinetic of model membrane into raft real-time by surface plasmon resonance on the Au covered glassy substrate.

Another example of approach to the manipulation of lipid molecules is the electric field-directed diffusion of charged lipids in supported membranes for spatially addressed microarrays. Field-directed diffusion of charged phospholipids in supported bilayer membranes into distributed partitions in a diffusion cell is shown. The balance between the field-induced drift and the thermal Brownian motion generates the concentration gradient of the charged lipids from partition to partition under an external electric field applied longitudinal to the partition walls. The concentration gradient across the partitions was found to primarily depend on the pore width and the distance between the pore and the partition wall. This field-directed diffusion approach provides a powerful tool for constructing various spatially addressed membrane arrays.

In conclusion, throughout this thesis, the reorganization of signal molecules on the model membrane has been extensively explored from the viewpoint of physical studies and device applications. The experimental/ theoretical analysis and several device concepts demonstrated here will provide a versatile platform for wide range of future applications by broaden the understandings of the raft domains and by applying as an microarray combined with raft-recognized proteins.

Keywords: supported lipid bilayers, lipid raft, liquid ordered domain, cholesterol intercalation, spontaneous curvature, monolayer and bilayer, charged lipid.

Student Number: 2009-30198

Contents

List of Tables

List of Figures

Chapter 1. Introduction

1.1 Lipid Membranes

1.1.1 Membrane Properties

A cell is a basic unit of living organism that is composed of variety organelles and molecules. The cell is covered with the plasma membrane that separates the interior of all cells from the outside environment. The cell membrane is selectively permeable to ions and specific molecules and controls the movement of substances in and out of cells. Above all, the fundamental function of cellular membrane is to protect the cell from its surroundings. This membrane consists of the lipid bilayer with embedded proteins in it as shown in **Figure 1.1**. These molecules play critical roles of cell life by performing the biological activities such as cell adhesion, cell signaling, budding, apoptosis and so on. Each lipid molecule is amphiphilic, consisting of hydrophilic head group and a hydrophobic tail (**Figure 1.1b**). Lipid bilayers are formed through the process of self-assembly. The cell membrane consists primarily of a thin layer of amphipatic phospholipids which spontaneously arrange with hydrophilic head group and hydrophobic tail group apart. The head group, polar or even charged, polarizes the small polar water molecules and is therefore strongly hydrophilic. The fatty acid tails, however, disrupt the local order of water and are more strongly attracted by themselves that by water. Therefore, the molecules self-assemble into a lipid bilayer under physiological conditions as shown in **Figure 1.1a**. It is energetically favorable to hide the hydrophobic tails from aqueous environments. Moreover, the membrane proteins are incorporated within the lipid bilayer floating in the see of lipids. The orientation of lipid molecules are intrinsically perpendicular to the plane of membrane keeping their position standing at outer-leaflet and stand on its head at inner-leaflet of bilayer morphology, respectively. One of the key features that distinguishes lipid bilayer from other membranes is lateral fluidity. That is to say, variety of lipids and proteins floating within the membrane moves here to there without any order. Thermal diffusion, called Brownian motion [1], is critical reason for membrane components move molecules to random space. However, the change of geometry, e.g., bending of the membrane, would provide certain order of moving direction for membrane components. Not only for bending membrane based on elastic-energy modification, but also intrusion of cytoskeleton or integral monotopic protein (I.M.P) [2], even the distributions of charged molecules can affect the reorganization of membrane components. Local changes in the physicochemical properties of bilayers, in turn, allow membrane deformation, and facilitate reorganization of membrane components.

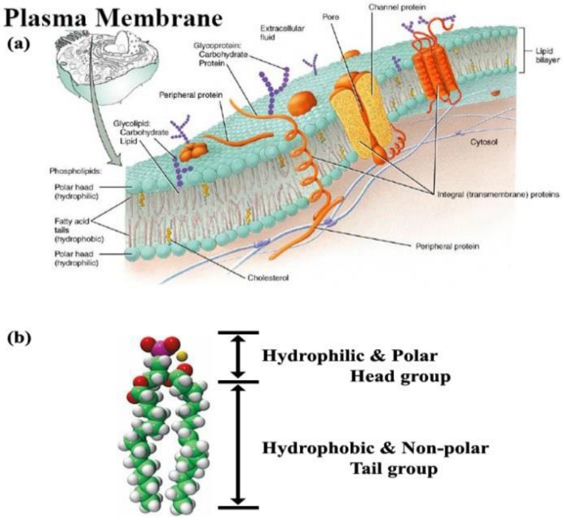

Figure 1.1 : (a) The plasma membranes of cells and (b) the phospholipids. The plasma membranes of cells composed of various types of lipids and membrane proteins. The lipid is amphiphilic molecule which has a hydrophilic head group, and hydrophobic fatty acid tails.

1.1.2 Model Membrane on the Solid Supports

The generation of switchable interfaces would give an opportunity that enables the active control of biofilm formation and macromolecule adsorption to solid supported lipid membranes. Furthermore, it will allow the design of new model system to study the heterogeneity of biological membranes and their dynamics, which play an extraordinary role for many biochemical and biological processes. As an effort to design the cellular membrane in vitro, supported lipid membranes (SLBs**)** [1] have been intensively studied over the last decade with the aim of mimicking the physical properties of lipid membrane. Schematic illustration of fabrication process for SLB membrane is shown in **Figure 1.2**. The substrate, we majorly use the glass as a substrate in our experiment, was piranha cleaned to giving hydrophilic surface by formation of hydroxyl (-OH) group on it. The surface interactions between the oxide solid supports and bilayer membranes are controlled by electrostatic, hydration, steric forces and van der Waals [3]**.** A subtle balance among these forces determines the kinetics of vesicle adsorption and fusion to the underlying support as well as membrane spreading across the surface. Lipid bilayers supported on silica substrates generally maintain about 10 Å layer of water [3] between the membrane and the solid surface. This thin water play a role as a lubricant layer which is essential for mobile and fluid in the plane of membrane. SLBs are continuous with mobile components both leaflets freely diffusion over the entire surface of the surface where the substrate covered with. In order to verify and estimate the lateral mobility, fluorescence recovery after photobleaching (FRAP) test [4] has been used. FRAP denote an optical technique capable of quantifying the two dimensional lateral diffusion of a molecularly thin film containing fluorescently labeled probes. The typical range of diffusion constants have been observed in the range of 1-5 $\mu m/s^2$ [1].

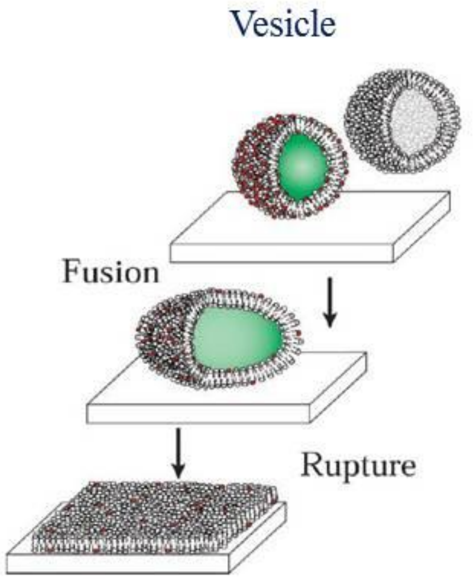

Figure 1.2 Formation and spreading of lipid bilayer by spontaneous rupture process from vesicle to supported lipid bilayers (from reference [3]).

Surface patterning of physicochemical properties through a standard photolithographic methods has been used as a new approaches in material synthesis [5], sensor microarrays [6], genomics [7], drug screening [8], proteomics [9]. Extending this strategy to fluidic SLBs membrane functions is desirable for understanding, emulating, patterning, and exploiting many functional roles of cellular membranes for fundamental research. Here, micro-patterned membrane surface will be introduced one by one. First of all, micro patterning of SLB membrane can be obtained by exposing deep-ultraviolet (UV) radiation on the membrane [4]. The principle of patterning through UV is explained that 'Deep-UV illumination (range of 185 - 254 nm) generates ozone and other reactive radicals from oxygen. In particular, O_2 becomes reactive oxygen atoms under 185 nm wavelength UV exposure, and these

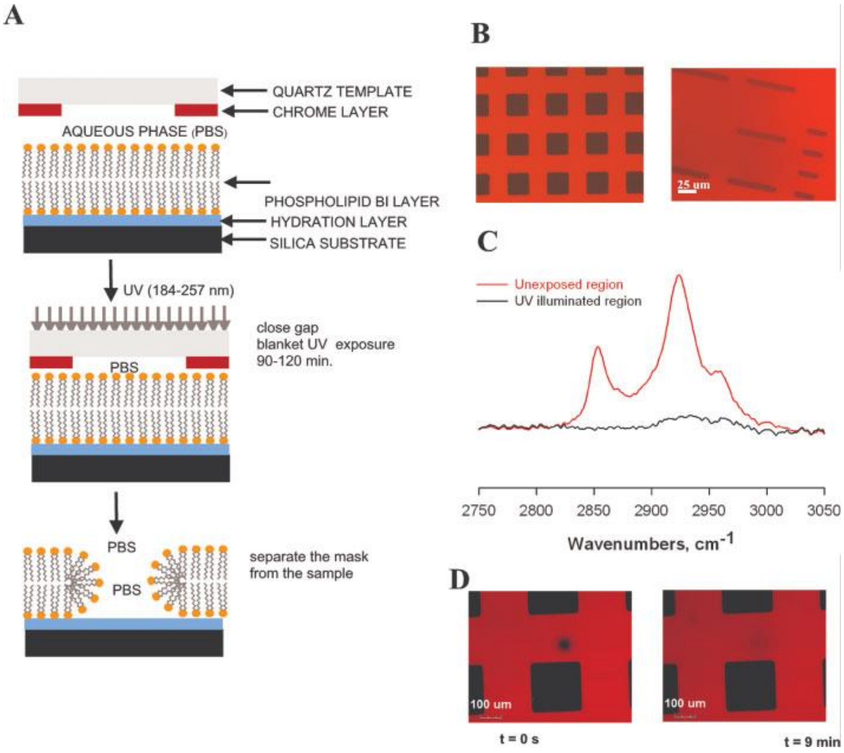

Figure 1.3 : Direct patterning of void arrays wthin bilayer membranes using deep-UV photolithography. (a) a schematic illustration of the process steps. (b) a typical epicluorescence image of the void arrays (100 μm × 100 μm) obtained using deep UV photolithography within a POPC bilayer membrane supported on a hydrophilic cover glass. (c) Spatially resolved ATR-FTIR microscopy spectra in the acyl-chain vibrational mode region (2750-3050 cm^{-1}) corresponding to the UV-illuminated and masked bilayer regions revealing the presence and absence of the vibrational mode adsorptions due to methylene and methl groups in lipid molecules. D) Two frames from time-lapse epifluorescence imaging (t = 0 and t = 9 min) revealing the fluorescence photobleach recovery for a spot in the vicinity of the void (from reference [4]).

oxygen atoms react with O to form ozone (O_3). O_3 itself adsorbs 254nm wavelength UV light and produces the reactive oxygen atom O (^1D) and singlet molecular oxygen ($^1O_2^*$). In aqueous environments, a water molecule can then react with O (^1D) and $^1O_2^*$ and form another radical, H_2O_2. These radicals chemically degrade and remove lipids with high spatial resolution, even in a entirely aqueous environment [4]. The schematic diagrams of direct patterning of void arrays within bilayer membranes using deep-UV photolithography are shown in **Figure 1.3.**

Another micro patterning of SLB membrane is membrane transfer by PDMS mold [10]. Spatially selective (patterned) removal of bilayer material can be achieved by using a PDMS stamp. Lipid bilayer membrane standing on the protrusion region of PDMS mold will translocate from mold to target surface. Bilayer region created by this stamping process keep their fluid and stable within the patterned surface. It also made the lipid-free region on blotted area and it can be used as membrane pattering as shown in **Figure 1.4**.

Conventional photolithography based pattering of metal-grid has been used as a membrane patterning methods. Using standard lithography technique, A wide range of materials including metals (Au, Al, Cr, Ti) and protein grids [11] plays a role as the effective barrier between patterned SLBs membrane as shown in **Figure 1.5**. Not only the patterning trough the lithographic methods, it have found that it is possible to partition fluid-supported membranes into corralled regions that retain their fluidity using simple mechanical scratches [3]. Mechanical scratching methods can be alternative method to create lipid-free region for membrane separating [3, 12]. Vesicle fusion is essentially irreversible. By flowing vesicle suspensions of

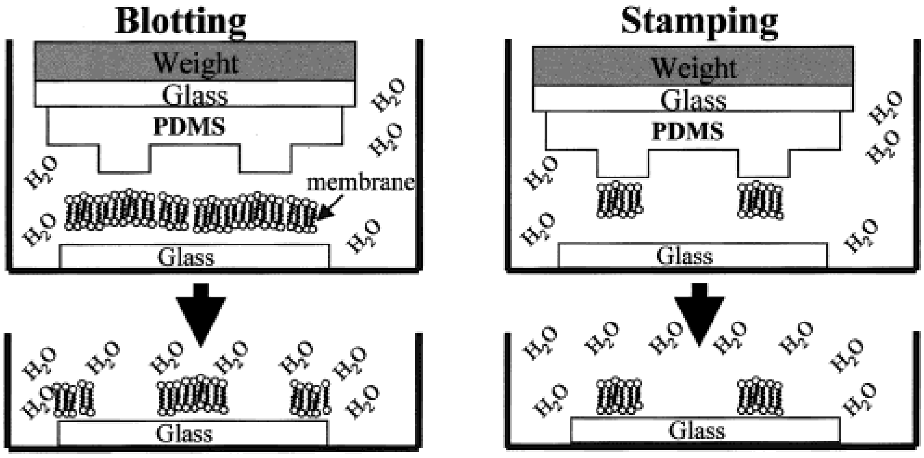

Figure 1.4 : patterning Barriers to Lateral Diffusion in Supported Lipid Bilayer Membranes by Blotting (left) and Stamping (right) (from reference [10]).

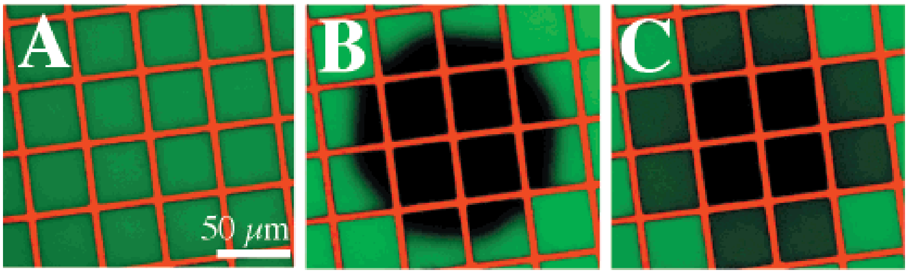

Figure 1.5 : (A) Fluorescence image of corrals of supported membrane (green) partitioned by a grid of diffusion barriers (red). In this case, barriers were created by microcontact printing a grid of fibronectin onto a silica surface followed by membrane deposition. (B) A circular region covering a number of corrals has been photobleached by selective illumination. (C) After 20 min, diffusive mixing leads to uniform composition within each corral; the barriers prevent mixing between separate corrals (from reference [12]).

different compositions under partial mixing conditions over a pre-patterned glass surface [11], each micropatterned region will catch whatever composition is passing by.

As mentioned above, the membrane is composed of thousand species of lipids molecules. They have distinct characters for each lipid molecule possessing different tail shape, length (thickness), shape of head group, polarity, net-charge. Among these properties, polarity and net charged are thought to be important factor for interaction between protein-protein, protein-lipids. In particular, charged molecules are known to play critical roles for biological activities. For example, charged environment, generated by abundant localization of charged lipids, facilitates efficient introduction of DNA, RNA or proteins for gene therapy or immunization trials [13]. Intercellular protein modification and trafficking, cell activation, e.g. protein translocation and deformation, K-channel activation in various concentration, are deeply associated to the charged environments [14, 15].

In order to estimate the role of environmental importance in plasma membranes, manipulation of charge lipids on the membrane has been attract great attentions over the last decade. Paul et al. [1] tried to partition of charged lipids on SLBs membrane using mechanical scratching methods. Kung et al. [16] showed strategy for modifying the individual corrals of a membrane microarray involves a secondary photolithographic step. The micro partitioned membrane itself is the substrate material for a spatially directed photochemical transformation that either eliminates functionality or activates the surface for attachment of some functionally interesting molecule (**Figure 1.6a**). Hovis and Boxer [17] introduce various concentration of charged membrane array through membrane transfer by stamping and consequential filling on membrane uncovered surface as shown in **Figure 1.6b**. Kam and Boxer [18] also represented fluidic channel induced variable introduction of vesicle for concentration gradient of charged components as shown in **Figure 1.6c**. A tangential electric field imparts a net force on the charged components in a fluid membrane, causing them to drift with a characteristic electrophoretic drift velocity. Due to this drift movement, geometrically well designed walls (ratchets) [19] demonstrated the charged membrane components could be manipulated two dimensionally within application of the single field as shown in **Figure 1.6d**.

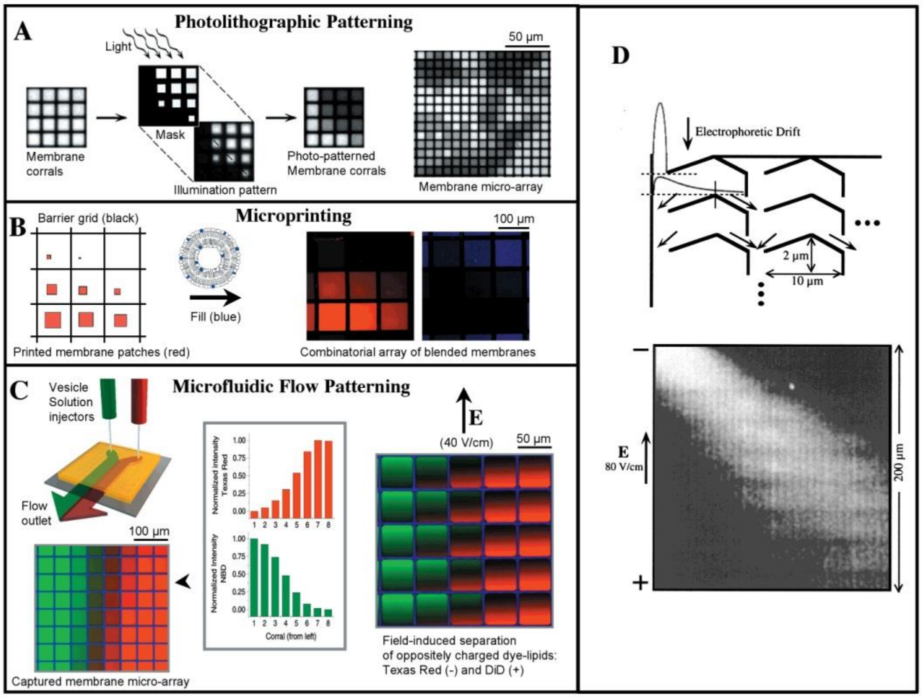

Figure 1.6 : Methods to manipulate charged lipids on model membrane system. (a) photolithographic patterning [16] (b) stamping membrane followed secondary photolithographic step [17] (c) microfluidic flow patterning [18] (d) membrane ratchet (from reference [19]).

1.2 Lipid Raft

1.2.1 Role of Lipid Rafts on Cellular Activities

Figure 1.7 shows the history of lipid rafts. Traditionally, it has been believed that various species of lipids and protein molecules randomly diffuse within the bilayer membrane. This is similar like the iceberg float in the plane of cell membranes according to the fluid mosaic model as demonstrated by Singer and Nicholson (1972) [20]. However, over the past few decades, there have been growing evidences that there are distinct domains where signaling molecules compartmentalized into. An early study by Yu et al. (1973) [21] indicated the existence of detergent-resistant sphingolipid-rich domains in the plasma membrane. Studies by van Meer et al. (1980) [22], 1987 [23] and by Lisanti and colleagues (1988) [24] found the asymmetric distribution of signal molecules and link between sphingolipids and GPI

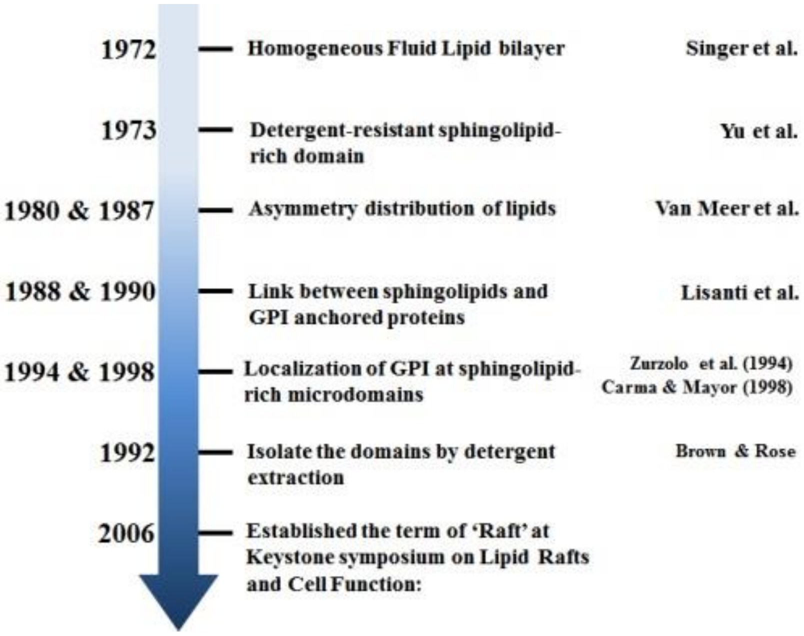

Figure 1.7 : The history of discovery related to lipid rafts

(glycosylphosphatidylinositol)-anchored proteins, respectively. And finally, Brown and Rose (1992) [25] found the method to isolate these domains by detergent extraction. The emerging observation of floating microdomains in the plasma membrane established the term ‘raft’. This term recently received a comprehensive definition at Keystone symposium on Lipid Rafts and Cell Function: ‘Membrane rafts are small (10-200 nm), heterogeneous, highly dynamic, sterol– and sphingolipid-enriched domains that compartmentalize cellular processes…’ [26]. The lipid rafts composed of sphingolipids (SPMs) and cholesterols (CHOLs) giving the liquid ordered domain (L_O), surrounded by liquid disordered (L_d) domains, and raft proteins show heterogeneity and compartmentalization on the cell membrane attracting great attention due to its vital roles in many biological functions, including signal transduction [27], vesicle budding [28], cellular deformation [29], cell apoptosis [30], and membrane trafficking [31].

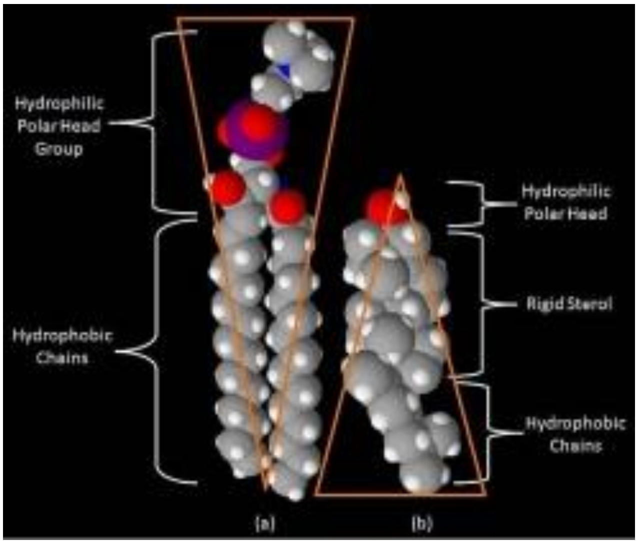

Figure 1.8 : The combination of sphingolipids and cholesterols

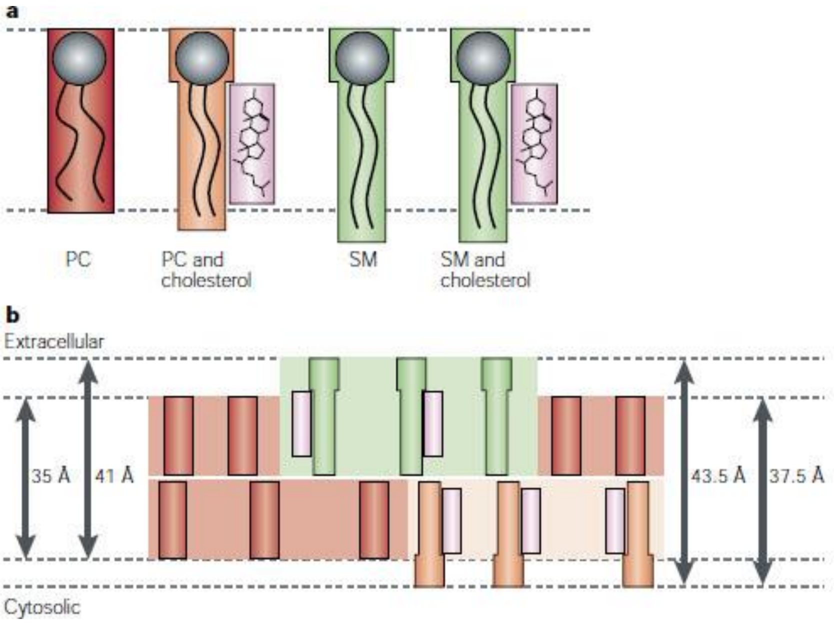

Figure 1.9 : (a) Cross sectional illustration of lipid moleculars and (b) height difference when they assembled into raft cluster (from reference [34]).

One of the most important physical features of the lipid rafts (L_O domain) other than surrounding lipids domains (L_d domain) are densely packed properties and consequent high bending rigidity. The major classes of lipids in the plasma membrane are phospholipids, sphingolipids, and sterols. The combination of sphingolipids and cholesterols with representative structures are shown in **Figure 1.8**. Detailed mechanisms that how SPMs and CHOLs interact to generate more densely packed domains are not clearly understood. Two models have been developed to explain how lipid rafts accumulate and remain in membrane as a domain. 1^{st} model suggested by Filippov et al [32]. They said 'Headgroups of sphingolipids interact with each other amide and hydroxy/carboxy group, therefore holding sphingolipids together, while cholesterol fills the space between the bulky sphingolipid headgroups and is additionally kept in place by hydrogen bonds and van der Waals interactions between its 3-OH group and the sphingolipid amide groups…’. London and brown attribute tight assembly in rafts to the interaction of mainly saturated acyl chains, which also prefer cholesterol packing [33].

Although the principle mechanism is obscure, it is apparent that the long and fully saturated hydrocarbon chains of sphingolipids and cholesterols are key components for forming a tightly packed domain. One the other hand, kink structure at the tail group of phospholipids hinders the interaction with cholesterol. The kinked structure of the fatty acyl chains of phospholipids results in a shoter molecular length relative to the straight spingolipids. For example, a bilayer composed of phosphatidylcholine is 3.5 nm thick, whereas a bilayer composed of sphingomyelin is 4.6 nm thick [34]. Hence, rafts should protrude from the background (L_d domain) by ~1 nm as shown in **Figure 1.9**, a difference in height that is clearly demonstrated by atomic force microscopy as shown in **Figure 1.10** [35]. This height difference could play a crucial role for molecular shorting both for lipids and proteins. Lipids have various shape and length of acyl chains. These hydrophobic chains prefer to assemble to release the energy generated by height difference of tail group. In this way, saturated lipids tend to get together, whereas unsaturated lipids independently diffuse around [36]. Hydrophobic length difference also play a role for protein sorting as shown in **Figure 1.11**. The proteins according to their length of hydrophobic regions tend to localize where the energy loss is minimized.

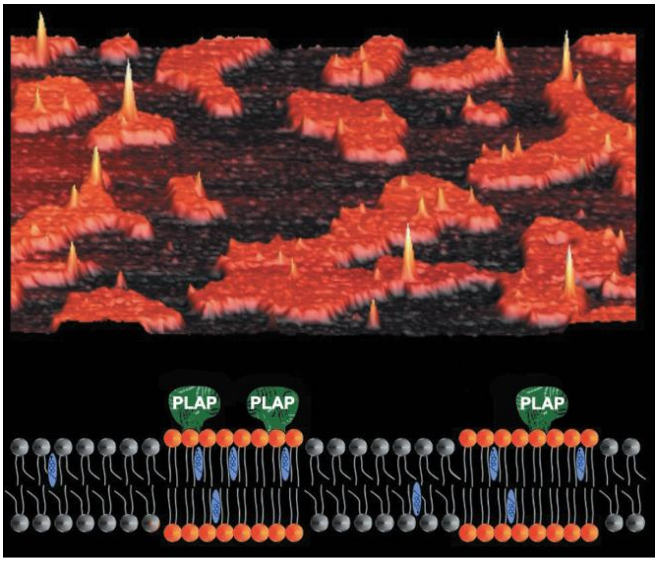

Figure 1.10 : Atomic force microscopy (AFM) image of lipid rafts (red regions) and its schematic diagrams of clustered regions surrounded by L_d domains (from reference [35]).

In this way, proteins may be sorted through height difference of lipid molecules. Thickness of the lipid molecules is not the only reason for protein sorting. Shape of hydrophobic regions of proteins also induces localization of proteins into specific lipid domain. In particular *glycosylphosphatidylinositol* (GPI)-anchored proteins prefer to locate at raft domain due to its covalently attached fatty acid such as *palmitates*.

This serves to anchor them to locate at the membrane where the saturated lipids are abundant. According to these characters, raft domains are thought to function as site for the selective concentration of proteins, acting as platforms enabling a sufficient quantity of protein to accumulate to enable their function.

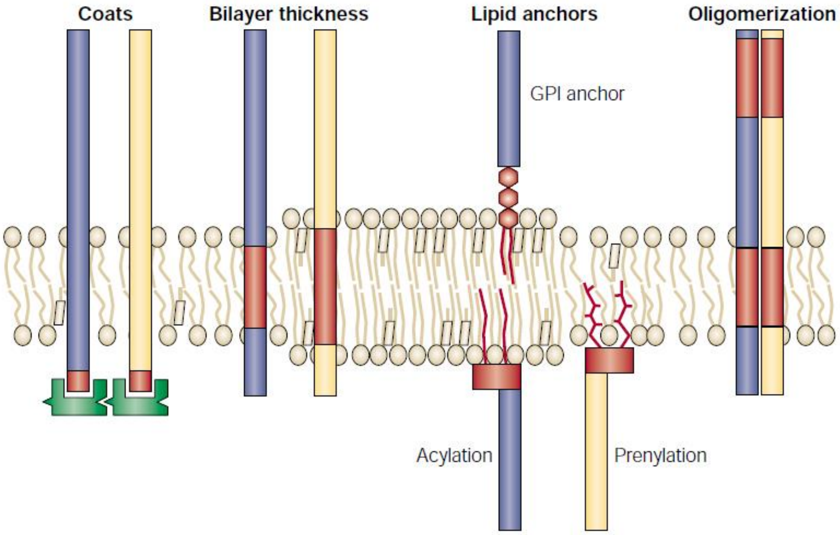

Figure 1.11 : Lateral sorting of membrane proteins according to the thickness of lipid membranes (from reference [36]).

Another important structural issue beside the microdomain in membrane is the curvature of the membrane. Cellular membranes change conformations in striking ways during such processes as movement, division, the extension of neuronal arbors and vesicle trafficking. Budding and fission occur with flux constantly maintaining the interaction between membrane-bound compartments. Curvature can be dynamically modulated by changes in lipid composition, influenced by integral membrane proteins, cytoskeletal proteins and scaffolding by peripheral membrane proteins, and active helix insertion into membranes [37] as schematically summarized in **Figure 1.12**. It is believed that three types of assembly should be recognized in cell membranes–rafts, clustered rafts domain, *caveolae* (a subset of clustered rafts)- and that the residue remaining insoluble after detergent extraction should be called detergent-resistant membrane (DRM) fractions [38].

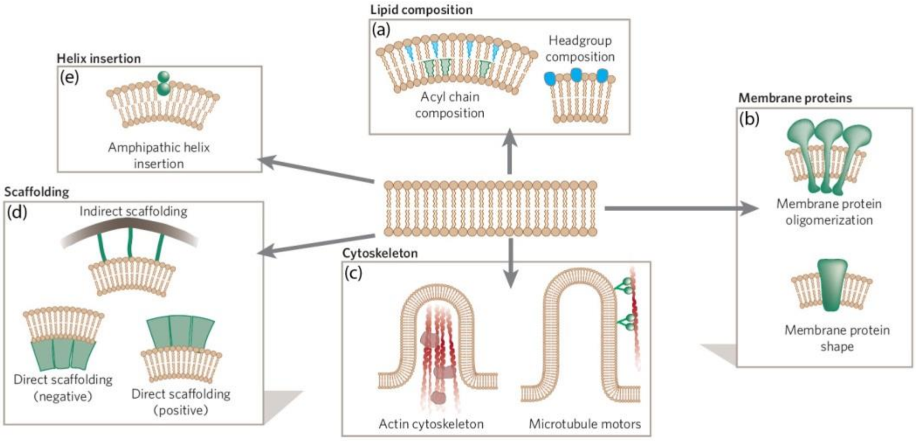

Figure 1.12 : Mechanisms of membrane deformation. The phospholipid bilayer can be deformed causing positive or negative membrane curvature. (a) changes in lipid composition (b) influence of integral membrane proteins that have intrinsic curvature or have curvature on oligomerization (c) changes in cytoskeletal polymerization and pulling of tubules by motor proteins (d) direct and indirect scaffolding of the bilayer (e) active amphipathic helix insertion into one leaflet of the bilayer (from reference [37])

Due to these intrinsic properties of raft domain, they are believed to play roles in various physiological phenomena. For example, lipid rafts have been regarded as the pathogenesis of *Alzheimer*’s, *Parkinson*’s, *prion* and cardiovascular disease, systemic *lupus erythematosus* and *HIV* [39]. But, exact and clearly relation between these unsolved diseases and raft domains has been remain to elucidate. Therefore, manipulation of these specific domains will open a give us an opportunities in medical and biological science.

1.2.2 Lipid Rafts on the Solid Supports

To understand the role of rafts in cells, a characterization of their dynamics is needed. Therefore, the local diffusion of single rafts have been tried to be controlled in the plasma membrane of living cells both in vivo and in vitro. For a physical understanding of cell membrane organization, synthetic lipid bilayers have been studied extensively as model system. Fluorescence microscopy based model systems have revealed a wealth of information about organization in lipid bilayers. Incorporated fluorescent molecules within a patch of membrane are imaged through the fluorescent microscope. This type of studies includes the imaging of phase separation in the lipid bilayers containing the sphingolipids and cholesterols. Manipulating the portion of key components, sphingolipids and cholesterols and phospholipids, lead phase separation of lipid molecules on the solid supports [35]. Although these methods demonstrate the existence of densely packed L_o domain, the shape and periodicity of raft domains cannot be controlled by showing random distributions in the shape of isolated island. Recently, the selective reconstitution of micrometer-scale L_o domain has been demonstrated in model membranes by adjusting the curvature of membrane [40] as shown in **Fig. 1.2.2a**. An elastic energy of membrane could reorganize membrane components and consequent phase separation of L_O domain by coupling between local curvature and topological character of solid supports. This indicates that the coupling between local curvature and microdomains in membranes could be important machinery for signaling events on the basis of curvature-mediated elasticity of membrane. With similar concepts, curvature-mediated raft formations on the SLBs systems [41, 42] were shown and these observations helps and adds the information for understanding physiological roles of raft domains in the real cell.

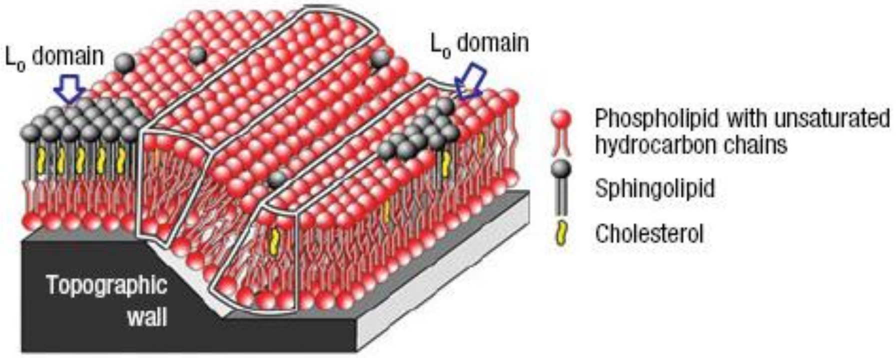

Figure 1.13 : The topographic wall produces elastic energy barriers at two edges. The coarsening process of nanorafts is restricted by the elastic energy barriers (from reference [40]).

1.3 Outline of Thesis

This thesis consists of 7 chapters from **Introduction** to **Concluding Remarks**. In **Chapter 1**, the general overview for describing the properties of lipid membrane, especially focused on the supported lipid bilayers as an artificial membrane and micro-patterning of cell components, is introduced. Among the various characters of lipid membrane, lipid rafts, as one of typical signal molecules that composed of SPMs and CHOLs, and their interaction with solid supports are overviewed in the physicochemical view. As an another typical molecules which deeply related to signaling process, importance and photolithograpy based membrane patterning of charge lipids introduced as well. In **Chapter 2**, the elasticity-based structural organization of artificial lipid membranes will be discussed in the view point of the scientific studies and device application. The concept of curvature-driven membrane reorganization of lipid molecules on biomimetic bud-pits template will be exploited with the experiments of raft domain at the corner of bud-neck regions. Moreover, site selective ligand-receptor binding events on the raft domain with marker proteins are will be discussed for biosensor applications. **Chapter 3** presents the binary membrane morphology, appositional formation of lipid monolayer and bilayer maintaining fluidity and continuity within a membrane. Stamping the dry *polydimethylsiloxane* (S-PDMS) mold on the hydroxylated glass offers sufficient hydrophobicity for generating lipid monolayer morphologies surrounded by unstamped lipid bilayer morphologies without any disruptions and lipid-free regions. Author will try to investigate the reason of the preferential localization of the signal lipids into ‘weak’ hydrophobic regions, and consequently generation of raft domains in the physical point of view. In **Chapter 4**, we will deal with the formative hypotheses of raft domain which has not been demonstrated clearly till now. Although it is obvious that combination of signal molecules, SPMs and CHOLs, is essential for generation of raft domain, not any groups directly observe the correlation between SPMs and CHOLs. Especially how the key components combine and how they cluster into micro domains is unclear since 1972. Author will discuss the plausible mechanism of raft generation at the viewpoint of molecular level and demonstrate the hypotheses by experimental observation. Author found the evidence of CHOL intercalation in raft formation for the first time and demonstrate it with our in vitro model membrane system. In **Chapter 5**, we will probe the real-time membrane formation and reconstitution of L_O domains within a fluid membrane for the first time by means of time-lapse epifluorescence microscopy coupled to the SPR microscopy. The uniqueness of this combinatorial spectroscopic technique is that it allows to monitor the structural parameters of raft domains such as packing density, refractive index (RI) of raft domains within the lipid bilayer both kinetic state and equilibrium mode. Distinguished from other sensing techniques of membrane bounded SPR devices, our systematic conformations of heterogeneous membrane force the L_O domains to aggregate at programmed position which enable the observations of phase-kinetics during raft formations. In **Chapter 6**, the field-directed diffusion of charged phospholipids in supported bilayer membranes into distributed partitions will be discussed within a diffusion cell. The balance between the field-induced drift and the thermal Brownian motion generates the concentration gradient of the charged lipids from partition to partition under an external electric field applied longitudinal to the partition walls. Our field-directed diffusion approach provides a powerful tool for constructing various spatially addressed membrane arrays.

Through the manipulation of signal molecules, our model membrane based approaches will provide a robust platform not only for understanding biological activities, but for designing highly sensitive patterned membrane arrays which could be applicable to DNA, RNA or proteins for gene therapy or protein arrays. Finally, some concluding remarks are made in **Chapter 7**.

Chapter 2. Reconstitution of Ring-raft on Mimicking Biological Bud-neck

2.1 Introduction

The geometrical shape and spatial distribution of the phase-separated domains, generated by heterogeneity-dictated compartmentalization membrane constituents, are believed to determine the diverse biological phenomena such as signal transduction [38], cellular deformation [28-30], viral infection [43], and membrane trafficking [44]. Among them, lipid rafts, called liquid-ordered (L_O) domains with compaction of CHOLs and SPMs possessing negative spontaneous curvature, exhibit distinct physical properties [45]. In the course of diverse biological activities associated with the plasma membrane where variety of lipids and membrane proteins are self-assembled in bilayer morphology, the plasma membrane-driven deformation such as bud-off mechanism (**Figure 2.1a**, cases I-IV) accompanying the bud-neck architecture (step III) is indispensable. However, within the framework of the lipid raft-associated membrane deformation, the compositional heterogeneity and spatial localization at the highly curved bud-neck region, name ‘ring-rafts’ [30], have not been explored and demonstrated in vitro for understanding the role of raft domains in bud-off mechanism such as budding [30], exo/endocytosis [46], fission [36]. A few groups [43, 47-50] have been tried to figure out the lipid trafficking and molecular reorganization when lipid-driven membrane deformation occurs. For example, how the spatial organization of lipids and proteins is established and how it fluctuated in response to external stimuli by focusing the insight at their geometrical properties in terms of spontaneous curvature (c_0). However, raft-dictated mechanical elucidations and observations between ‘ring-rafts’ and pinch-off mechanism remain to be the central question for the secretory and endocytic pathways [38] since Huttner at el. [30] have assumed the existence of ‘ring-raft’ sitting on either side of a bud-neck. The nano-scaled and transient appearance during the bud-off process have ring-rafts as mysterious creature.

Here, we have investigate the effects of the spatial local curvatures on the formation and stability of raft domain, ring-rafts [30], and sequential protein recognitions in model membrane on the biomimetic bud-neck architectures for the first time by means of time-lapse epifluorescence microscopy coupled to the confocal microscopy. Our concept lies primarily in elasticity driven-molecular reorganizations of L_O domains surrounded by liquid-disordered (L_d) domains. The molecular shape [40, 51-53] helps to release the increase of the elastic energy of membrane by transporting membrane molecules. That is, cylindrical-shape lipids prefer to locate at planar membrane surface where spontaneous curvature (c_0) is zero ($c_0 = 0$), and cone-shape lipids reorganize into negatively curved membrane structure ($c_0 < 0$) while the inverted cone-shape molecules prefer to locate positive curved area ($c_0 > 0$). The L_O domains, giving the negatively curved surface ($c_{Lo} = -1/53\ \text{Å}^{-1}$) [52], might be one of the presumable subjects by migrating themselves at the corner of highly curved bud-neck architecture as shown in **Figure 2.1b** and **c**.

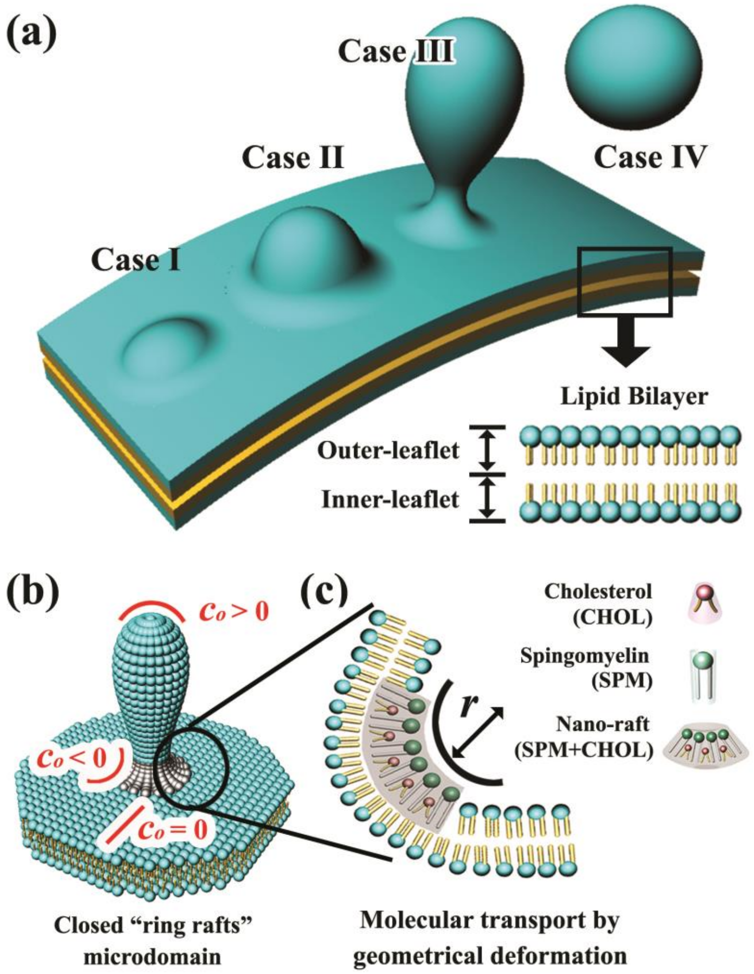

Figure 2.1 : Formation of raft domains at the NC-membranes giving nanometer scale spontaneous curvature (c_0=1/r). (a) Schematic diagrams of progressive budding steps (cases I~IV) from bilayer membranes (b) Closed loop-like raft domains locating at negatively curved ($c_0 < 0$) bud-neck regions giving highly curved ($r \approx$ 100 nm) membrane architecture. (c) Preferential phase-separation domain at the outer leaflet of bilayers due to molecular shape based reorganization process.

2.2 Membrane Formation on Bud-Neck Template

2.2.1 Bud-neck Templates

we have investigate the reorganization of the spatial raft domains on the formation of closed loop "ring rafts" [30] and sequential protein recognitions in model lipid bilayers for the first time. The solid support provides geometrical characters having bud pits like positively curved surfaces ($c_0 > 0$) and planar surfaces ($c_0 = 0$). Negatively NC-bud-neck ($c_0 < 0$) regions are achieved at the boundary between positively curved and planar surfaces for mimicking the budding process (**Figure 2.1a, Case III**) of living cell as shown in **Figure 2.1.** For the viable reconstruction gives geometrical properties of living cell membrane in the shape of bud pits, solid supports should be made with single material for identical physicochemical properties such as surface interaction, adhesion strength between membrane and solid supports except for the geometrical constraint. Since time-lapse reorganization on solid supports is one of our key concepts of our *in vitro* membrane system, solid supports should be biocompatible for lipid membrane. Moreover, Fabrication of solid supports showing geometry in nanoscale is critical requirement for reconstitution of closed loop type raft domains after coverage of membrane allowing the lateral diffusion of membrane components on the supports. The *polydimethylsiloxane* (PDMS) is the ideal choice by fulfilling all the conditions mentioned above. The PDMS is a well-known elastomer which has unique advantages. In particular, it has good biocompatibility, high oxidative and thermal stability, optical transparency [54]. Moreover, it has long history as a well characterized material used to replicate micron to nanoscle structures in the field of soft lithography. The negatively nanocurved- (NC-) structure is achieved by melting process of the

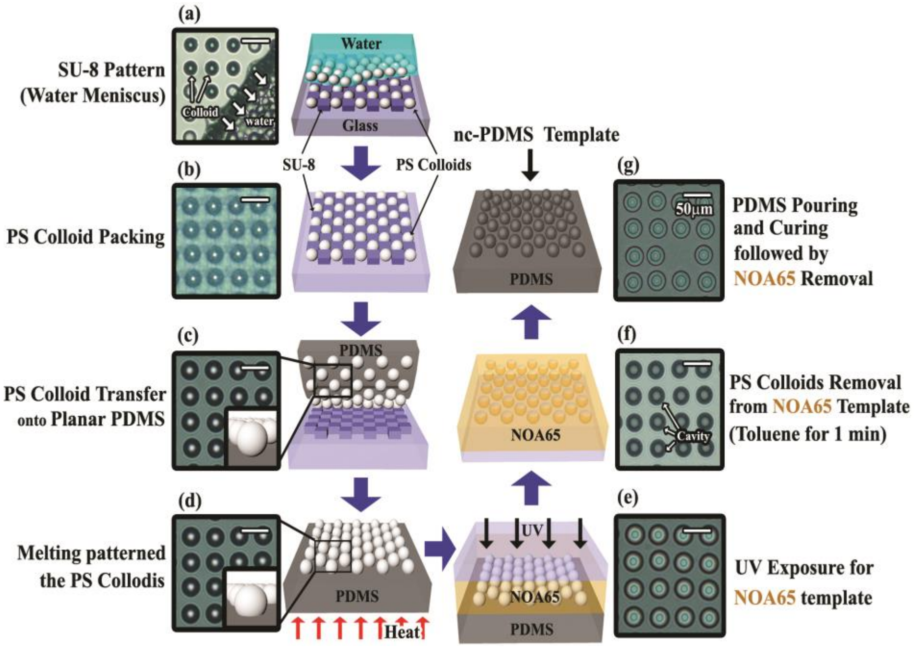

Figure 2.2 : Schematic illustrations of fabrication process for three-dimensional (3-D) NC-PDMS template and systematic control of NC-surface. a,b) Polystyrene (PS) colloidal particles were assembled onto the periodically patterned SU-8 template through a convective assembly process[26] followed by transfer process on to the planar PDMS template (c) and subsequent exposure to hotplate (d) to obtain NC-topography. e,f) The UV curable polymer (NOA65) was spun onto melted colloidal particles followed by covered with the cover glass and exposed to UV for 2 min (e). After peeling from PDMS and removal of PS particle (f) from Noa 65 template, PDMS was poured and cured followed by NOA65 template removal process in the solution (dichlorometane:methanol=100:15) and consequent construction of NC-PDMS template (g).

colloidal particle and sequentially replaced by PDMS. Fabrication process of nanocurved-PDMS (NC-PDMS) will be explained below. After preparing the NC-PDMS, the lipid bilayer structure on the NC-PDMS template is obtained by plasma treatment to make the PDMS surface hydrophilic to keep membrane molecules fluid which is key character that distinguish SLBs from other films [55, 56]. Various compositions of membrane components on NC-PDMS template demonstrate phase-separating of L_o domains at the NC-surfaces ($c_0 < 0$) surrounded by liquid disordered (L_d) phase on positively curved surfaces ($c_0 > 0$) and planar surfaces ($c_0 = 0$). These studies will demonstrate the curvature-dictated assembly of raft domain into shape of 3-D closed loops and protein-bindings on continuous membranes.

Our method to fabricate NC-PDMS is shown in **Figure 2.2** in detail. Briefly, the polystyrene (PS) colloidal particles were assembled onto the periodically patterned SU-8 template (**Figure 2.2a** & **b**) through a convective assembly process [57] followed by transfer process onto the planar PDMS template (**Figure 2.2c**). Subsequently, transferred PS particles are melted on the hotplate [58] (**Figure 2.2d**) to obtain the NC-topography. The ultra violet (UV) curable polymer (NOA65) was spun onto the melted colloidal particles followed by covered with the cover glass and exposed to UV for 2 min (**Figure 2.2e**). After peeling the planar PDMS template from cover glass, the melted PS particles involved in NOA template removed by immerging at toluene solution for 1 min (**Figure 2.2f**). The elastomeric material, *Sylgard 184* silicone elastomer (Dow Corning Corp.) mixed with curing agent in a 10:1 ratio, was poured onto hollowed balls to fill the space with PDMS and cured on the hotplate at 80℃ for 3 hours. By removing of NOA65 template from the cured PDMS in the solution (dichlorometane:methanol=100:15), we can achieved NC-PDMS template as shown in **Figure 2.3a**. Author used the diameter of 25 μm PS particle.

The NC-surfaces showing nano scaled curvature radius ($r = 1/c$) at the boundary between bud pits-like surface and planar surface are achieved according to the melting time (t_m) of colloidal particles on the hotplate as shown in **Figure 2.3b**. At $t_m = 50$ min, we can achieve the curvature radius (r) about ~900 nm as shown in **Figure 2.3c**. Author can control the curvature radius (r) from ~100 nm to micro-scale as function of melting time (t_m) shown in **Figure 2.3d**.

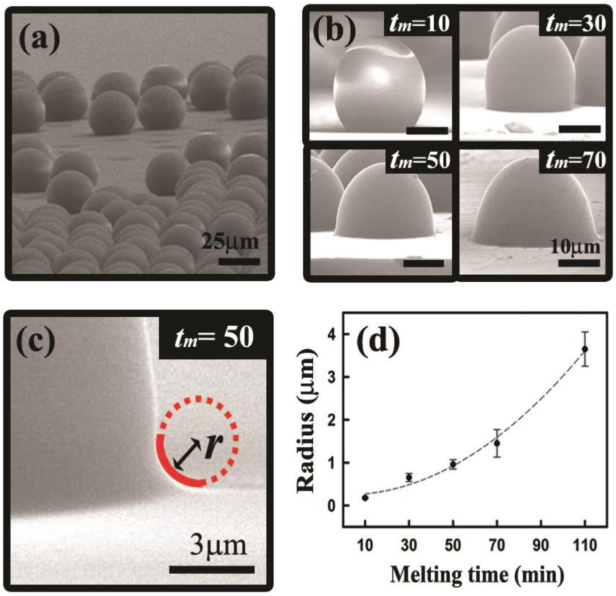

Figure 2.3: Manipulation of curvature radius (r) depending on particle melting time (t_m) of colloid. a-c) The SEM image of NC-PDMS template made of diameter of 25 µm particles (a) and NC-surface (b) with various NC-curvature radius (r), and magnified SEM image of curved region at the value of melting time (t_m=50 min showing $r \approx 700$ nm). d) Curvature radius (r) as function of melting time (t_m) is shown in (d).

2.2.2 Model Membrane on the Template

Author now demonstrates how the SLBs membrane can be expressed on the NC-PDMS template with showing continuous and fluid both on the curved and planar surfaces within the patch of membrane. **Figure 2.4** shows the schematic illustration (**Figure 2.4a**) and confocal micrograph of fluorescent lipids (**Figures 2.4b-h**) on supported lipid bilayers (SLBs) covered NC-PDMS template (t_m = 30 min giving the $r \approx$ 400 nm). The NC-PDMS template was exposed to standard plasma treatment [59] to modify the surface property from hydrophobic into hydrophilic. The treatment of the PDMS surface with plasma introduces polar functional group, primarily *silanol* (-SiOH) groups, on the PDMS surface, which has been documented by a decrease of the contact angles from 120 to 20 degree [60]. Binary **B1** vesicle mixture, composed of 1,2-dioleoyl-sn-glycero-3-phoph-ocholine (DOPC) as a base for the formation of the SLBs with 1 mol% negatively charged lipids labeled with red fluorescent dyes, texas red 1,2-dihexadecanoyl-sn-glycero-3-phosp-hoethanola-mine (TR), are exposure to hydrophilic NC-PDMS template more than 5 min.

The confocal fluorescence microscope shows distributions of membrane components on NC-PDMS template with the side view (**Figure 2.4b**) and top views at each value of Z-axis (**Figure 2.4c-h**), respectively. The distribution of fluorescent TR molecules (**Figure 2.4b**) shows similar shape of scanning electron microscop (SEM) image (not shown) of NC-PDMS template. In order to analyze in detail, we shows distribution of TR at each Z-axis values. As seen at **Figure 2.4c**, a little light was detected at the center of micrograph at the value of Z = 0 μm. whereas the circle-shape distributions of TR are

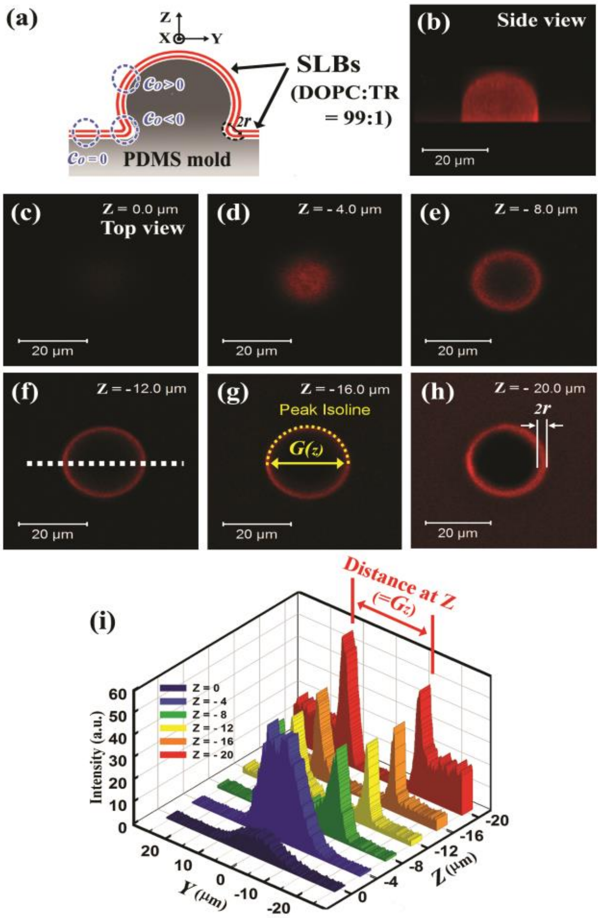

Figure 2.4: a,b) Schematic diagram of formation of SLBs on the NC-PDMS template by rupturing the binary mixture (DOPC:TR=99:1) membrane and side view of confocal micrograph (b) of SLBs covered NC-PDMS template (t_m = 30 min giving the $r\approx500$ nm). c-h) The confocal micrographs at each value of z-axis, Z=0 μm (c), Z=-4μm (d), Z=-8 μm (e), Z= -12 μm (f), Z=-16 μm (g), Z=-20 μm (h) and corresponding cross-sectional intensities along the white dotted line (depicted at Fig. 2.4f) at each Z-axis value (i).

observed indicating that the SLB membrane is completely expressed on the NC-PDMS template (**Figure 2.4c-h**). The distance between 'peak isoline' as each Z values are defined as gap distance G(z) of TR are observed indicating that the SLBs membrane is perfectively expressed on the NC-PDMS template by analyzing the distribution of 'peak isoline', defined as gap distance G(z), at each micrographs. **Figure 2.4i** represents corresponding cross-sectional intensities along the white dotted line (depicted at **Figure 2.4f**) at each Z-axis value. The gap distance is $G_{(-12)}$ = 21.4 μm compared to the $G_{(-20)}$ = 16.1 μm. These data shows the diameter near the bud-neck region is shallow than the diameter of the middle of bud-pits region. And as we expected, amount of fluorescence intensity at the outside of the circle was detected while inside of circle has no intensities at Z = -20 μm. These data give us the information that a patch of continuous SLB membrane is formed on the NC-PDMS template without any disruptions. In the physical words, an appropriate adhesion energy [59] for fluid membrane is achieved by plasma treatment and surface tension of lipids is big enough not to be disrupted by elastic distortion of membrane at the bud-neck area ($r \approx$ 400 nm). Actually, a thin water layer approximately 1-2 nm thick is trapped between the support and the head groups of the lower leaflet of the bilayer [3]. This water layer acts as a lubricant allowing both leaflets of the bilayer to remain fluid. However, it is impossible to fit the exact distribution of SLBs on NC-PDMS template in nanometer scale through the fluorescent microscopic image due to the dispersal effect of fluorescent dye. Therefore, by comparing distribution of TR with confocal microscope with SEM image of NC-PDMS, we can verify the existence of SLB membrane on the NC-PDMS template. Author measures the diameter of NC-PDMS template at various Z values, and figure out that the diameter of template is perfectively same value of $G_{(Z)}$ at each Z values. For example, the diameter at Z = -12 μm was 21.5 μm, compared to the $G_{(-12)}$ =

21.4 μm (data not shown). Author also verified the membrane fluidity through the fluorescence recovery after photo-bleaching (FRAP) studies [4] with the 1 mol% TR molecules included membrane at 99 mol% DOPC lipids on the NC-PDMS template (t_m = 10 min giving the $r \approx$ 100 nm) as shown in **Figure 2.5**. The phospholipids, used as a base for the formation of the SLBs, were 1,2-dioleoyl-sn-glycero-3-phoph-ocholine (DOPC). For imaging the SLBs, a negatively charged lipids labeled with red fluorescent dyes, *texas red 1,2-dihexadecanoyl-sn-glycero-3-phosp-hoethanola-mine* (TR, Molecular Probes, Eugene, Oregon) were mixed with DOPC at 1 mol%. The lipid mixture, 33:33:33 (mol: mol: mol) DOPC: SPM: CHOL, all purchased from Avanti Polar Lipids, Birmingham, Alabama) was prepared, doped with TR and *ganglioside* GM_1 (brain, ovine-ammonium salt, Avanti Polar Lipids, Birmingham, Alabama) at 1 mol% according to the each purpose, respectively. The alexa fluor 488 labeled *cholera toxin B subunit* (Alexa-488 CTxB, molecular probe, Eugene Oregon) is used as a raft maker protein diluted to a concentration of 10 μg/ml with Tris buffer (100 mM NaCl and 10 mM Tris at pH 8.0). All lipids were dissolved in chloroform. The rapid solvent exchange method [55] was employed to evaporate chloroform and to hydrate with Tris buffer (100 mM NaCl and 10 mM Tris at pH 8.0) simultaneously. Small unilamellar vesicles (SUVs) were produced by extruding 20 times through a 50 nm filter. The residual SUVs remained in the tris buffer solution were removed with the DI water after the SLBs was formed after the substrate was exposed to the SUVs solution for 5 min The texas red dyes and *alexa fluor 488* dyes were monitored using both with an confocal microscopy (Carl Zeiss LSM710, Karl Zeiss, Carl Zeiss Korea) and an epifluorescence microscopy (Eclipse E600-POL, Nikon). Whole processes were performed in room temperature. The measurements of the fluorescence intensity molecules in supported lipid membranes were carried out using an image analyzing program of Image J (National Institute of Mental Health, USA). Formed SLB membrane by vesicle rupture process had been kept for 3 days showing the stable coverage on the NC-PDMS template and followed by FRAP tests both on the planar areas (**Figure 2.5a-c**) and on the bud-pit areas (**Figure 2.5d-f**). The bleached regions (yellow dotted circles) with UV for 1 minute were recovered with surrounded lipid molecules by Brownian motion after 20 min at both of area. A quantitative analysis of our system reveals an diffusion coefficient of 1.36 ± 0.1 $\mu m^2/s$ at both of the bud-pits surface and the planar surface giving identical diffusion constant, in good agreement with lipid bilayers on glass [4, 42] and oxidized PDMS substrates [61]. Our FRAP studies indeed confirm that the continuity and fluidity of the binary membrane are completely preserved.

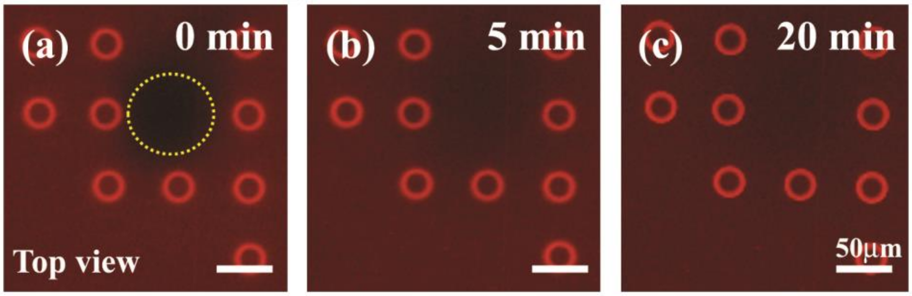

FRAP of TR on the planar SLBs (DOPC:TR = 99:1)

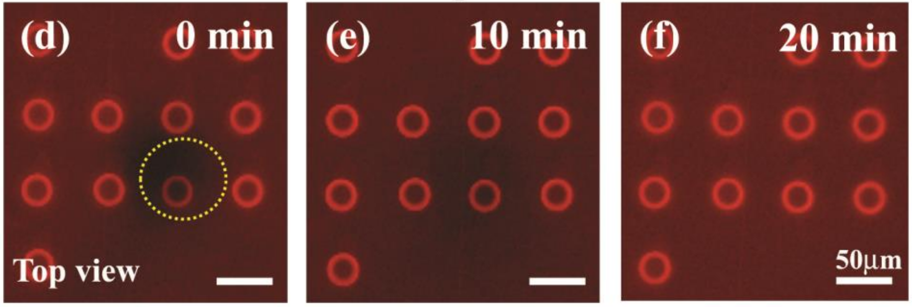

FRAP of TR on the curved and planar SLBs

Figure 2.5: a,b) the fluorescence recovery after photo-bleaching (FRAP) studies [4] with the 1 mol% TR molecules included membrane at 99 mol% DOPC lipids on the NC-PDMS template (t_m = 10 min giving the $r \approx$ 100 nm). FRAP test on the planar SLBs (a-c) and both on curved and planar SLBs (d-f). The yellow dotted circle indicated the area where UV light is exposed.

2.3 Curvature Elasticity-driven Membrane Reorganization

2.3.1 Membrane Reorganization on Bud-neck Template

On the basis of the outcomes made above, we implemented combinatorial introduction of diverse lipid mixtures on the NC-PDMS template to demonstrate which lipid molecules are crucial for phase-separating into L_O phases at NC-surfaces. Whole fluorescence micrographs were taken after 36 *h* of vesicle rupture procedure that is sufficient for phase-separating into L_O phases at the control value of NC-PDMS template ($t_m = 50$ min giving the $r \approx 700$ nm). The compositional properties of each SLB types are represented in **Table 1.**

Table 1. The compositional properties of each vesicle mixture

SLB types	Composition of SLB
B1	99% DOPC, and 1% TR **(Fig. 2)**
B2	66% DOPC, 33% CHOL and 1% TR **(Fig. 3a)**
B3	66% DOPC, 33% SPM and 1% TR **(Fig. 3b)**
B4	98% DOPC, 1% GM_1 and 1% TR **(Fig. 3c)**
B5	65% DOPC, 33% SPM, 1% GM_1 and 1% TR **(Not shown)**
B6	65% DOPC, 33% CHOL, 1% GM_1 and 1% TR **(Not shown)**
B7	33% SPM, 32.5% CHOL, 32.5% DOPC, 1% GM_1, and 1% TR **(Fig. 3d)**
B8	33% DOPC, 33% SPM, 33% CHOL and 1% TR **(Not shown)**

In order to identify the effect of the CHOL and saturated SPM, we express the both of SPM/GM_1-free **B2** membrane (**Figure 2.6a**) and CHOL/GM_1-free **B3** membrane (**Figure 2.6b**) to the NC-templates, respectively. Although the CHOL and SPM molecules are key components for raft formations, individual introduction to NC-PDMS fail to phase-separate into L_O domains. Similar process is performed with the ternary **B4** membrane (**Figure 2.6c**), but fail to shows any difference as well. No particular changes (**Figure 2.6a-c**) during 36 *h* give us the information that the SPM, CHOL and GM_1 couldn't lead phase-separation into the L_O domain when they work alone. Author also performed the identical experiments with quaternary **B5** CHOL-free membrane (data not shown) and SPM-free **B6** membrane (data not shown), but cannot find any differences compare to former experiments. These data give us the information that the SPM (or CHOL) and GM_1 and their combination doesn't lead phase-separation into the L_O domain[62]. However, when quintuplicate **B7** mixture (**Figure 2.6d;** SPM+CHOL+DOPC+GM+ TR) was introduced to the NC-PDMS template, the black lines around the edge of bud pits structure were observed. In order to investigate which lipid components lead to phase-separation into raft domain, the identical experiment was performed with quaternary GM_1-free **B8** mixture. The identical black lines at the same regions were detected (data not shown). Our combinatorial introduction of membrane to NC-PDMS studies indeed confirms that the CHOL and SPM are critical components for L_O domain formation and subsequent phase-separation in the shape of 'ring-raft' domains. Besides, phase-separation of rafts domain is mostly activated at the negatively curved surface. As we mentioned above, we used NC-PDMS template ($t_m = 50$ min giving the $r \approx 700$ nm). **Figure 2.6e** shows the time-lapse microscopic observation after rupturing the **B7** mixture in time, and the corresponding fluorescent intensity of TR as function of distance from center of bud-pits. The fluorescent intensity of TR near the center of bud-pits gets increase as function of time, while that of TR at the NC-regions gets decrease.

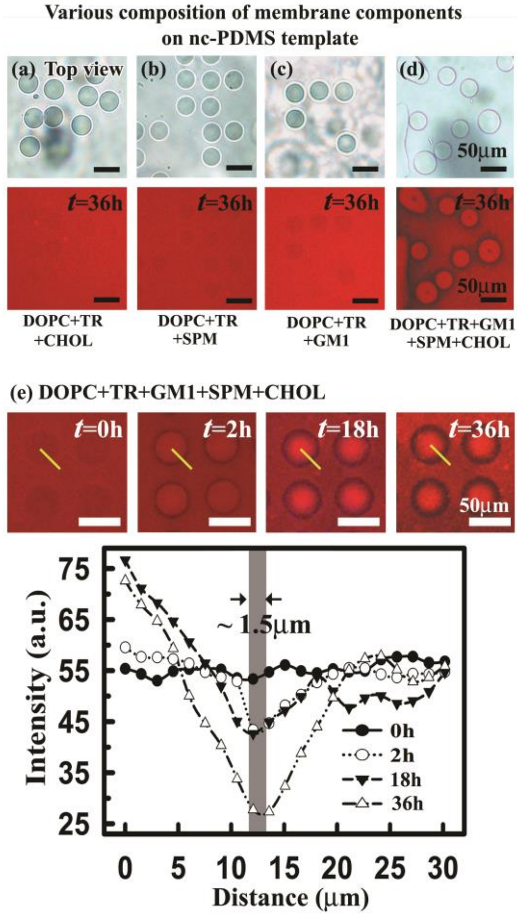

Figure 2.6 : The microscopic (top row) and fluorescence textures (bottom row) by rupturing various composition of membrane components on NC-PDMS template. a-d) The ternary mixture SPM/GM$_1$-free B2 membrane (a), with CHOL/GM$_1$-free B3 membrane (b), with SPM/CHOL-free B4 membrane (c), and the quintuplicate B7 membrane (d) after formation of SLB membrane for 36 *h*. The time evolution of B7 membrane in time is shown in (e).

This can be interpreted the growth of L_O domains at the corner of NC-regions in time. Interestingly, we find out that the range of darkest intensity at $t = 36$ *h* is about 1.5 μm (shown in gray region between two black arrows at **Figure 2.6e**) which is two times of curvature radius ($\approx 2r$). Underlying concept of organizing lipid domain at the NC-surface can be explained by spontaneous curvature of the L_O domain ($c_{Lo} = -1/53$ Å^{-1}) [52]. Author already estimates the preferential localization of raft domains at curved surfaces at previous papers [52]. The intrinsic curvature originated from asymmetric molecular shapes of lipids [63], generally has a more negative value due to a small head group of a cholesterol molecules than the L_d phase ($c_{Ld} = -1/160$ Å^{-1}) [64]. When the outer leaflet of lipid monolayer is under structural deformation by the negative curvature of NC-PDMS template, the L_O domains will experience less severe elastic distortions than the L_d domains. This means that the curvature gradient of the NC-PDMS surfaces will provide a driving force for the transport of L_O domains to release the increase of the elastic energy. As a result, the preference of 'nanoraft' into at the NC-surface than planar surface lead phase-separation at the edge of bud-pit structures as seen at **Figure 2.6d**. The 'height mismatch' of lipids molecules also helps the phase-separation and growth into bigger raft domains. Lipid raft domains tend to be thicker than surrounding membrane. This comes from that the saturated hydrocarbon chains of SPM (~4.6 nm thick) is thicker than the unsaturated hydrocarbon chain of DOPC (~3.5 nm thick) demonstrated by atomic force microscopy [35]. These 'height mismatch' [28] at the edge of phase-separated domain would give arise the increase of 'line tension' which is energetically unfavorable by exposing of hydrophobic part of raft components to water molecules. If membranes allow themselves to deform at the boundary so as to prevent the creation of hydrophobic surface by protruding rafts, the line tension would be reduced. However, in our system, instead of rolling up or detaching from the solid supports, the ‘ring-raft’ domain prefers to locate to the NC-region. Author postulates that energetically unfavorable ‘line tension’ also lead the rafts aggregates to accumulate bigger domain to reduce the total line tension at NC-surface in our system. According to these data, we can conclude that geometry of membrane structure, with radius in nanometer scale, might be major factor for spatial migrating and coarsening of ‘nanoraft’ units in the shape of ‘ring-rafts’ as providing excellent platforms for gradual aggregations of nanoraft into L_O domains.

2.3.2 Ring-rafts and Protein Localization at NC-surface

On the basis of the results made above, we reconstitute spatial distributions of L_O domain into ‘ring-rafts’ within a patch of model membrane and sequential protein-binding as shown in **Figure 2.7**. Prior to reconstitution of L_O domain on the NC-PDMS template, we rupture CHOL-free **B5** mixture (DOPC:TR:GM_1:SPM=65:1:1:33) to the template (t_m=30 *min* giving the $r \approx$ 500 nm; SEM image in **Figure 2.7a**) In order to confirm the existence of L_O domain, well known raft-marker protein, *alexa fluor 488 labeled cholera toxin B subunit* (CTxB-488), was additionally introduced 36 *h* after the formation of the SLB membrane on NC-PDMS template. The CTxB protein has highly affinity to glycolipid receptor GM_1 which would highly concentrate on the L_O domain (**Figure 2.7b**). The confocal microscope was used to identify the 3-D distributions of target lipids. First of all, we found that the TR uniformly distribute on the NC-PDMS template without any fluorescence depletion regions showing that no L_O domain was formed as a control test **(Figure 2.7c)**.The GM_1-bound CTxB-488 (**Figure 2.7d**) distribute uniformly, namely uniform distribution of GM_1, on the NC-PDMS template (Not shown).

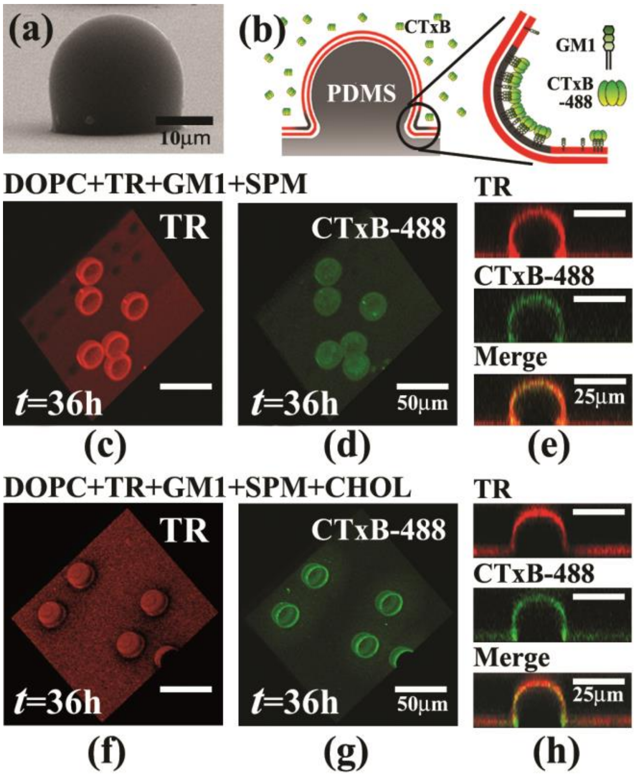

Figure 2.7 : Reconstitution of spatial L_O domain into a 3-D form of closed loop within a patch of model lipid bilayers and protein (CTxB-488) binding on the NC-PDMS template. a) The SEM image of NC-PDMS template made of diameter of 25 μm particles (t_m=30min giving the r≈500nm). b) Schematic illustrations of the CTxB protein binding to glycolipid receptor GM1 with highly affinity. c-e) Distribution of TR (c), CTxB-488 (d), and cross-sectional view of single bud-pit (e) when covering the NC-PDMS template with quaternary mixture (DOPC:TR:GM1:SPM=65:1:1:33) of cholesterol excluded membrane. f-h) c-e) Distribution of TR (c), CTxB-488 (d), and cross-sectional view of single bud-pit (e) when covering the NC-PDMS template with quintuplicate mixture (DOPC:TR:GM1:SPM:CHOL=33:1:1:32.5:32.5) membrane to the NC-PDMS

The **Figure 2.7e** shows the series of the cross-sectional micrographs of target lipid (TR; top row), protein (CTxB-488; middle row) and merged image (TR+CTxB-488; bottom row). These confocal images confirm that TR and bounded CTxB cap the NC-PDMS template with uniform and constant coverage without any disruption of membrane. By contrast, expression of the quintuplicate **M7** mixture to the NC-PDMS template shows contrasting results compared to the **M5** membrane which excludes the CHOL lipids. Author observed that closed loop shaped TR-depleted areas at the NC-surface showing that L_O domain was formed as shown in **Figure 2.7f.** The distribution of CTxB-488 (**Figure 2.7g**) also supports our observation of ring-raft domains at the NC-surfaces. That is, more intensive fluorescent light of CTxB-488, namely location of GM_1, was detected near the NC-surface, and the cross-sectional micrographs (**Figure 2.7h**) verify the formation of L_O domain at NC-surface. Author also performed 'continuity test' to confirm that black regions at NC-surface comes from whether ring type 'lipid-free' zone by disrupting the lipid membrane or phase-separation of L_O domain by expelling the TR-DHPE lipids from L_O domain. Author exposes fluorescence labeled proteins, *avidin*-FITC, which will bind to hydrophilic surface of solid supports if there are 'lipid-free zone' [65, 66] in our system. However, no non-specific binding of *avidin*-FITC protein was detected which indicate that black ring-shape regions are L_O domains (data not shown). on the NC-PDMS template. The **Figure 2.7(e)** shows the series of the cross-sectional micrographs of target lipid (TR; top row), protein (CTxB-488; middle row) and merged image (TR+CTxB-488; bottom row). These confocal image confirm that TR and bounded CTxB covered NC-PDMS template with uniform and constant coverage. Author also confirms that the continuity quaternary membrane are completely covered and preserved. By contrast, expression of the quintuplicate mixture (DOPC:TR:GM1:SPM:CHOL=33:1:1:32.5:32.5) membrane to the NC-PDMS template shows different results compared to the quaternary mixture membrane which excludes the CHOL lipids. Author observed that closed loop shaped TR depleted areas at the NC-surface showing that L_o domain was formed as shown in **Figure 2.7f.** The distribution of CTxB-488 (**Figure 2.7g**) also supports our observation of closed loop type raft domains at the NC-surfaces. That is, more intensive fluorescent light of CTxB-488, namely location of GM1, was detected near the NC-surface. The **Figure 2.7h** shows series of the cross-sectional micrographs of target lipid (TR; top row), protein (CTxB-488; middle row) and merged image (TR+CTxB-488; bottom row). Our selective membrane introduction to NC-PDMS studies indeed confirms that the saturated SPM and CHOL are critical components for 'nano raft' formation and subsequent phase separating into L_o domain. Moreover, intrinsic curvature mediated spatial reconstitutions of raft domain into a 3-D form of closed loop within a patch of model lipid bilayers. Author also performed 'continuity test' to confirm that black regions at NC-surface comes from whether ring type 'lipid-free' zone by disrupting the lipid membrane or phase separation of Lo domain by expelling the Txrd-DHPE lipids from Lo domain. Author exposes fluorescence labeled proteins, *avidin*-FITC, which will bind to hydrophilic surface of solid supports if there are 'lipid-free' zone [65, 66] in our system. However, no non-specific binding of *avidin*-FITC protein was detected (data not shown).

2.4 Discussion & Conclusion

In conclusion, the approach described here offers the practical reconstruction and stability of ring-rafts in model membrane for the first time by means of time-lapse fluorescence microscopy coupled to the confocal microscopy. The spatial local curvatures which mimic the intermediate process of budding were achieved with single PDMS material and exposure of diverse mixtures confirms that the combination of SPM and CHOL is essential for Lo domain at the bud-neck architecture. Curvature mediated reorganization within the membrane will give clues for understanding the mechanical correlation between local curvature and biological phenomena such as generations of budding, invaginations [27, 49], and virus intake process (*e.g. Influenza virus hemagglutinin*) [43]. First of all, our concepts shows geometric deformation of membrane can transport and localize the specific class of lipids molecules, known as lipid rafts, into shape of ‘ring-type’ by escaping from the conventional isolated ‘island-type’ lipid raft pattern[4, 15, 28]. Our reconstitution of ring-rafts in vitro could be expended to identify the physical and functional roles of ‘ring-raft’ [30] in the course of budding process. Author also carried out ‘field directed diffusion test’ [56] to confirm that whether closed shape of L_O domain at NC-area prohibits lipid mixing or transporting between bud–pits and donor membrane, and confirm that these ‘ring-type’ rafts play as an barrier between two regions as shown in **Figure 2.8**. This phenomenon might occur at apical membrane of living cell which is believed to be happened near the either side of a neck within the membrane. Since ‘ring-rafts’ can play an important role as a barrier to lipid diffusion, which can facilitate fission by restricting the amount of lipid molecules involved in the fission reaction and thereby reduce dissipation of energy as mentioned by Huttner at el [30]. Secondly, our system could offer the opportunities to uncover the general explanation why membrane division protein, dynamin, destined to locate at bud-neck region. Raft domains are thought to function as site for the selective concentration of proteins, acting as platforms enabling a sufficient quantity of protein, including *dynamin* [67], to accumulate to enable their function [27]. However, general explanation or mechanistic factors for gathering of the *dynamin* into bud-neck regions remain to obscure. Author conjectures that it might aggregate at bud-neck due to ‘ring-type’ raft domains as we shown in this thesis. In conclusion, our results could represent clues for understanding the relations between curvature [28-30] and lipid compactions [68], and consequential protein migration and clustering [49, 50] for scientific research and for applied science by providing the platform in vitro.

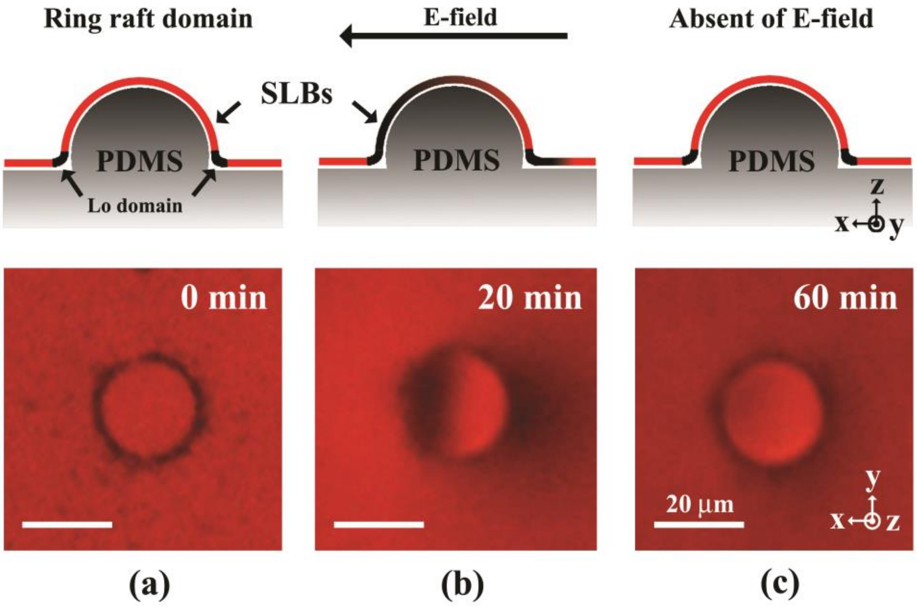

Figure 2.8: The schematic illustrations (upper line) and epifluorescence micrographs (bottom line) indicating the procedure of ‘field directed diffusion test’. Spatial reconstitution of loop shape Lo domain before, at t = 0 min (a) and after, at t = 20 min applying the electric field of 45 V/cm (b) followed by cutting the electric field for 40 min at t = 60 min (c).

Materials & methods

Formation of SLBs and an imaging method**:** The phospholipids, used as a base for the formation of the SLBs, were 1,2-dioleoyl-sn-glycero-3-phophocholine (DOPC). For imaging the SLBs, a negatively charged lipids labeled with red fluorescent dyes, texas red 1,2-dihexadecanoyl-sn-glycero-3-phosphoethanola-mine (TR, Molecular Probes, Eugene, Oregon) were mixed with DOPC at 1 mol%. The sphingomyelin (SPM; brain, porcine), cholesterol (CHOL), *ganglioside* (GM_1 ; brain, ovine-ammonium salt) were purchase from from Avanti Polar Lipids (Birmingham, Alabama). The alexa fluor 488 labeled *cholera toxin B subunit* (Alexa-488 CTxB, molecular probe, Eugene Oregon) is used as a raft maker protein diluted to a concentration of 10 μg/ml with Tris buffer (100 mM NaCl and 10 mM Tris at pH. 8.0). All lipids were dissolved in chloroform. The rapid solvent exchange method [55] was employed to evaporate chloroform and to hydrate with Tris buffer (100 mM NaCl and 10 mM Tris at pH. 8.0) simultaneously. Small unilamellar vesicles (SUVs) were produced by extruding 20 times through a 50 nm filter. The residual SUVs remained in the tris buffer solution were removed with the DI water after the SLBs was formed after the substrate was exposed to the SUVs solution for 5 min The texas red dyes and alexa fluor 488 dyes were monitored using both with an confocal microscopy (Carl Zeiss LSM710, Karl Zeiss, Carl Zeiss Korea) and an epifluorescence microscopy (Eclipse E600-POL, Nikon). Whole processes were performed in room temperature. The measurements of the fluorescence intensity molecules in supported lipid membranes were carried out using an image analyzing program of Image J (National Institute of Mental Health, USA).

***Application of the electric field*:** The electric field-directed experiment in our study is similar to the electrophoresis experiment[56]. Across the two Pt wires being used as two electrodes stands away 1.5 cm apart, the direct current electric field of 45 V/cm was applied from a standard power supply.

Chapter 3. Cellular Signal Pathways across Mono-Bilayer Junction

3.1 Introduction

The living cell coordinates its components against the numerous signals through the signaling pathways associated with the transportation of the messenger molecules [69, 70] or the generation of the reaction cascades [71] in the forms of cell deformation [29], membrane trafficking [36], and domain organization [72-74]. Since most of signaling events are mediated by the cellular membrane where the diverse lipids and membrane proteins are assembled in bilayer architecture, elucidating physicochemical factors which migrate and compartmentalize the signaling components [75, 76] into spatial domains within a patch of membrane are crucial for understanding the role of membrane in signaling. As one of regulatory factors, the membrane morphology has been believed to integrate the certain type of membrane constitutes (*e.g.* receptor protein complex, signal lipids) toward specific domains, called *lipid raft* [77, 78]. The lipid rafts, the dynamic assemblies of sphingomyelins (SPMs) and cholesterols (CHOLs), have been considered to play a central role in gathering signaling-participative proteins [45, 66, 79] to variable extents showing morphological variations within the bilayer architecture, but remain as the open question to answer the correlation between the signaling and the membrane morphology. Macroscopically, the cell membrane exhibits two types of morphologies depending on the relative positions of individual membrane proteins. One case is that trans-membrane proteins [2, 36, 71, 75] occupy both the outer and inner leaflets of the membrane (**Figure 3.1a**, left). The other cases are that a large family of membrane proteins are floated around the membrane without penetrating into the layers of the lipids [36]. For example, the integral monotopic protein (IMP) [2] is occupied only in a single leaflet, either the outer or inner leaflet, of the membrane (**Figure 3.1a**, middle and right). At this moment, the monolayer-bilayer junction (MBJ) within continuous membrane is destined to occur. As an effort to mimic the MBJ where majority of signals are propagated across the membrane, numerous physicochemical approaches have been tried to reconstitute appositional binary membrane in model system [80, 81]. However, the lipid-free gap [82-86], separating the lipid monolayer region from the bilayer region at the substrate boundary between the hydrophilic and the hydrophobic surfaces, prohibits floating lipids from being mixed each other showing incomplete reconstruction of native cellular junctions. In order to reconstitute leaflet of a monolayer at opposing the IMP, two distinct essential prerequisites, which are comparable to property of the IMP, are required. That is the hydrophobicity which avoids discontinuity at the boundary between lipid monolayer and bilayer membrane, and embedded dimension around of ~2 nm height. Despite the actual existence in cellular membrane, the reconstitutions of connective MBJ in model membrane and the consequential assembly of raft molecules into specific domain for effective ligand-receptor binding (**Figure 3.1b**) has not been explored so far in supported lipid membrane (LM) even at the significant roles in the course of signaling pathway [27-31]. Therefore, it is extremely crucial to establish a reliable and practical strategy of integrating continuous and fluid binary supported LM which gives an opportunity toward designing bio-functional surface. Besides usage of this platform which applicable to preferential behavior of signal molecules will become robust tools for biological science for in vitro studies.

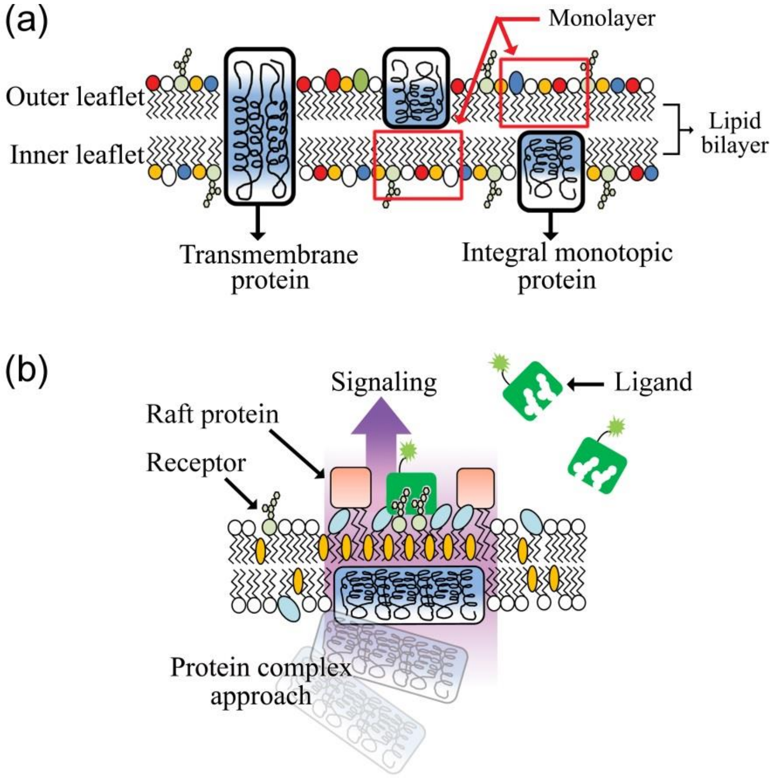

Figure 3.1 : Representation of the MBJ**. (**a) The native plasma membrane consist of two opposing monolayers of diverse lipids floating the large family of proteins exhibiting the MBJ. (b) Regulatory signal events are initiated by approach of signal protein complex. Preferential segregation of signal lipids and accompanying protein sorting at monolayer morphology could occurs with consequent binding of signal proteins due to the receptor-ligand recognition.

3.2 Continuous Membrane across the Mono-Bilayer Junction

3.2.1 Modification of the Surface Hydrophobicity.

Author now describes how the surface energy of S-PDMS transferred glass can be modified to find ‘weak’ surface hydrophobicity at which reconstitutions of supported lipid monolayer. The fabrication process of S-PDMS transferred glass was explained at **Materials and Methods** in detail. Briefly, before the contact with dry PDMS mold, a glass substrate was first cleaned with a solution of piranha. The PDMS preferentially transfers onto more hydrophilic surface features due to the hydrolysis reaction of PDMS material with hydroxyl (-OH) group on glass during stamping [87, 88]. Piranha cleaned glass was contacted to PDMS mold and subsequent exposure to hotplate while they keep contacted. Author have found that temperature can vary the surface hydrophobicity [89]. The contact angle gradually increases as temperature increases while they keep contacted to glass as shown in **Table 2**. Author also represents surface energy (γ_{sv}) which will be discussed later. **Figure 3.2a** shows the microphotographs of contact angle (θ) of water before (θ_1 = 6°, inset) and after (θ_2 = 80°) stamping of the PDMS mold at 200℃ for 3 min. To test the surface hydrophobicity at the aqueous environments, we performed water drop test at selectively patterned surfaces showing distinct wettability. Transfer of S-PDMS to half of 2 cm × 2 cm cleaned glass, hydroxyl (-OH) group terminated, contacted with bulk PDMS mold and being exposed to aqueous environment by dropping the water droplet at the boundary between stamped (white rectangle) and unstamped (filled with water) area as depicted in **Figure 3.2b**. The schematic illustrations of selective transfer process of S-PDMS on cleaned glass are shown (in upper inset in **Figure 3.2b**).

Table 2 : Contact angles ($\theta_{C.A.}$) of water (H_2O) & the surface energy (γ_{sv}) on various substrates

Surface	**$\theta_{C.A.}$ (H_2O) (deg)**	**γ_{sv} (mJ/m^2)**
Piranha cleaned glass	< 6.0	72.4
S-PDMS glass (Room temp.)	36.0	62.0
S-PDMS glass (50℃)	45.0	56.6
S-PDMS glass (100℃)	48.5	54.6
S-PDMS glass (150℃)	60.6	47.5
S-PDMS glass (200℃)	80.1	35.4
S-PDMS glass (250℃)	84.0	33.0
S-PDMS glass (300℃)	90.1	29.2
Bulk PDMS	105.6	19.7
Octadecyltrichlorosilane (OTS)	109.1	17.6

***** Surface tension (γ_{sv}) of different surface before and after PDMS stamping calculated from mean advancing water contact angle (γ_{lv} =72.8 mJ/m^2 and β = 0.0001247 (mJ/m^2)$^{-2}$.

Moreover, it is essential to design bio-functional arrays and devices [90, 91] at the unit of micro-scale. These characters were demonstrated by water vapor test [86] with micro-fabricated PDMS mold by conventional photolithography. The schematic picture of micro-patterned PDMS mold, casted and peeled from piranha cleaned glass at 200 ℃ for 3 min, was shown (in **Figure 3.2c**) with showing scanning electron microscopy (SEM; upper inset) micrograph of micro-patterned PDMS mold and Atomic force microscopy (AFM; bottom inset) micrograph of stamped area. It is found that the thickness of S-PDMS region was at the range of 3-4 nm (data not shown) which is comparable scale of thickness of the lipid layer. To test for differences in chemistry between the underlying substrate and S-PDMS material, water from humid air was allowed to condense on the micro-patterned (50 μm × 50 μm separated by 15 μm grid patterns). Upon the patterns, clear patterns were formed. This data is good accordance with data shown by Karin Glasmästar at el [86]. A clear pattern of the expected dimensions was shown, demonstrating a contrast in hydrophilicity/hydrophobicity between the contact/noncontact regions as shown in **Figure 3.2d**.

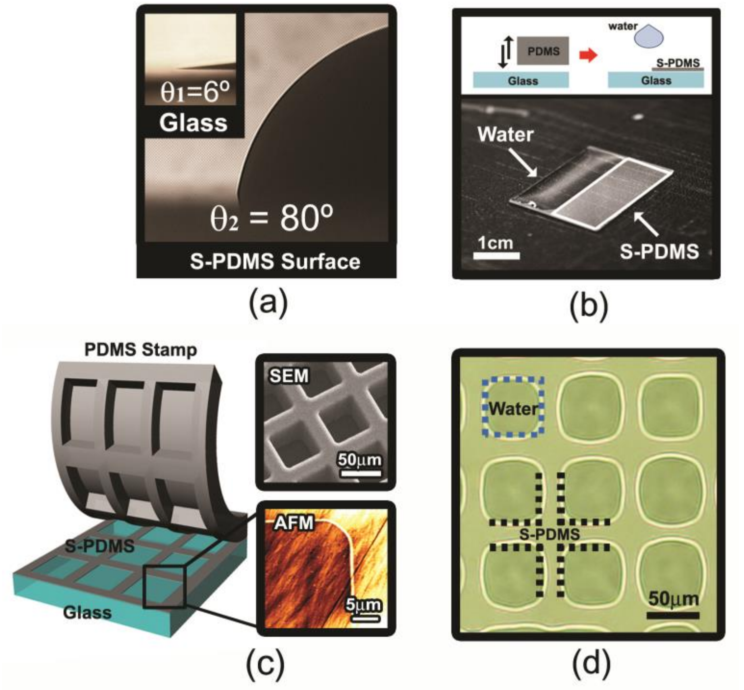

Figure 3.2 : Water vapor test and water drop test at selectively patterned surfaces showing distinct wettability (a) The Microphotographs of contact angle of water before ($\theta_1 = 6°$, inset) and after ($\theta_2 = 80°$) stamping of the bulk PDMS at 200℃ for 3 min. (b) Transfer of S-PDMS to half of 2 cm x 2 cm cleaned glass showing distinct wettability is demonstrated by dropping the water drops on the boundary between stamped (white rectangle) and unstamped area. The schematic illustrations of selective transfer process of S-PDMS on cleaned glass are shown in upper inset. (c) The schematic picture of micro-patterned PDMS mold to piranha cleaned glass showing Scanning electron microscopy (SEM; XL30FEG, Philps) micrograph of PDMS mold (upper inset) and Atomic force microscopy (AFM; AutoProbe CP, Park Scientific) micrograph of stamped area (bottom inset). (d) The microphotograph of water vapor test on 50 μm x 50 μm separated by 15 μm grid PDMS patterned stamp (the scale bar is 50 μm).

3.2.2 Continuous Binary Lipid Membrane

Supported lipid films have been reconstructed through the vesicle fusion on planar surfaces using one of three techniques. First, Tamm and McConnell [92] observed spontaneous adsorption of lipid films forming continuous bilayers that are weakly bound to the surface through a 1-nm-thick water layer. Thin water layer provides the fluidity of lipid molecules in bilayers morphology and thus provide a bio-functional films. On the other hand, lipid films can be formed on self-assembled monolayer (SAM) and polymer surfaces by using the balance of hydrophobic, steric, and electrostatic forces acting on lipids [93]. Among them, hydrophobic force is an important factor for reconstructing the binary membrane. Since the steric interactions takes place in the plane of the monolayer and the electrostatic interaction depend deeply on the ionic strength of the solution. Therefore, for our system, it is proper to focus on the surface hydrophobic interaction at a water-hydrophobic interface. The interfacial free energy of lipids has been reported to vary between 50 and 19 mJ/m^2 [94]. In order to establish fluid and connective membrane on the hydrophilic supports, it is essential to form 'weak' hydrophobic barrier (Type I; **Figure 3.3a**) for lipid monolayer architecture. If the hydrophobic energy of barrier is too strong, lipids stick to the 'strong' hydrophobic barrier and result in discontinuous binary membrane (Type II; **Figure 3.3b**) by acting like geometrical barrier as explained above. Author estimates 'strong' and 'weak' surface energy (γ) through contact angle (θ) and an equation of state of interfacial tension has been developed [87]:

$$\cos\theta = -1 + 2\sqrt{\frac{\gamma_{\mathrm{sv}}}{\gamma_{\mathrm{lv}}}}\, e^{-\beta(\gamma_{\mathrm{lv}}-\gamma_{\mathrm{sv}})^2} \qquad (1)$$

Where, γ_{sv} γ_{sl} and γ_{lv}, where the subscripts sv, sl, and lv refer to the solid-vapor, solid-liquid, and liquid-vapor interfaces, respectively. if γ_{lv}, θ , and empirically derived parameter β are known, then γ_{sv} is also known. γ_{sv} was determined using a Microsoft excel that we wrote employing values of 0.0001247 mJ/m$^{2)-2}$ for β and 72.8 mJ/m^2 for γ_{lv} of water. Detailed explanation for the **equation 1** is described at **Materials and Methods**.

In the light of the above idea, supported lipid films are reconstructed through the vesicle fusion method [92]. The phospholipids, used as a base for the formation of the connective binary supported membrane (CBSM) membrane, were 1,2-dioleoyl-sn-glycero-3-phoph-ocholine (DOPC, white headgroup in **Figure 3.3a**) and negatively charged lipids labeled with red fluorescent dyes, Texas Red 1,2-dihexadecanoyl-sn-glycero-3-phosp-hoethanola-mine (TR-DHPE, red headgroup in **Figure 3.3a**) mixed with the ratio of 99:1. To enable fluorescence visualization, we use the starting vesicles doped with a 1 mol% TR probe. The 1-nm-thick water layer provides the fluidity of lipid molecules in bilayers [56, 95]. To demonstrate the connective MBJ system through S-PDMS (**P**) transfer method, we directly compare the membrane properties on the octadecyltrichlorosilane (OTS) self-assembled monolayer (**O**) formed with identical experimental conditions. The OTS was selected since it shows the comparable thickness of the single layer with S-PDMS and representative material for generating lipid monolayer morphology as well. The AFM data obtained both at **P** and **O** regions (data not shown) show great accordance with data reported earlier by Wang et al. [96] Templates for the **P** and **O** patterns comprised of 50 μm × 50 μm square regions separated by 10 μm (**Figure 3.3a**, inset) and 15 μm (**Figure 3.3b**, inset) distance were shown by SEM images and consequent vesicle fusion on the **P** and **O** stamped substrates forming binary membrane were shown in **Figure 3.3a** and **Figure 3.3b**, respectively. A high-contrast fluorescent pattern comprising two regions of distinctly different fluorescence intensities is immediately discerned: (I) bright and homogeneous region within the patterned square (‘**G**’ for unstamped glass); (II) weaker, yet homogeneously fluorescent, background regions (‘**P’** and ‘**O’**). The patterns correspond directly to the patterns of surface hydrophobicity and topography generated by mold stamping. In particular, the unstamped **G** regions exhibit stronger, homogeneous fluorescence due the probe doped lipid bilayer. By contrast, the stamped **P** or **O** regions show weaker, homogeneous fluorescence due to the probe-doped lipid monolayer. Our results show great accordance with the previous studies which established the a lipid mono layer [97] on hydrophobic surface, whereas the lipid bilayers [56] on hydrophilic surface. Author also observes the fluorescence intensity contrasts in hydrophilic (**G)** and hydrophobic regions (**P** or **O**) along the white dotted line (**Figure** 3.3**a,b**). Corresponding data are depicted as yellow line profiles, displaying stronger intensity (I_2) on hydrophilic regions and weaker one (I_1) on hydrophobic regions. Average values derived from more than 20 independent samples yielded the intensity ratios of ~1.74 (I_2/I_1) at **O** regions, ~1.51 (I_2/I_1) at **P** regions, respectively. These data are similar with data of Howland et al [83]. The ‘migration test’ [82] of charged lipids is tested to verify the connectivity of MBJ between hydrophobic and hydrophilic regions. As mentioned above, the lipid mixture used to form the binary membrane contained 1 % negatively charged TR-DHPE. Following the appliance of a field of 40 V/cm for 20 min (t = 20), the negatively charged lipids within the square pattern are expected to move toward opposite direction of electric-field. In case of **P/G** patterns, faint accumulations and depletions of charged lipids within square regions (G) at t = 20 represent only accumulation of the TR molecules which positioned at the inner leaflet of membranes are geometrically blocked by S-PDMS molecules, while continuity of membrane through the outer leaflet of bilayer structure allows the mixing between two regions (**Figure 3.3a**, middle). To further definite verification of membrane connectivity, we apply boundary through mechanical scratching method [1] along the blue dotted line at t = 20

(**Figure 3.3a**, inset of middle) and applying the electric field of 40 V/cm for 10 min (*t* = 30). Cross-sectional fluorescence intensity (yellow line) at white dotted line shows abrupt depletion of TR-DHPE at right-side of scratched line (blue dotted line) showing similar drift velocity (~0.11 ± 0.01 μm/s at DOPC:TR-DHPE=99:1 estimated from the mid-point trajectory method [97]) at square regions. In the case of O/G pattern, by contrast, TR lipids within the square pattern are found to accumulate toward the right-side of **G** regions having the field-induced drift motion showing a constant velocity ~0.13 ± 0.01 μm/s, while identical lipids on the grid pattern (**O**) show dubitable accumulation (**Figure 3.3b**, middle) at *t* = 20. Corresponding fluorescence intensity profiles (yellow lines) along white dotted lines demonstrates accumulation of charged species within the **G** regions. Similar results have been reported earlier by Han et al [82]. This comes from the strong hydrophobicity of S-OTS that prohibits lipid mixing of two distinct regions by forming lipid-free gaps. Additive stamping was performed to confirm our connective property on binary architecture by S-PDMS stamping. Periodically aligned 'line and space' patterns of **P** (100 μm width) and **O** regions (200 μm width) in orthogonal direction were used for direct comparison of distinct connective characters on an identical solid supports (**Figure 3.4**). The generation of lipid-free gaps could be explained with the competition between a 'lipid surface tension' ($\gamma_{\text{L-L}}$) and a surface hydrophobicity of the geometrical barriers [85]. In order to construct the BMJ, interfacial energy (γ) and height (*h*) of hydrophobic barriers that transferred from stamps should be in suitable range (γ = 19-50 mJ/m^2) and comparable to the thickness of the monolayer (L_t = 2~3 nm) [98], respectively. Since membrane morphology is determined by hydrophobic characters of barriers on the solid supports, it is desirable to provide 'weak' hydrophobicity (**Figure 3.3a**, Type I) which allows fluid and connective membrane at MBJ. That is why we select the specific S-PDMS transfer condition (200℃ for 3 min) for suitable surface properties constituting lipid monolayer against to the weak barriers. The method to calculate the γ is explained in **Methods.** By contrast, if the hydrophobic energy of barrier is too ‘strong’ enough to beat the $\gamma_{L\text{-}L}$, lipids stick to the ‘strong’ hydrophobic barrier and result in discontinuous binary membrane (**Figure 3.3b,** Type II) as they generate lipid-free gap at the boundary.

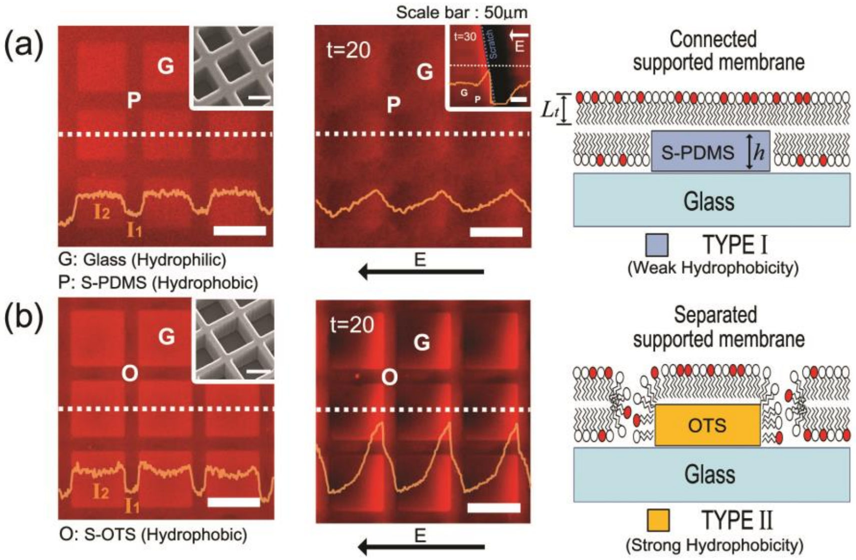

Figure 3.3 **:** Direct comparison of binary membrane fabricated with S-PDMS (top) and S-OTS (bottom) patterned substrate. The phospholipids, used as a base for the formation of the CBSM cell, were DOPC (white head group) and TR-DHPE (red head group) mixed with the ratio of 99:1. The 50 μm x 50 μm squares separated by 10 μm (a) and 15 μm (b) patterned PDMS mold (SEM images are shown in upper-right insets) were used. Epifluorescence images and corresponding cross-sectional (white dotted lines) intensities (yellow lines, I_1 for P and O regions and I_2 for G region, respectively) of a supported phospholipid binary membrane formed by vesicle fusion over the S-PDMS (Type I; a) and S-OTS (Type Ⅱ; b), followed by applying the electric field of 40 V/cm for 20 min with direct comparison of diffusion conformations before (left column) and after (middle column). Especially, the epifluorescence image before scratching is shown at *t* = 20. Mechanical Scratching method are performed along the blue dotted line at *t* = 20 and consequence micrographic image (*t* = 30) in the presence of E-field were shown in inset. (whole scale bars are 50 μm long). Conclusive illustrations of CBMS showing connective membrane at MBJ (TYPE I, a), while showing lipid-free gap at boundary of two distinct morphologies (TYPE II, b).

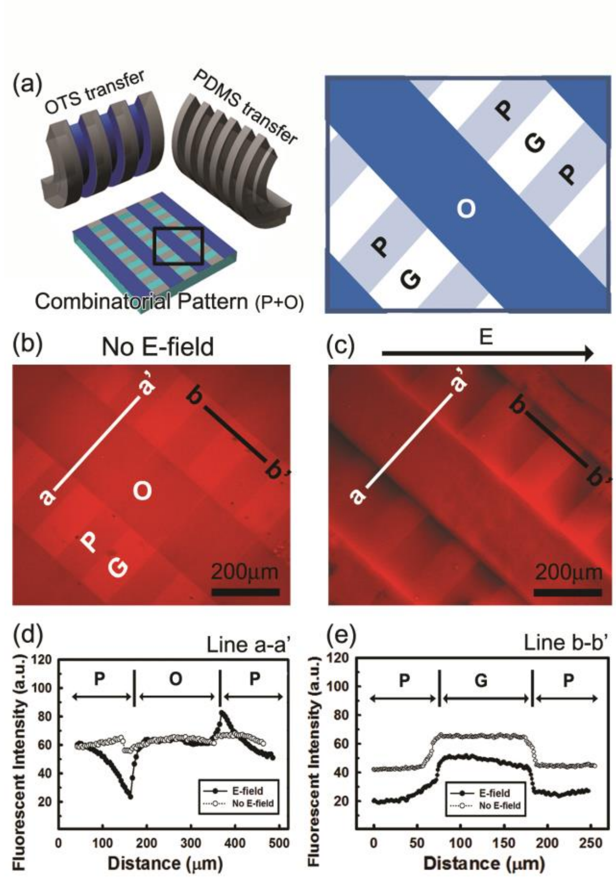

Figure 3.4 : The combinatorial pattern (P+O pattern) for verifying our connective property on binary lipid architecture. (a) Schematic diagram of the additive transfer process (left) for P regions (100-μm-width line and space) and O regions (200-μm-width line and space) in perpendicular direction. Magnified illustration of the rectangular-grid pattern (black square, left) is represented (right). b,c) Epifluorescence images of a supported phospholipid binary membrane formed on combinatorial pattern before (b; t=0) and after (c; t=20) applying an electric field of 40 V/cm for 20 min. d,e) Corresponding crossectional intensities on line a-a’ (d) and line b-b’(e) at the absent (white circle) and present (black circle) of an electric field.

3.3 Selective Growth of Rafts on Mono-Bilayer Membrane

3.3.1 Surface Hydrophobicity Dependence

As predicted, the site-selective reconstitution of the signal domains might occur at continuous MBJ depending on underlying properties of surface. Prior to imposing the raft mixtures to our CBSM system, the diverse lipid mixture containing each raft components are introduced to S-PDMS patterned surface as shown in **Figure 3.5**. Selective stamping was achieved with photolithographic patterned master consisted of 50 μm × 50 μm square areas standing out 50 μm from PDMS stamp (**Figure 3.5**, inset). The distributions of red dye (TR) and green dye (NBD) were represented at top and bottom lines, respectively. First, the vesicles which contain both of raft components, denoted as **M1** membrane, (**Figure 3.5a**; 1% TR-DHPE, 33% NBD-CHOL, 33% SPM, 1% GM_1 and 32% DOPC) were expressed on S-PDMS stamped glass and confirm the formation of monolayer/bilayer morphology at S-PDMS stamped/unstamped surfaces. Author observed the high-contrast fluorescent pattern comprising two regions of distinct fluorescence intensity, that is, brighter for bilayer region and weaker for monolayer region. The character of fluorescence intensity of TR-DHPE shows bright at **G** regions (I_2) and darker at **P** regions (I_1). However, very interesting result was observed at the range of green spectrum. That is, the distribution of NBD-labeled CHOL molecules shows opposite tendency of fluorescent contrast profiles against the TR-DHPE molecules showing brighter intensity at **P** regions (I_1) and darker at **G** regions (I_2). Despite the monolayer architecture on the **P** regions, the fluorescent intensity is brighter than **G** regions as shown in bottom line of **Figure 3.5a**. To test whether the distribution of CHOL enrich patterns come from Fluorescence resonance energy transfer (FRET) occurring between TR and NBD, the TR-DHPE excluded **M2** membrane was prepared to our pattern. No fluorescent signals were observed at the range of red spectrum shown in **Figure** 3.5**b**. However, the identical distribution of NBD-CHOL molecules was obtained showing brighter intensity at **P** regions and darker at **G** regions. Author used the NBD-CHOL that NBD labeled at the head group (and tail group) of CHOL molecules, but no diffusive difference were observed between head-NBD labeled and tail-NBD labeled CHOL (data not shown). The vesicle mixtures which contain the individual key components of rafts are also tested. The CHOL-free **M3** membrane (**Figure 3.5c**) and the SPM-free **M4** membrane (**Figure 3.5d**) films are formed on S-PDMS patterned glass, respectively. Author found that both of SPM and CHOL molecules prefer to localize at '**P**' regions than '**G**' regions. This was demonstrated by the yielded the NBD intensity ratios of ~2.10 (I_1/I_2) for SPM (**Figure 3.5c**) and ~1.85 (I_1/I_2) for CHOL (**Figure 3.5d**) over the **P** stamped samples, respectively. The introduction of **M5** membrane (**Figure 3.5e**) to our system was performed as control experiments to verify the preferential localization of raft components at **P** regions comes from NBD-dye itself or not. Consequential results show the identical distributive tendency of TR-DHPE by exhibiting (I) darker and homogeneous region within the **P** regions; (II) brighter, yet homogeneously fluorescent **G** regions in the both range of red and green spectrum (**Figure 3.5e**). It is concluded from this result that the SPMs and CHOLs prefer to localize on hydrophobic surface than hydrophilic one. This result shows good accordance with the comments that the Park and Lee et al. [93] reported. In the conformation of monolayer at a water-hydrophobic interface, the saturate lipids, the SPMs for our system, prefer to locate in more hydrophobic area [93, 99, 100]. Moreover, Vlasova et al. [100] demonstrated that the affinity of hydrophobic compounds for hydrophobic surfaces is higher than for hydrophilic surface. This could give the clues to interpret the favorable localization of CHOLs on S-PDMS region since the composition of CHOLs is majorly made up of the hydrophobic steroid rings.

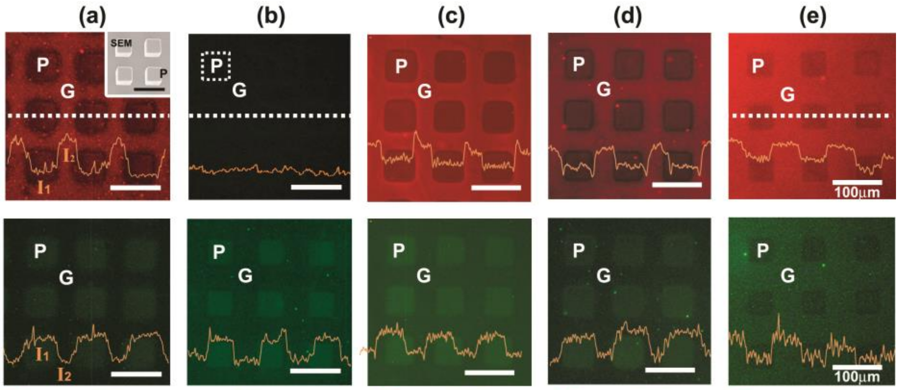

TR-DHPE + NBD-CHOL + SPM + GM1

NBD-CHOL + SPM + GM1

TR-DHPE + NBD-SPM + GM1

TR-DHPE + NBD-CHOL + GM1

TR-DHPE+NBD-PE/PS +GM1 (Bace lipid: DOPC)

Figure 3.5 : **Selectivity of raft components on surface hydrophobicity.** The various vesicles including different raft components are exposed to P patterned surface. Lipid mixtures including NBD-CHOL, SPM, GM1, DOPC with TR-DHPE (a), and without TR-DHPE (b) were exposed to S-PDMS pre-patterned glass. The SEM image of PDMS mold was represented (a, inset). Individual raft components with NBD-SPM (c), with NBD-CHOL (d) were exposed mixing with TR-DHPE, GM1, DOPC, respectively. (e) raft component-free mixtures also test. Corresponding cross-sectional contrast intensities (yellow lines; I_1 for P region and I_2 for G regions, respectively) along the dotted white lines were shown in each micrograph.

3.3.2 Selective Raft Formation and Protein Binding

Based on the preferential localization of raft components on S-PDMS region, we accomplished time-lapse microscopic observations to investigate whether the favorable migration of raft components into L_O domains and consequent ligand-receptor binding occur within fluid CBSM as shown in **Figure** 3.6**.** Author previously demonstrated the coarsening of unit rafts, called 'nanorafts', into microscopic scale depending on the topographic character of solid supports which is essential for controlling the L_O domain in a supported membrane system[40]. After preparing the hydrophobic patterns ('**P**' for S-PDMS and '**O**' for S-OTS) on glass, the raft component included **M6** membrane is introduced and monitored. As direct comparisons at each region, the fluorescence recovery after photo-bleaching (FRAP) studies[4] on the raft-mixture membrane were carried out **(Figure 3.6a)**. Our FRAP studies indeed confirm that the continuity and fluidity of the CBSM are completely preserved in the **P** region (**Figure 3.6a1**, the diffusion coefficient of ***D*** = 0.375 ± 0.05 $\mu m^2/s$) and in **G** region (**Figure 3.6a2**, *D* = 1.06 ± 0.1 $\mu m^2/s$) except for in **O** region (**Figure 3.6a3**, not estimated by dubitable diffusion). White dotted circles (**Figure 3.6**) indicate where the photo-bleaching performed. As predicted, no aggregation of nanorafts is monitored at the **O** region (**Figure 3.6b**). By contrast, nanorafts aggregate and grow into macroscopic L_O domains only in the **P** regions (**Figure 3.6c**). Since the TR-DHPE molecules are strongly excluded in the course of nanorafts-coarsening process, the formation of L_O domains are monitored by the distribution of the TR-DHPE. Importantly, it seems that nanorafts initially present in the **G** regions actively participate in the formation of L_O domains in the **P** regions. This is clearly shown by the fact that the L_O formation is much faster at the boundaries than at the center of **P** regions. The corresponding cross sectional (along the yellow dotted line) intensities as function of time on CBMS membrane supports our conclusion (**Figure 3.6c**). The standard raft-marking process, the specific binding of *cholera toxin unit B* (CTB) to glycolipid receptor $GM_{1,}$ was implemented as a model for ligand-receptor recognition process and applicability for biomedical microarray. **Figure 3.6d** and **e** shows the L_O domain microarray which was incubated with solution of *Alexa Fluor 488-labelled CTB* (CTB-488) for 1 *h* and washed with phosphate buffered saline (pH. 7.4). The strong green fluorescence at **P** region illustrates that the CTB-GM_1 binding processes are highly concentrated in these regions. These data can be interpreted to the conjecture that preferential segregation of signal lipids and accompanying protein sorting which are key factors for the signaling event occurs at monolayer than bilayer morphology.

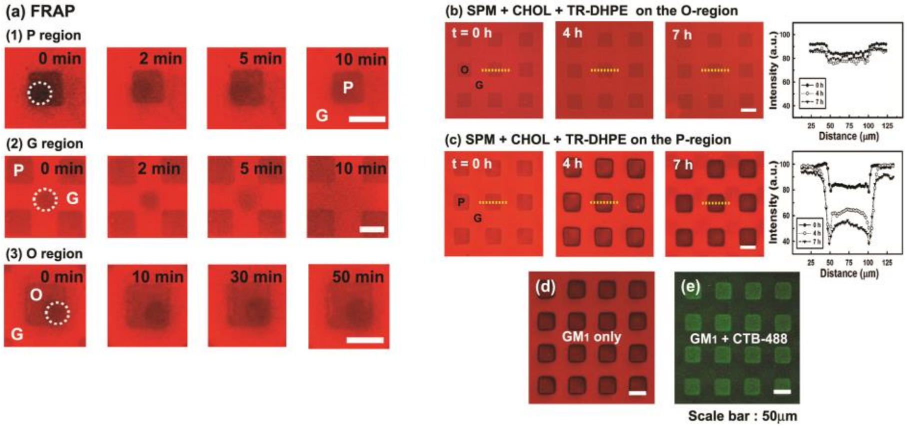

Figure 3.6 : Growth of lipid raft by monolayer-bilayer connectivity and protein binding. (a) FRAP studies on the TR-DHPE molecules on the **P** (a.1), **G** (a.2) and **O** (a.3) regions bleached with UV light (white dotted circle) for 1 min (the scale bar is 50 μm). **b,c,** Epifluorescence images and corresponding cross-sectional (yellow dotted lines) intensities as function of time of supported binary membrane on patterned **O** region (b) and **P** region (c) using heterogeneous membrane (33% SPM, 33% CHOL, 32% DOPC, 1% GM$_1$, 1% TR-DHPE). d,e), Selective reconstitution of the CTB-GM$_1$ binding process in the L_O domain microarray (d) after incubation of solution of *Alexa Fluor 488-labelled CTB* (CTB-488) for 1 *h* (e). (the scale bar is 50 μm)

3.4 Discussion & Conclusion

In this study, Connective binary lipid membranes are implimented by constructing connective appositional formation of lipid monolayer-bilayers depending on the surface hydrophobicity. Author denotes ‘weak’ hydrophobicity which gives monolayer morphology and connective to the bilayer. This is suitable for connective CBSM system. Controlled surface in a systematic way associated with transfer of the residual low-molecular-weight oligomers was established as function of temperature by giving ‘weak’ hydrophobicity. After patterning the distinct patterns, the lipid morphology, self-assembled into CBSM binary architecture without showing lipid-free gap, is demonstrated membrane connectivity in direct comparisons with stamped *octadecyl-trichlorosilane* self assembly monolayer (S-OTS SAM) from water vapor to vesicle exposure test. It is found that raft components prefer to locate on the 'weak' hydrophobic area. Exposure of raft mixture vesicle consequently demonstrate the formation of L_O domains and confirm by selective binding of raft marker protein on the fluid CBSM.

Constructing binary lipid membrane *in vitro* requests not only understanding of membrane formation on the solid supports and physicochemical characters about surface of solid supports as well. Tamm and McConnell [92] observed spontaneous adsorption of lipid films forming continuous bilayers that are weakly bound to the surface through a 1-nm-thick water layer. Thin water layer provides the fluidity of lipid molecules in bilayers morphology and thus provide a bio-functional films. To construct bilayer structure with 'weakly' bounded to solid surface, balanced forces including hydration, electrostatic, steric and long ranged van der Waals force are involved [56, 101]. Hence, for constructing monolayer structure, it is essential to constructing 'weak' but enough to 'strong' to attract tail part of lipid molecules. For reconstruction of CBMS morphology *in vitro*, appropriate surface hydrophobicity is essential that has surface hydrophobicity stabilizing the lipid in monolayer morphology. The interfacial free energy per unit area ($\gamma_{L\text{-}S}$) for lipid monolayer at a water-hydrophobic interface is reported to vary between 50 and 19 mJ/m^2 [93]. Forming the connective appositional formation of lipid monolayer-bilayer requires the 'weak' hydrophobic energy which does not breaking balance with the surface tension of lipid molecules. Several approaches have been attempted by lying hydrophobic 'Barrier' on the hydrophilic surface and trying to construct binary membrane. However, due to the too ‘strong’ hydrophobicity of barrier, there is the lipid-free gap [82-86], separating the lipid monolayer domain from the bilayer domain at the substrate boundary between the hydrophilic and the hydrophobic surface. Therefore, it is essential that if there is ‘weak’ hydrophobicity (Type II; **Figure 3.1b**) which allows not only fluid and connective membrane between lipid monolayer and bilayer, but thickness of barrier (blue ‘W’ as shown in **Figure 3.1b**) similar to that of lipid monolayer. It is found that S-PDMS, known as residual low-molecular-weight oligomers (LMWOs) [86-88, 102, 103], does show ‘strong’ hydrophobic properties enough to form the lipid monolayer and ‘weak’ hydrophobic ones (see the **Table 2**) to exhibit connective and fluid binary structures as well. These characters are demonstrated by compared with ‘strong’ hydrophobic barrier (S-OTS) as shown in **Figure 3.3** and **Figure 3.4**.

Biological membranes comprise multiple lipid components that segregate into coexisting phase. Spatially controlled heterogeneity of the membrane components exhibits biological phenomenon including signal transductions and cell-cell recognition. Specially, the lipid rafts, composed of sphingolipids and cholesterols giving the L_O domain showing heterogeneity on the cell membrane, have been attract great attention due to its vital roles in many biological functions**.** Owing to significant importance of reorganizing the signal molecules *in vitro* system, reorganization of membrane components on the fluid CBSM according to characteristics of the underlying solid surface would give great interests. In the light of the above idea, we found the preference of signal molecules, e.g. SPM and CHOL, on the ‘weak’ hydrophobic areas as shown in **Figure 3.5**. Our results can be interpreted the comment the Park and Lee et al [93] mentioned. They pointed out the hydrophobic energy as a source to transfer a molecule of lipid from the hydrophobic surface to solution. This values is the interfacial free energies per unit area(γ) of monolayer at a water-hydrophobic interface. The range for monolayer morphology has been reported to vary between 50 and 19 mJ/m^2, where the higher interfacial free energies (γ) are associated with saturated lipids and lower interfacial free energies were associated with unsaturated lipids at the specific range. This means, it needs more energy to transfer of saturated lipids from surface to solution. That is to say, saturate lipids prefer to locate in more hydrophobic area. In our system, it is plausible for the SPMs to be found at hydrophobic area, since it is well known saturated lipids. For the CHOLs, we should solve the reason why they prefer the S-PDMS surfaces. The hydrophobic character of cholesterol within the single monolayer is obviously demonstrated by hydrophobic interaction with proximate phospholipids, which leads to a liquid-ordered phase [99], but not for interaction with hydrophobic polymer-water surfaces. Vlasova et al. demonstrate that the affinity of hydrophobic compounds (cholesterol) for hydrophobic surfaces is higher than for hydrophilic surface [100]. This results are good accordance with our data. For our system, we postulated that the orientation of CHOL molecules within the monolayer structure, the steroid ring part that is major components for hydrophobicity of cholesterol are expected to keep in contact with S-PDMS regions while hydrophilic components of cholesterol toward water, facilitate the preference of cholesterols at S-PDMS region. As a results, by showing the preference of signal molecules on the hydrophobic regions, we report controlling the reconstitution of the L_O domains in a selective manner by predefining underlying surface energy using PDMS stamping (**Figure 3.6**). Our surface hydrophobicity based approach differs from other methodologies to accumulate L_O domains by Yoon at el [40], established to growing Lo domain by locally modulating the surface curvature, and by Okazaki at el who modulates the coverage of the surface by the polymeric bilayer domains [104].

The approach described here offers a new way of constructing connective lipid membrane in model membrane system *in vitro*. Moreover, the CBSM system would potentially be of significant interest as a useful platform for understanding of phenomena occurring at the cell interfaces. Our CBSM provides a practical route to mimic the cellular environment by overcoming the lipid-free gap between lipid monolayer and bilayer domain. Moreover, incorporation of different classes of biomaterial such as DNA, living cell, other signal proteins will lead more functional flexibility for studying biochemical process. In particular, it gives the morphological reproduction of fluid lipid-monolayer facing I.M.P. [2] which occupies one leaflet of membrane as well (shown in the left illustration of the **Figure 3.7a**). Since it is well known that Lo domains are primarily formed at the outer leafleat of native living cell membrane, reconstructing of the CBSM systems with inner leaflet-substitutable materials are indispensable for understanding the interaction between outer and inner leaflet within bilayer morphology as well as the formations of Lo domain. By substituting the I.M.P., our CBSM system will open the new way to lipid sorting (shown in middle illustration of the **Figure 3.7a**), specially for saturated lipids, and will be used for protein arrays for raft proteins (shown in right illustration of **Figure 3.7a).** Not only restricted on signal molecule events and protein induced re-compartmentalization of outer leaflet, it can also applicable to understanding the interleaflet dynamics of lipids in cellular membranes as well. For example, our CBSM system can mimic the signal transduction which occurs when a signaling molecule activates a cell surface reorganization. In our case, the I.M.P plays a signal molecule by approaching and involved in the one leaflet of membrane. Sequential reorganization of membrane components, e.g. signal lipids and raft proteins, result in raft formation as shown in **Figure 3.7b**. Our CBSM system gives information about an interaction between lipids and faced I.M.P. which cannot be achieved through the conventional lipid binary structures due to the denaturation of membrane proteins when it come in contact with solid supports [105] at the *in vitro* system. Therefore, the CBSM structures of the heterogeneous lipids will hold promise of a new class of functional devices range from signal transduction, chemical and biological analysis/detection, and materials engineering with target protein [97, 105, 106].

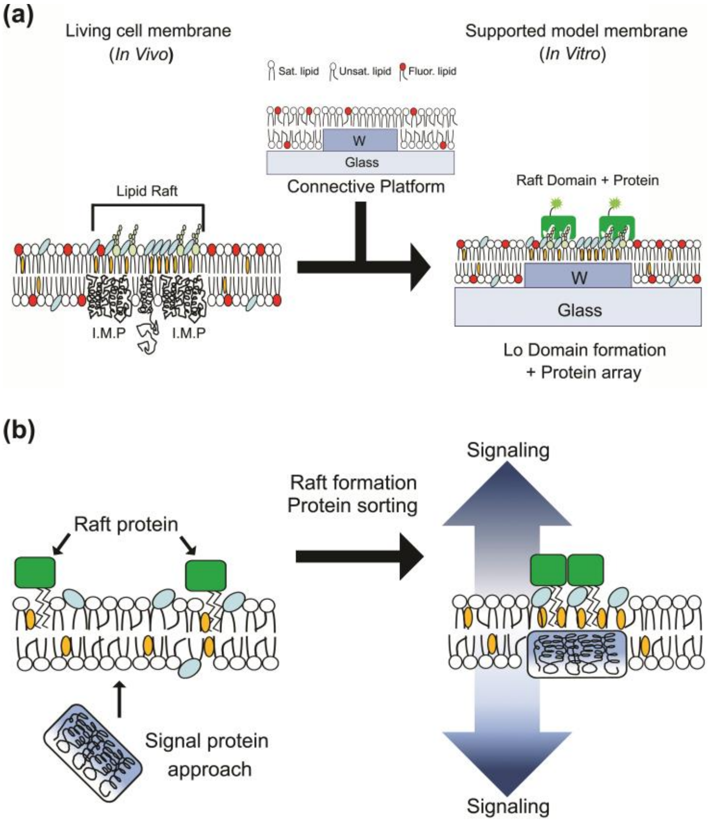

Figure 3.7 : A model for hydrophobicity-mediated lipid raft formation. (a) Possibility of mimicking the Integral monotopic protein (I.M.P) on the living cell membrane (left; in vivo) by reconstituting connective model membrane (middle, in vitro) used for protein arrays for raft proteins (right, *in vitro*). (b)

Plausible mechanism of raft formation for signal transduction which occurs when a signaling molecule activates a cell surface reorganization. The I.M.P plays a signal molecule by approaching and involved in the one leaflet of membrane. Sequential reorganization of membrane components, e.g. signal lipids and raft proteins, result in raft formation

Materials & methods

Fabrication of PDMS mold stamp. Before coating the photoresist, the glass substrate was immerged in acetone for more than 30min followed by in deionized (DI) water for 10 min. Whole cleaning process were performed in the standard ultra-sonicator at room temperature. After blowing with N2 gun, standard negative photoresist (SU-8 2050, MICROCHEM) was spun onto the glass substrate according to the vendor’s instructions. The coated glass was aligned and exposed through a photo-mask using a mask aligner (MA-6, EVG). After exposure process, SU-8 patterning process was performed giving the film thickness of 50 μm. The elastomeric material, Sylgard 184 silicone elastomer (Dow Corning Corp.) mixed with curing agent in a 10:1 ratio, was poured onto the mold and subsequently cured for more than 3h at 80 ℃.

Formation of SLBs and an imaging method. The phospholipids, used as a base for the formation of the supported LMs, were 1,2-dioleoyl-sn-glycero-3-phoph-ocholine (DOPC). For imaging the supported LM, a negatively charged lipids labeled with red fluorescent dyes, texas red 1,2-dihexadecanoyl-sn-glycero-3-phosp-hoethanola-mine (TR-DHPE, Molecular Probes, Eugene, Oregon) were mixed with DOPC at 1 mol%. The cholesterol, and two kind of fluorescence NBD labeled at head and tail group of cholesterol, 5-cholesten-3ß-ol 6-[(7-nitro-2-1,3-benzoxadiazol-4-yl)amino] caproate (NBD labeled at Head group) and 25-[N-[(7-nitro-2-1,3-benzoxadiazol-4-yl)methyl]amino]-27-norcholesterol (NBD-labeled at tail group), N-[12-[(7-nitro-2-1,3-benzoxadiazol-4-yl)amino]dodecanoyl]-sphingosine-1-phosphocholine (NBD-SPM; NBD labeled at tail group of SPM), 1-palmitoyl-2-{12-[(7-nitro-2-1,3-benzoxadiazol-4-yl)amino]dodecanoyl}-*sn*-glycero-3-phosphoserine (NBD-PS; labeled at tail group of PS), 1-palmitoyl-

2-{12-[(7-nitro-2-1,3-benzoxadiazol-4-yl)amino]dodecanoyl}-*sn*-glycero-3-phosphoethanolamine (NBD-PE; NBD labeled at tail group of PE), and *ganglioside* (GM_1; brain, ovine-ammonium salt) were purchase from from Avanti Polar Lipids (Birmingham, Alabama). These lipids mixed according to their purpose.

Table 3. The compositional properties of each membrane mixture

Membrane types	Membrane composition
M1	33% SPM, 33% NBD-CHOL, 32% DOPC, 1% GM_1 and 1% TR-DHPE
M2	33% SPM, 33% NBD-CHOL, 33% DOPC and 1% GM_1
M3	33% NBD-SPM, 65% DOPC, 1% GM_1 and 1% TR-DHPE
M4	33% NBD-CHOL, 65% DOPC, 1% GM_1 and 1% TR-DHPE
M5	33% NBD-PE (or NBD-PS), 65% DOPC, 1% GM_1 and 1% TR-DHPE
M6	33% SPM, 33% CHOL, 32% DOPC, 1% GM_1, and 1% TR-DHPE

All lipid mixtures were dissolved in chloroform. The rapid solvent exchange method[107] was employed to evaporate chloroform and to hydrate with Tris buffer (100 mM NaCl and 10 mM Tris at pH. 8.0) simultaneously. Small unilamellar vesicles (SUVs) were produced by extruding 20 times through a 50 nm filter. The residual SUVs remained in the tris buffer solution were removed with the DI water after the supported LM was formed after the substrate was exposed to the SUVs solution for 5 min The Texas red lipids were monitored using an epifluorescence microscopy (Eclipse E600-POL, Nikon). Whole processes were performed in room temperature

Preparation of S-PDMS pattern. In order to prepare a glass substrate having hydrophilic surface property, it is immersed in piranha solution (3:1 (v/v) H_2SO_4:H_2O_2) at 120 ℃ for more than 10 min followed by ultra-sonication in DI water for 10 min. The PDMS mold mentioned above is placed on the cleaned glass. The contacted PDMS mold and glass are heated at 200 ℃ for 3 min using standard hot plate in order to make distinct S-PDMS transfer from PDMS mold. After heating, the PDMS mold is gently removed from the hydroxylated glass.

Formation of CBSM membrane on the S-PDMS surface. Schematic illustration of fabrication process for CBSM (**Figure 3.8**) where patterned PDMS molds were used for reconstituting lipid bilayer-monolayer structures with single vesicle rupture process. The glass was piranha cleaned to giving hydrophilic surface by formation of hydroxyl (-OH) group on it. Selective stamping was achieved with photolithographic patterned master. The pattern consisted of 50 μm x 50 μm square areas standing out 50 μm from PDMS stamp were contacted with hydroxylated glass (**Figure 3.8a**) and subsequent peeling process (**Figure 3.8b**) gives a selective square patterning of S- PDMS on the glass. Note that the S-PDMS, residual low-molecular-weight oligomers transferred from the PDMS mold, alters the surface property from hydrophilic to hydrophobic. In other word, the regions for lipid bilayer formation changed into that for lipid monolayer. In this way, we can reconstitute self-assembly CBSM with a single step of vesicle exposure to S-PDMS patterned glass

(**Figure 3.8(c)** and **(d)**).The phospholipids, used as a base for the formation of the CBSM cell, were 1,2-dioleoyl-sn-glycero-3-phoph-ocholine (DOPC, White headgroup in **Figure 3.8(d)**) and negatively charged lipids labeled with red fluorescent dyes, texas red 1,2-dihexadecanoyl-sn-glycero-3-phosp-hoethanola-mine (TXRD-DHPE, Red head group in **Figure 3.8(d)**) mixed with the ratio of 99:1

Formation of OTS SAM (S-OTS) on the prepared PDMS. To make the *octadecyltri-chlorosilane* (OTS) on the PDMS surfaces, we dipped PDMS mold into a toluene-based-10 mM OTS solution for more than 5 min at room temperature followed by immerging at toluene solution (100%) for washing for 10 min. After blowing with N2 gun, Immerged OTS SAM coated PDMS is dried on the hot plate for more than 5 min to evaporate residual toluene solvent absorbed in the PDMS mold [108].

Application of the electric field. Pt wire was used as an electrode. 45 V/cm direct current field was applied through the standard power supply. The length of each electrode on the opposite side was 1.5 cm. The measurements of the fluorescence intensity molecules in supported lipid membranes were carried out using an image analyzing program of Image J (National Institute of Mental Health, USA).

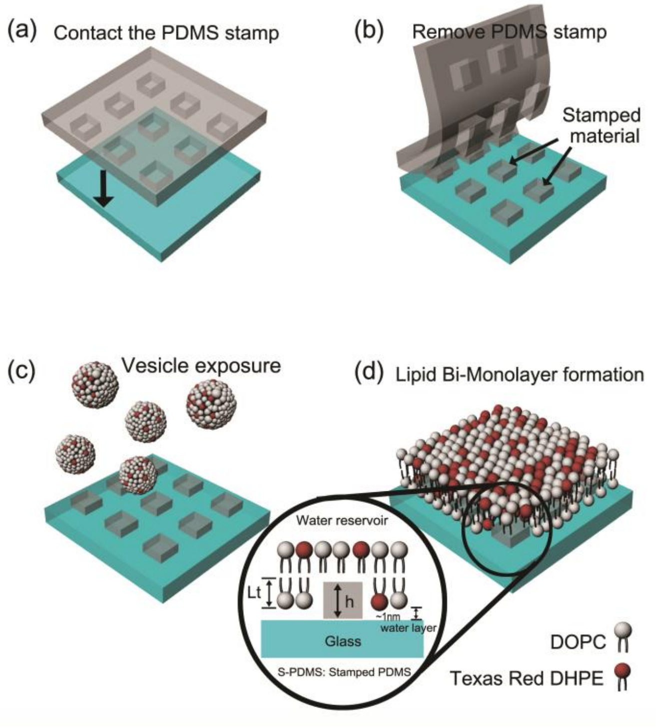

Figure 3.8 : Reconstitution process for CBSM. (a) Glass cleaning with Piranha solution followed by contacting with periodically patterned PDMS mold at 200℃ for 3 min. (b) PDMS mold removal. The S-PDMS residues on 50 μm x 50 μm square areas standing out 50 μm from PDMS stamp transferred into the cleaned glass. c,d) Vesicle exposure to S-PDMS patterned glass (c) and self-assembly formation of CBSM (d). Steps c,d are performed in deionized (DI) water. Crossectional schematic illustration of CBMS is shown in inset. The geometrical parameters of CBSM cell are the thickness of the lipid layer (L_t) and that of S-PDMS molecules (h). The phospholipids, used as a base for the formation of the CBSM cell, were DOPC (White head group) and TXRD-DHPE (Red head group) mixed with the ratio of 99:1.

Surface tension calculations. Young's equation ($\gamma_{lv}\cos\theta = \gamma_{sv} - \gamma_{sl}$) describes the thermo-dynamic equilibrium of the three surface tensions related to a droplet of liquid on a surface : γ_{sv} γ_{sl} and γ_{lv}, where the subscripts sv, sl, and lv refer to the solid-vapor, solid-liquid, and liquid-vapor interfaces, respectively. Only two of the parameters in Young's equation (γ_{lv} and θ) are easily measured or obtained, which leaves on equation and two unknowns (γ_{sv} and γ_{sl}). To more easily determine solid-vapor surface tension (γ_{sv}), an equation of state of interfacial tensions has been developed:

$$\gamma_{\mathrm{sl}} = \gamma_{\mathrm{lv}} + \gamma_{\mathrm{sv}} - 2\sqrt{\gamma_{\mathrm{lv}}\gamma_{\mathrm{sv}}}e^{-\beta(\gamma_{\mathrm{lv}}-\gamma_{\mathrm{lv}})^2} \qquad (1)$$

When this equation is combined with Young's equation, the following equation is obtained:

$$\cos\theta = -1 + 2\sqrt{\frac{\gamma_{\mathrm{sv}}}{\gamma_{\mathrm{lv}}}}e^{-\beta(\gamma_{\mathrm{lv}}-\gamma_{\mathrm{sv}})^2} \qquad (2)$$

Hence, if γ_{lv}, θ, and empirically derived parameter β are known, then γ_{sv} is also known. γ_{sv} was determined using a Microsoft excel that we wrote employing values of 0.0001247 $(\mathrm{mJ/m^2})^{-2}$ for β and 72.8 $\mathrm{mJ/m^2}$ for γ_{lv} of water.

Chapter 4. Intermolecular Behavior of Raft Components for Raft Domain Formation

4.1 Introduction

The cellular membrane coordinates diverse lipids together with a large family of proteins through the molecule transportations and reaction cascade in the form of membrane heterogeneity and compartmentalization. Especially, sterol– and sphingolipid-enriched domains, called rafts [26], attracted enormous interest since they are believed to deeply related to pathogenesis of incurable diseases (e.g. *Alzheimer*'s, *Parkinson*'s, *prion*, cardiovascular disease, systemic lupus erythematosus and *HIV* [39]) and physiological consequences in processes such as endo/exocytosis [28], cell deformation [29], cell apoptosis [30], membrane trafficking [31], and domain organization [27]. Despite the significant roles in solving unconquered human diseases, former studies established the information only to find the compositions, size, and physical properties of lipid raft domains. This might come from that the research of 'lipid rafts' was began from the discovery of the detergent-insoluble raft domains [25]. Thus, research trend has been forced to investigate relationship between raft domains and physiological processes and their functions as pathogenesis [27-31]. Moreover, intrinsic characters of nano-sized assembly [109] and their fluidic nature within lipid membrane make it difficult to investigate and manipulate. A series of hypothetical organized models have been investigated [110] to understand the intermolecular behavior between raft components. Nevertheless, fundamental concept about generating principles, governing factors, and their intermolecular behavior between raft constituents which is critical for forming the raft domains, are relatively lack of definitions and has not been demonstrated experimentally so far.

4.2 Models of Raft Formation

Here, we assume the plausible hypotheses of generating principle of raft domains as shown in **Figure 4.1**. Lipid raft domain could be the assembly of ‘raft-unit’ which means the combinations of sphingomyelin (SPM; depicted in red) and cholesterol (CHOL; depicted in blue) molecules as shown in left of **Figure 4.1**. Nano-scaled ‘raft unit’ aggregates into spatial region of cell membrane and result in highly packed and thicker [35] domain than surrounding phospholipids. The combinatorial way of two constituents could be categorized into two fashions. First of all, randomly floating individual raft-units could coalesce at spatial regions and successive growth of this assembly result in the Lo domain within the membrane. Author designates this mechanistic generating principle as ‘**Random Fashion**’ as shown in **Figure** 4.1**.** Secondly, ‘**Prescribed Fashion**’ could be another plausible mechanism of generating the Lo domains as shown in **Figure 4.1b**. Living cell may prescribe the specific molecule-enrich domains at spatial position as the programmed schedules for cell life. Consecutive intercalation of counter-molecule into preformed specific molecule-enrich domains could be another generating mechanism for densely packed raft aggregates. For examples, the individual SPM molecule could intercalate into the CHOL-rich regions (**Figure 4.1b(i)**) and opposite situation could happen. That is, individual CHOL molecules diffuse rapidly intercalate into the SPM rich regions, also called as SPM clusters, as shown in **Figure** 4.1**b(ii)**. Actually, the CHOLs tend to aggregate into cluster at CHOL to phospholipid mole ratios in excess of 0.3 [111] and forms separate domains [112, 113] at ratios in excess of 1 (i.e.,

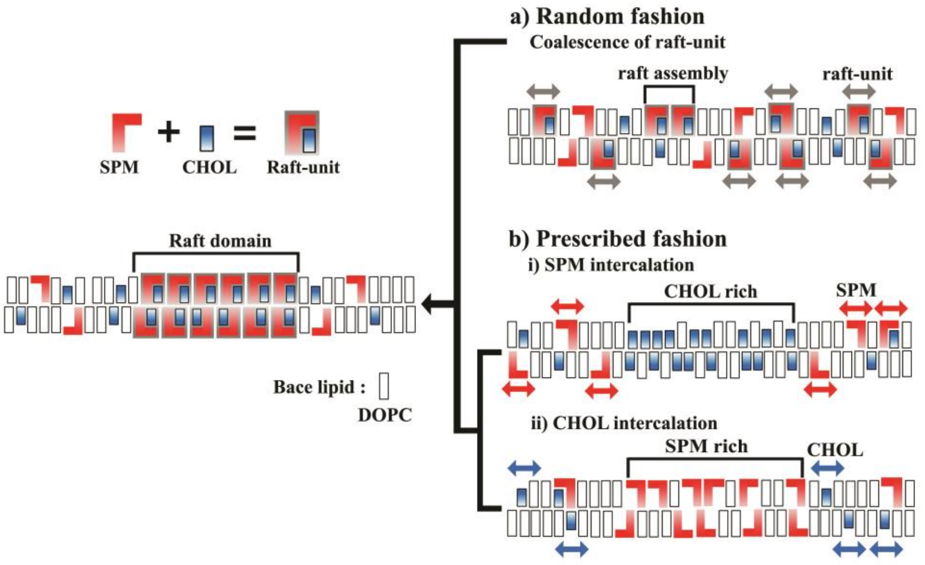

Figure 4.1 : hypothetical scenarios of generating principle of raft domains. The combinatorial way of two constituents could be categorized into two fashions. (a) Random fashion; the coalescence of randomly floating individual raft-units and successive growth into raft domains. (b) Prescribed Fashion; intercalation of a molecules into counterpart molecule-enrich regions at spatial position. (b.i) The SPMs intercalate into CHOL-rich region and (b.ii) the CHOL's intercalations into SPM-rich regions.

50 mol% sterol) [114] by forming of CHOL-rich domains contributing both physiologic and pathologic cellular process [115]. As another programed domains, the evidence of SPM-rich domain formation in the absence of CHOL also has been found due to hydrogen bonds between their headgroups [116]. The cohesive intermolecular forces between SPMs and CHOLs, derived from hydrogen bonding between the 3-OH group of CHOL and the SPMs [117], lead intermolecular packing surrounded by unsaturated PC molecules [118]. Therefore, our hypotheses of generating domains with

‘**prescribed fashion**’ are not ridiculous, but probable scenarios for raft compartmentalization. On the basis of the hypothesis models for understanding principles behind the dynamics of intermolecular behaviors in rafts formations, mimetic systems for specific molecule-rich domains is the basic essentials for investigating the hypothesis of ‘**prescribed fashion**’. Moreover, successive lateral diffuse of counter-molecule which would intercalate into preformed specific molecule-enrich domains is a significant requirement. Actually, the SPM and CHOL molecules inherently prefer to locate at outer-leaflet of plasma membrane [110, 119] showing compositional asymmetry between opposing lipid monolayers. Therefore, practical reconstruction maintaining the compositional heterogeneity and compartmentalization of raft components in lateral and vertical would be desirable. To meet the conditions, we present heterogeneous binary membrane which keeps fluid and continuous properties on supported lipid bilayers membrane (SLBM) by using the dry PDMS stamping method [88, 102]. This method provides platforms not only by allowing mixing of distinct lipid membrane only at outer-leaflet of SLBM, but by forcing them to meet at the boundary that would help to understand the formative mechanism of the raft domain. Our manipulation of raft domains is expected to play a crucial roles for not only studying the fundamental biophysics, but also opening an opportunities in medical science.

4.3 Reconstruction of Heterogeneous Membrane

Surface patterning of bio-molecules in aqueous environment has been established to define the physicochemical and biological functions of cellular constituents in variety field such as proteomics [120], genomics [121], drug screening [122] and lipidomics [123]. Among them, patterning methods of membrane constituents [4, 124, 125], particularly strategies for coalescence into raft domains [40, 52], attract great attention due to their roles in varies functions on cell life [27-30]. Thus, directive engineering of heterogeneous constituents into binary pattern is essential for investigating our hypothetic models into Lo domains. Since raft components are known to aggregate at outer-leaflet of bilayer architecture in cellular membrane, it would be desirable if we phase-separate Lo domains at the outer-leaflet of membrane *in vitro* for biomimetic purpose. Here, we present a microfluidic based membrane arrays which enable mixing of heterogeneous raft components at the outer-leaflet of membrane system keeping connectivity between monolayer (**M**) and bilayer (**B**) morphologies. The PDMS mold plays bifunctional material. Firstly, it guides the vesicle along the channels to form the lipid bilayer structure at restricted regions as shown in **Figure** 4.1**a**. Secondly, it also works as a stamp to modify the chemical properties of PDMS-contacted regions from hydrophilic to hydrophobic which is proper for **M** morphologies by transferring residual-PDMS (R-PDMS; depicted in dark gray at **Figure 4.1a**) [87, 88, 102, 103] as well.

The vesicles composed of green fluorescent dyes, *4-(4-(didecylamino)styryl)-N-methylpyridiniumiodide* (D291) and 1,2-dioleoyl-sn-glycero-3-phoph-ocholine (DOPC) at the molecular ratio of 1:99. Author already describes how the surface energy of R-PDMS transferred glass can be modified to find surface hydrophobicity at which reconstitutions of supported lipid monolayer at previous papers [89, 126]. The fabrication process of R-PDMS transferred glass was explained at **Methods** in detail. Briefly, before the contact with dry PDMS channel, a glass substrate was first cleaned with a solution of piranha. The PDMS preferentially transfers onto more hydrophilic surfaces due to the hydrolysis reaction of PDMS material with hydroxyl (-OH) group on glass [87, 88]. Piranha cleaned glass was contacted to PDMS mold and subsequent

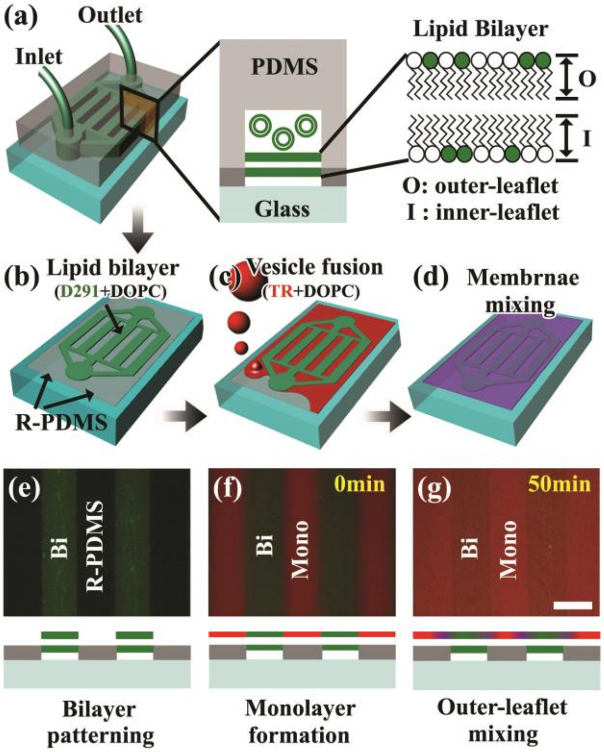

Figure 4.2 : microfluidic based heterogeneous membrane arrays. (a) Representative schematic illustration of bilayer membrane showing opposing two monolayer, outer-leaflet (O) and inner-leaflet (I) by injecting vesicle mixture (D291:DOPC=1:99). (b) Detaching the PDMS mold leaving residual-PDMS (R-PDMS) on mold contacted regions. Standing bilayer membranes are surrounded by R-PDMS barriers. (c) The backfilling of secondary vesicle mixture (TR:DOPC=1:99) on R-PDMS regions representative monolayer architecture. (d) Membrane mixing across the membrane only at the O-layer while molecules at I-layer displaying confined diffusion. (e-f) Microscopic pictures (top) and schematic illustrations (bottom) of membrane configuration along the cross-sectional area at each step. Scale bar, 100 μm.

exposure to hotplate at 200℃ for 3 min. Author have found that temperature can vary the surface hydrophobicity at previous paper [89]. Author uses micro channel that 100 μm periodically apart. That is to say, width of **B** region and **M** regions are identical at the value of 100 μm, respectively. Through the vesicle rupture process, the channel-guided bilayer membrane are achieved showing opposing two monolayer, outer-leaflet (O) and inner-leaflet (I), as shown in **Figure 4.2a**. Patterned bilayer membrane surrounded by R-PDMS region is obtained as shown in **Figure 4.2b**. Microscopic picture (top) and schematic illustration (bottom) of membrane configuration along the cross-sectional area are shown in **Figure 4.2e**. As next step, the voids can be refilled by fusion of secondary lipid vesicles (**Figure 4.2c**) composed of labeled with red fluorescent dyes, TR and DOPC at the molecular ratio of 1:99. Fluorescence data show the existence of distinct bilayer (D291+DOPC; green) and monolayer (TR+DOPC; red) membranes without any disruptions as depicted in **Figure 4.2f**. Membrane mixing of D291 (green) and TR (red) is represented by color of ‘purple’ as shown in **Figure 4.2d**. Continuous and consequent membrane mixing is demonstrated by fluorescent micrograph of the distinct two regions taken after 50 min (**Figure 4.2g)**.

4.3.1 Membrane Mixing

In order to verify the mixing process occurs only at the outer-leaflet of membrane, diffusive characters of each membrane (green for **Bi**, red for **Mono**) was represented (**Figure 4.3**). In these experiments, we use PDMS pattern consisted of 100 μm width walls at the intervals of 150 μm. The green membrane (width of 150 μm) expressed through the microfluidic channel, and consequent backfilling of red membrane (width of 100 μm) were performed. Thus, the D291 starts to move from **B** to **M** (**Figure 4.3a.i**) while the TR moves from **M** to **B** (**Figure 4.3a(ii)**). The data demonstrate the mixing properties of both dye-labeled molecules without any ‘lipid-free’ gap [82, 83]. Interestingly, distributive character of D291 molecules are differs from that of TR during the sufficient mixing time (t = 3days). Time-lapse reorganizations show that TR molecules located at the outer-leaflet of membrane move freely both on bilayer and monolayer regions result in uniform fluorescent intensity, while the D291 molecules don’t shown uniform distribution as shown in **Figure 4.3a**. The presence of R-PDMS region prevents D291 molecules that positioned at inner leaflet of bilayer from mixing while the identical molecules locating on outer-leaflet can diffuse without any obstacles. This confirms the mixing of two kinds of dye-labeled molecules occurs only at the outer-leaflet of membrane shown at our previous paper [89]. Author also verified the membrane fluidity through the fluorescence recovery after photo-bleaching (FRAP) studies [4] with the 1 mol% TR molecules included membrane at 99 mol% DOPC lipids both on bilayer and monolayer regions showing distinct intensity at the ratio of ~1.74 (**B**/**M**) which is similar with Howland et al [83]. Our FRAP studies indeed confirm that fluidity of the binary membrane are completely preserved in the bilayer region (**Figure 4.3b.i**), the diffusion coefficient of 1.06 ± 0.1 $\mu m^2/s$) and in monolayer region (**Figure 4.3b.ii**, the diffusion coefficient of 0.375 ± 0.05 $\mu m^2/s$) at room temperature (*RT*), respectively.

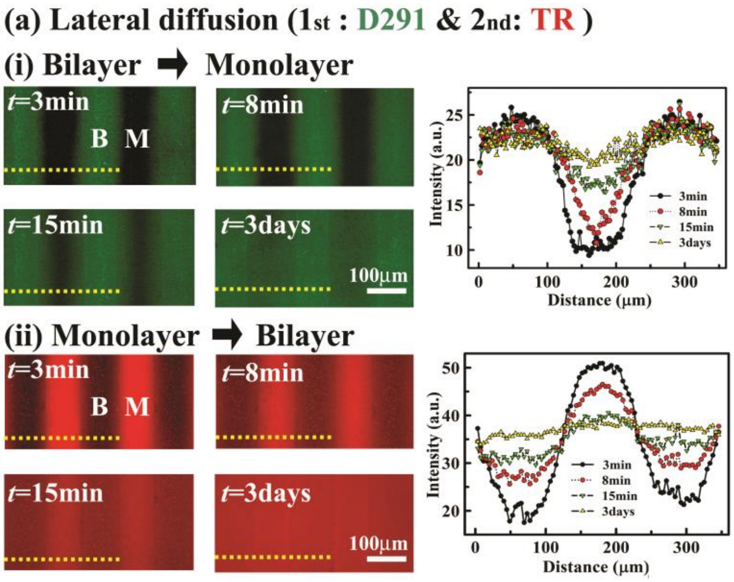

(a) Lateral diffusion (1st : D291 & 2nd: TR)

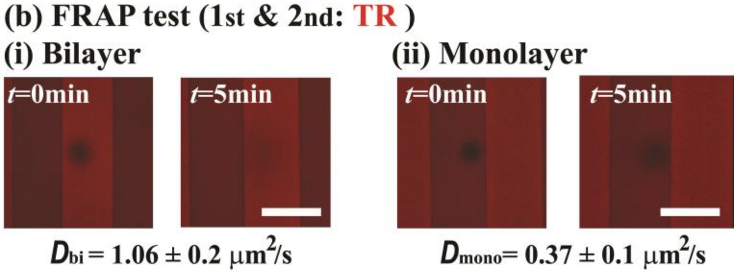

(b) FRAP test (1st & 2nd: TR)

Figure 4.3 : Lateral diffusion across the distinct membrane. (a) Time-lapse diffusion characters of the D291 (a.i) and the TR (a.ii) involved membrane and corresponding fluorescent profiles along the yellow dotted lines at each time value. The micrographs show that D291-involved membrane (D291:DOPC=1:99) were firstly expressed in the form of bilayer and consequently move to monolayer while secondary expressed TR-involved membrane (TR:DOPC=1:99) diffuse from monolayer to bilayer. (b) The FRAP test in distinct membrane morphology representing diffusion coefficients of 1.06±0.1 $\mu m^2/s$ for bilayer (b.i) and 0.375 ± 0.05 $\mu m^2/s$ (b.ii) for monolayer at *RT*, respectively. Note that the vesicle mixture (TR:DOPC=1:99) on both morphology is identical. Scale bar, 100 μm.

4.3.2 Lateral Mobility of Signal Lipids

On the basis of the outcomes made above, diffusive characters of two key molecules, SPMs and CHOLs, were implemented on bilayer and monolayer structure, respectively. Prior to exam which hypothetic model is probable, lateral mobility of key molecules on the solid support both on bilayer and monolayer membrane are critical. Our connective binary supported membrane (CBSM) [126] would be useless if no lateral mobility of SPMs and CHOLs are detected. Furthermore, in order to verify '**Prescribed Fashion**' which is one of plausible mechanism of generating the Lo domains as shown in **Figure 4.1b**, CHOLs-rich (or SPMs-rich) region are prerequisites for our system. It is well known that below the transition temperature (T_t), lipid matrix contains clusters of closely packed molecules [127, 128]. Author performed FRAP test at *RT* that is below the T_t of SPMs (T_t = 40℃) [127] and that of CHOLs (T_t = 41℃) [128], assuming the membrane below the $\boldsymbol{T_t}$ of two signal molecules would contain clusters of closely packed domains. For example, SPM-rich membrane means the cluster of SPMs are abundant at *RT*. Thus, interpreting the distributive properties of dye-labeled SPMs (NBD-SPMs) and CHOLs (NBD-CHOLs) could give the information of diffusive characters within SPM-rich and CHOL-rich membrane, respectively. The molecular structure of NBD-labeled SPMs and CHOLs are shown in **Figure 4.4a** and **b**, respectively.

First of all, the vesicles mixture (33% NBD-SPMs, 66% DOPC, 1 % *ganglioside* GM1) were exposed to PDMS stamped supports as shown in **Figure 4.4a**. Author observed that the diffusion coefficient of NBD-SPMs on the monolayer region ($D_{\text{SPM-MONO}}$= 1.75 ± 0.5 μm^2/s) and on **B** region ($D_{\text{SPM-BI}}$= 2.66 ± 0.75 μm^2/s) at *RT*, respectively (**Figure 4.4a**). FRAP measurements reveal that both bilayer and monolayer are independently fluid exhibiting probe diffusion coefficient of (~1-3 μm^2/s) in excellent agreement with previous papers [129, 130]. Secondly, the mixture membrane (33% NBD-CHOLs, 66% DOPC, 1 %, GM_1) shows similar mobile characters on both regions. Actually, the CHOLs tend to aggregate into cluster at cholesterol to phospholipid mole ratios in excess of 0.3 [111] and forms separate domains [112, 113] at ratios in excess of 1 (*i.e.*, 50 mol% sterol) [114] by forming of CHOL-rich domains contributing both physiologic and pathologic cellular process [115]. Author needs to prepare the vesicles that contain cholesterols over 50% for separated domains. However, it is inherently impossible to form supported lipid membrane due to the non-rupture process of vesicles. Negative intrinsic curvature of CHOLs prohibits vesicle to rupture on supports if it contains CHOLs over 40% of vesicle mixture [131].

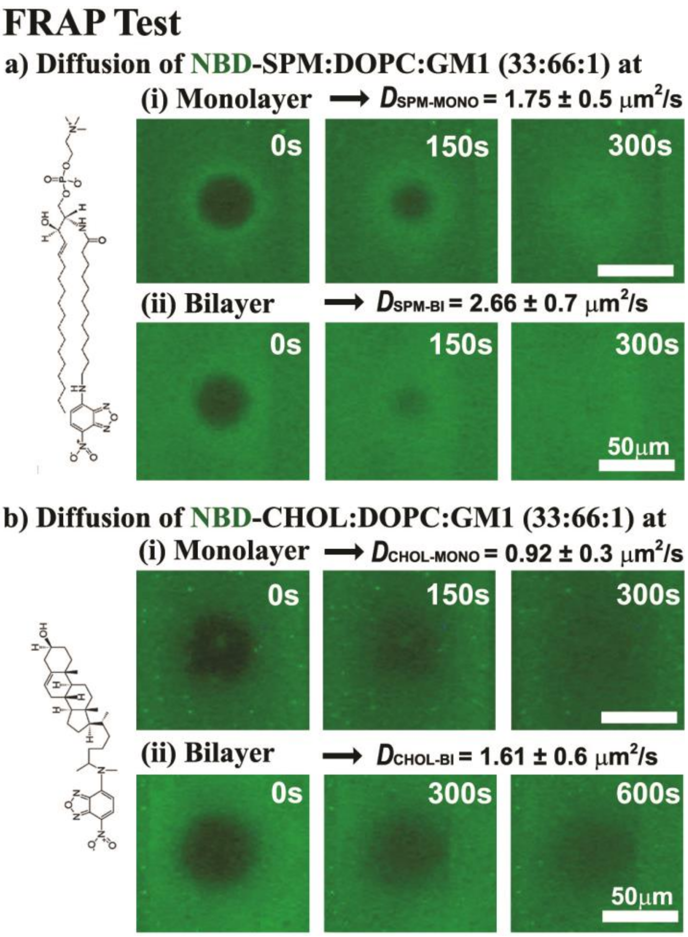

Figure 4.4 : Diffusive characters of SPMs and CHOLs on our CBSM. Molecular structures and diffusion properties of dye-labeled SPM (33% NBD-SPMs, 66% DOPC, 1 % GM1) and dye-labeled CHOLs (33% NBD-CHOLs, 66% DOPC, 1 % GM1) involved membrane. (a) Diffusion coefficient of NBD-SPMs on the monolayer region (a.i; $D_{\text{SPM-MONO}}$= 1.75 ± 0.5 μm^2/s) and on bilayer region (a.ii; $D_{\text{SPM-BI}}$ = 2.66 ± 0.75 μm^2/s) at *RT*, respectively. (b) Diffusion coefficient of NBD-CHOLs on the monolayer region ($D_{\text{SPM-MONO}}$= 1.75 ± 0.5 μm^2/s) and on bilayer region ($D_{\text{SPM-BI}}$= 2.66 ± 0.75 μm^2/s) at *RT*. Scale bar, 50 μm.

Therefore, we use 33% of CHOLs were used for our system. The diffusion constant of NBD-CHOLs on the **M** region is value of $D_{\text{CHOL-MONO}}$= 0.92 ± 0.3 $\mu m^2/s$, while on the **B** region shows the value of $D_{\text{CHOL-BI}}$= 1.61 ± 0.6 $\mu m^2/s$, which also great accordance with the value of previous experiments [127, 128]. These data underscore the diffusivity of raft constituent lipids is mobile both on bilayer and monolayer region on the model membrane. Especially, mobility of both molecules on the **B** regions is more diffusive than on the **M** regions at the ratio of ~ 1.6 ($D_{\text{BI}}/D_{\text{MONO}}$) through sufficient data (n=20).

4.4 Interactive Behavior of Raft Components

4.4.1 Cholesterol Intercalation into Sphingomyelin-rich Domain

To test which hypothetic model among the ‘**Prescribed Fashion**’ is dominant, diffusive behavior of two raft constituents are implanted on our CBSM. Interactive behavior between two molecules, SPMs and CHOLs, might be monitored at the boundary of bilayer and monolayer region. This is because the TR molecules are strongly excluded in the course of nanorafts-coarsening process [40]. Therefore, the location of L_O domains are monitored through the distribution of the TR-DHPE, and this shows the intermolecular behavior between two raft components. The vesicles mixture (33% CHOLs, 65% DOPC, 1% GM1, and 1% TR) were injected to micro channels while PDMS mold contacted to the hydrophilic substrate as they form the membrane in bilayer structure. After detaching the mold in water, secondary mixture (33% SPMs, 65% DOPC, 1% GM1, and 1% TR) were consequently backfilled with generating the monolayer lipid film on the R-PDMS. Interestingly, the distribution of Lo domains generated at the boundary (t =

36*h*) decreases as it close toward SPM rich regions. This clearly means the fact that the raft formation is much faster at the boundaries and

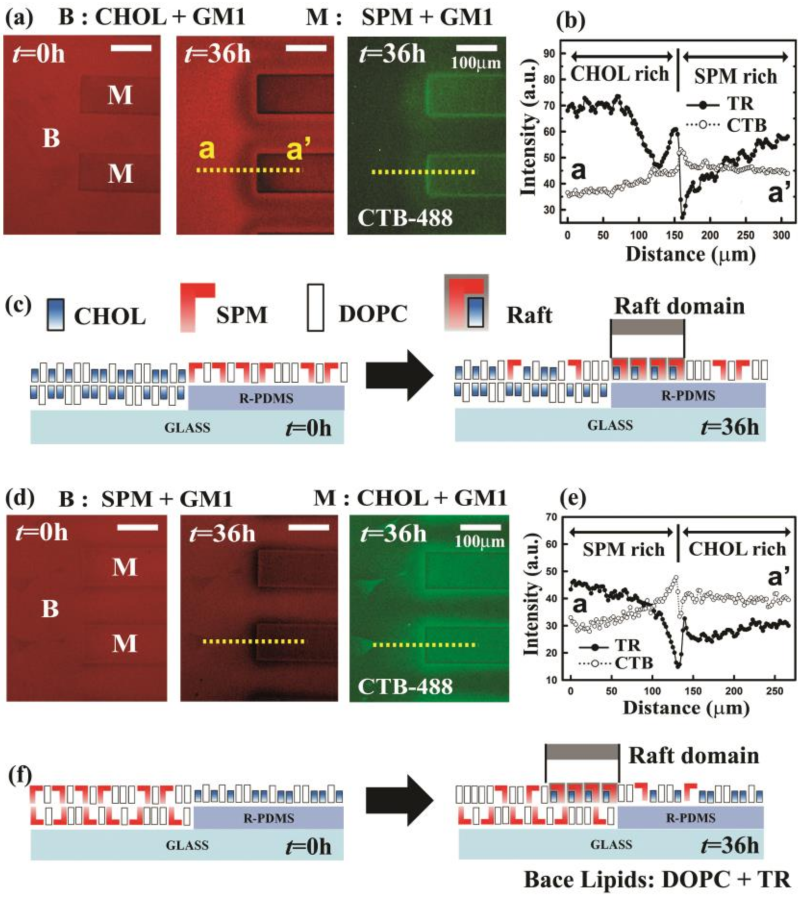

Figure 4.5 : the intermolecular behavior between two raft components. (a) Phase behavior by mixture between 1st membrane (33% CHOLs, 65% DOPC, 1% GM1, and 1% TR) and 2nd membrane (33% SPMs, 65% DOPC, 1% GM1, and 1% TR). Green dyed CTB (CTxB-488) were introduced at *t* = 36 *h*. (b)The fluorescent intensity profiles along the line a-a'(yellow dotted line) as function of distance. (c) Schematic illustrations of raft formation before (*t* = 0 *h*) and after (*t*=36*h*) membrane mixing across the membrane. (d) The fluorescent micrographs of distinct membrane before (*t* = 0 *h*) and after (*t* = 36 *h*) membrane mixing across the membrane and protein binding between CTB-GM1. (e) Fluorescent intensities of TR and CTxB-488 as function of distance and (f) Schematic illustrations of raft formation before (*t* = 0 *h*) and after (*t* = 36 *h*) membrane mixing across the membrane at *RT*. Note that the raft domains are formed at SPM-rich membrane. Scale bar, 50 µm.

generative ratio gradually decreases near the center of **M** regions (**Figure 4.5a**). The specific bindings of green dye-labeled cholera toxin unit B (CTxB-488) to glycolipid receptor $GM_{1,}$ confirm that the black domains indicate the raft domains. **Figure 4.5b** shows the distributions of TR and CTxB-488 across boundary. The direct comparison of corresponding cross-sectional intensities along the line a-a' (yellow dotted) as function of distance supports our conclusion (**Figure 4.5b**). Abrupt increase (for TR) and decrease (for CTB) of fluorescent intensities at the boundary between bilayer and monolayer are monitored. This phenomenon could be interpreted with the result that the molecule at B region intercalates into M region. That is, CHOLs intercalate into SPM rich regions as depicted in **Figure 4.5c.** Accumulation of raft domains at the boundary is observed through the time-lapse fluorescence microscopy *in vitro*. The diametrical experiments were performed to convince our interpretation. The vesicles mixture (33% SPMs, 65% DOPC, 1% GM1, and 1% TR) were prepared, followed by backfilling the secondary mixture (33% CHOLs, 65% DOPC, 1% GM1, and 1% TR). Lo domains are expectably observed at the boundary between bilayer and monolayer regions. However, the distributive formation of Lo domains is obviously opposite as shown in **Figure 4.5d**. The distribution of Lo domains generated at the boundary (at $t = 36h$) also decreases as it close toward SPM rich regions. The CTxB-488 binding to Lo domains confirms that Lo domains are generated at SPM rich regions. The cross-sectional profiles (**Figure 4.5e**) obviously support the intercalation of CHOLs into SPMs as shown in **Figure 4.5f**.

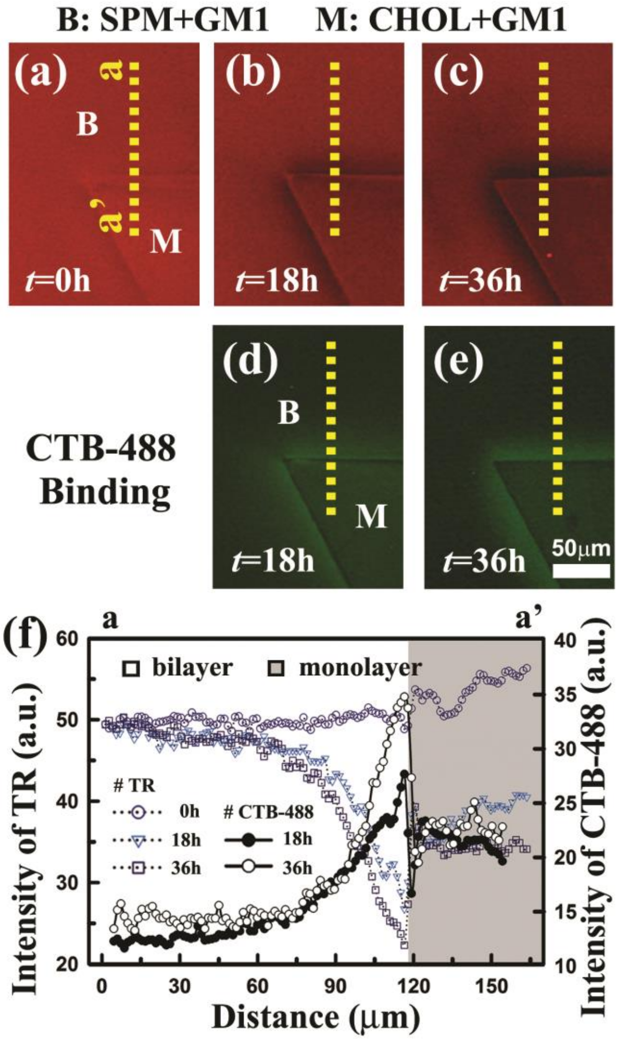

Figure 4.6 : Growth of lipid raft and protein binding. (a-c)Time-lapse phase separation by formation of raft domains at the boundary and (d,e) protein binding. The vesicles mixture (33% SPMs, 65% DOPC, 1% GM1, and 1% TR) were prepared, followed by backfilling the secondary mixture (33% CHOLs, 65% DOPC, 1% GM1, and 1% TR). The growth of lipid raft was observed by direct comparison of micrographs at *t*=18*h* (b) and *t*=36*h* (c). Diffusive character of CTxB-488 confirms that the raft domains accumulate at the boundary of distinct membrane and represented in graph at (f). Scale bar, 50 μm.

4.4.2 ‘Prescribed fashion’ vs ‘Random fashion’

As another plausible formative mechanism, ‘**Random Fashion**’ was implemented. Author already designates that assembly of floating individual raft-units at random spots with performing a role as building blocks of the Lo domain. Author prepares the raft mixture (32.5% CHOLs, 32.5% SPMs, 33% DOPC, 1% GM1, and 1% TR) which contains both of SPMs and CHOLs to form a set building block, designated as raft-unit that signifies the compaction of single SPM and CHOL. Previous studies [28, 35, 52] have observed the conventional isolated and island-type raft (ITR) patterns on the planar substrate, postulating that raft-unit aggregate at random spot due to uncertain reasons. Author already demonstrates the plausible scenario, **‘Prescribed Fashion’**, which comes from the intercalation of CHOL into SPM clusters as mentioned above. To test whether which formative scenario for raft domains is dominant, we prepare the heterogeneous membrane that composed of SPM enrich membrane and ‘Raft-unit’ rich membrane. First of all, we introduce SPM mixture (33% SPMs, 65% DOPC, 1% GM1, and 1% TR) to microfluidic channel for SPM enrich membrane (**Figure 4.7a**). After consequent backfilling of R-PDMS region with raft mixture for 36*h*, they show expected phase separation (**Figure 4.7b.i**) at the SPM membrane-sided boundary by CHOL intercalation as mentioned above. The CHOL molecules included in raft mixture (*t* = 0 *h*; inset) move to SPM rich membrane and result in black domains by expelling the TR molecules at the boundary **Figure 4.7b.ii**). Interestingly, ITR patterns in random fashion are observed at SPM rich membrane **(Figure 4.7b.iii**). The specific bindings of CTxB-488 confirm that distinguishable black patterns are Lo domains (**Figure 4.7b iv-vi**). These ITR patterns were not observed at all through the experiments for '**Prescribed fashion'** as separation occurs at the SPM membrane-sided boundary (e.ii & e.v) due to the intercalation of CHOLs from B to M region.

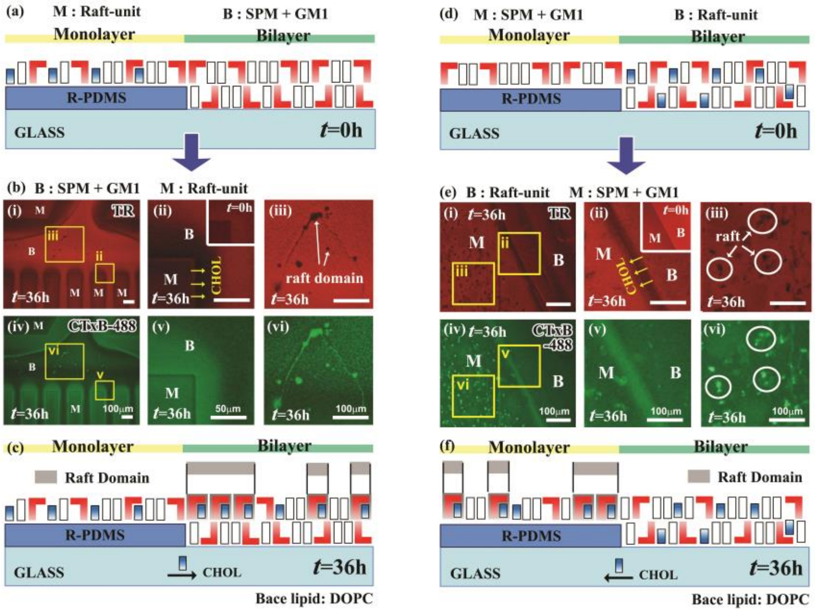

Figure 4.7 : (a) Schematic diagram of before (t = 0 h) mixing of distinct membrane that was prepared with the vesicles mixture (33% SPMs, 65% DOPC, 1% GM1, and 1% TR), followed by backfilling the secondary raft mixture (32.5% CHOLs, 32.5% SPMs, 33% DOPC, 1% GM1, and 1% TR). (b) Fluorescent Microscopic pictures of TR (top; i-iii) and CTxB-488 (bottom; iv-vi) after mixing membrane constituents (t = 36 h). Expected phase separation occurs at the SPM membrane-sided boundary (b.ii & b.v) due to the intercalation of CHOLs from M to B region. The phase behavior at t=0h was shown in inset. (b.iii & b.vi) Unexpected island-type raft (ITR) domains are observed at random location. (c) The schematic illustrations of two type of raft domains one at boundary and another at SPM-rich (=bilayer) membrane.

(d) Schematic diagram of membrane conformation by raft mixture (32.5% CHOLs, 32.5% SPMs, 33% DOPC, 1% GM1, and 1% TR), followed by backfilling the secondary SPM mixture (33% SPMs, 65% DOPC, 1% GM1, and 1% TR). (e) Microscopic graphs of TR (top; i-iii) and CTxB-488 (bottom; iv-vi) after mixing membrane constituents (*t* = 36 *h*). Expected phase The phase behavior at *t*=0*h* was shown in inset. (e.iii & e.vi) Random distribution of ITR domains observed in M region demonstrated by binding of CTxB-488. (f) Illustration of two type raft domains both on SPM-rich (=monolayer) membrane. Scale bar, 100 μm.

Shown in **Figure 4.5**, author interprets that these submicron scaled ITR domains comes from the assembly of building blocks which should be distinguished from CHOL intercalation directed domain formation at the boundary. The CHOL molecules located at R-PDMS regions (*t* = 0 *h*) move to SPM rich regions due to the osmotic pressure. The molecular ratio of CHOLs within distinct membrane makes them diffuse from monolayer to outer-leaflet of bilayer regions (*t* = 36 *h*) as shown in **Figure 4.7c**. Two type of raft domains were generated at different locations, one at boundary and another at SPM-rich (=bilayer) membrane. Author concludes former comes from ‘Prescribed Fashion’, and latter occurs due to ‘Random Fashion’. Our findings were verified by diametrical experiment with changing the order of lipid mixtures. As depicted in **Figure 4.7d,** raft mixture were expressed first, followed by backfilling of R-PDMS regions with SPM mixture. The fluorescent micrograph shows two distinct raft domains (**Figure 4.7e.i**). The SPM membrane-sided line-shaped rafts are the first one (**Figure 4.7e.ii**), and ITR domains at SPM rich membranes are next (**Figure 4.7e.iii**). Binding of CTxB-488 demonstrate that these black domains are raft aggregates (**Figure 4.7b iv-vi**). Since our CBSM system allows the diffusion of CHOLs from bilayer to monolayer, both of ITRs and raft domains at boundary are observed at monolayer region.

4.5 Discussion & Conclusion

To understand the role of rafts and derived physiological processes including the unconquered diseases, a characterization of dynamic behavior between raft components is essential. As an effort to reconstitute of raft domain, spatial manipulation of diffusive single rafts into Lo domains have been investigated in the basis of physicochemical and biological comprehensions both *in vivo* and *in vitro*. Previous studies **figure**d out that raft are composed of sphingolipids, sterols, and raft proteins. However, the intermolecular behavior between key constituents of raft domain has been remained to be obscure. In particular, no researches have answered the questions such as ‘how the raft components are packed?’ or ‘how the CHOL plays a role as glue for packing the sphingolipids for raft aggregates?’ The approach described here offers plausible scenarios of formative mechanism in raft domain followed by series of experimental results on the solid supports based on hypothetical organizing mechanisms. Author uses the CBSM system which also offers expression of distinct membranes and allows mixing membrane components at the boundary of monolayer and bilayer architectures. This systematical platform provides an opportunity to understand interactive behaviors of two key raft components. Through the experiment of the ‘**Prescribed Fashion**’, we found that intercalation of CHOLs into SPM enrich membrane is prerequisites for forming raft domains. The mixing behavior between the CHOL rich and SPM rich membrane provides information that generation of Lo domains requires intercalation of CHOLs into preformed SPM clusters. Since the rafts are thought to form by self-association of sphingolipids because of their long and saturated hydrocarbon tails [109], our data demonstrate the existing assumption for the first time that the voids between the frame supports, made of hydrocarbon chains caused by the rather bulky headgroups of sphingolipids, would be filled by cholesterols [132-134]. The CHOL molecules has known to essential for formation, the precise nature of their intermolecular behavior with sphingolipids has been unclear before our finding of CHOL intercalation to SPM enrich regions so far.

In this thesis, we could conjecture that raft aggregates and resultant domain formation could occur through two distinct fashions. The first one is the intercalation of CHOL into SPM clusters. The growth of raft domains toward the SPM enrich membrane elucidate the intercalative diffuse of CHOLs to SPM rich area and consecutive accumulation of raft unit and resultant raft domains. Secondly, the assembly of units of raft at random spot into micro scaled domains could be one another, as they play as building blocks of house. Author defines former as '**Prescribed fashion**', and later as '**Random Fashion**'. To **figure** out which fashion is dominant remains to our later work. However, our findings are expected to offer information how to prevent them to aggregates and help to take precautionary measures to avoid raft domain-induced disease such as Alzheimer's, Parkinson's, prion, cardiovascular disease, systemic lupus erythematosus and HIV [39]. Incorporation of different classes of biomaterial such as DNA, living cell, other signal proteins will lead more functional flexibility for studying cellular activities to understand not only signal process if it incorporated with raft proteins, but cellular communications which require mixing between heterogeneous membranes.

Materials & methods

Fabrication of PDMS mold stamp. Before coating the photoresist, the glass substrate was immerged in acetone for more than 30min followed by in deionized (DI) water for 10 min. Whole cleaning process were performed in the standard ultra-sonicator at room temperature. After blowing with N2 gun, standard negative photoresist (SU-8 2050, MICROCHEM) was spun onto the glass substrate according to the vendor’s instructions. The coated glass was aligned and exposed through a photo-mask using a mask aligner (MA-6, EVG). After exposure process, SU-8 patterning process was performed giving the film thickness of 50 μm. The elastomeric material, Sylgard 184 silicone elastomer (Dow Corning Corp.) mixed with curing agent in a 10:1 ratio, was poured onto the mold and subsequently cured for more than 3h at 80℃.

Formation of SLBs and an imaging method. The phospholipids, used as a base for the formation of the SLBs, were 1,2-dioleoyl-sn-glycero-3-phoph-ocholine (DOPC). For imaging the SLBs, a negatively charged lipids labeled with red fluorescent dyes, texas red 1,2-dihexadecanoyl-sn-glycero-3-phosp-hoethanola-mine (TR, Molecular Probes, Eugene, Oregon) and green flurescent dyes, 4-(4-(didecylamino)styryl)-N-methylpyridinium iodide (D291, Avanti Polar Lipids, Birmingham, Alabama) were mixed with DOPC at 1 mol%, repectively. The cholesterol, and two kind of fluorescence NBD labeled at head and tail group of cholesterol, 5-cholesten-3ß-ol 6-[(7-nitro-2-1,3-benzoxadiazol-4-yl)amino]caproate (NBD labeled at Head group) and 25-[N-[(7-nitro-2-1,3-benzoxadiazol-4-yl)methyl]amino]-27-norcholesterol (NBD-labeled at tail group), N-[12-[(7-nitro-2-1,3-benzoxadiazol-4-yl)amino]dodecanoyl]-sphingosine-1-phosphocholine (NBD-SPM; NBD labeled at tail group of SPM), and *ganglioside* (GM_1 ; brain, ovine-ammonium salt) were purchase from Avanti Polar Lipids (Birmingham, Alabama). These lipids mixed according to their purpose. All lipid mixtures were dissolved in chloroform. The rapid solvent exchange method [107] was employed to evaporate chloroform and to hydrate with Tris buffer (100 mM NaCl and 10 mM Tris at pH 8.0) simultaneously. Small unilamellar vesicles (SUVs) were produced by extruding 20 times through a 50 nm filter. The residual SUVs remained in the tris buffer solution were removed with the DI water after the SLBs was formed after the substrate was exposed to the SUVs solution for 5min The Texas red lipids were monitored using an epifluorescence microscopy (Eclipse E600-POL, Nikon). Whole processes were performed in room temperature.

Formation of binary supported membrane on the R-PDMS surface. The glass was piranha cleaned to giving hydrophilic surface by formation of hydroxyl (-OH) group on it. Selective stamping was achieved with photolithographic patterned PDMS mold. The pattern consisted micro channel that 100 μm periodically apart, standing out 50 μm from PDMS stamp were contacted with hydroxylated glass. Injection of first vesicle mixture along the micro channel result in bilayer membrane, and subsequent peeling process gives a selective patterning of bilayer membrane surrounded by R-PDMS regions. Note that the R-PDMS, residual low-molecular-weight oligomers transferred from the PDMS mold, alters the surface property from hydrophilic to hydrophobic. In other word, the regions for lipid bilayer formation changed into that for lipid monolayer. Secondary backfilling of R-PDMS regions with secondary mixture generate connective binary membrane which allows diffusive mixing between 1st and 2nd membrane.

Chapter 5. Kinetics of Raft Formation by Real-time Surface Plasmon Resonance

5.1 Introduction

Supported membranes on the solid, whether being fixed to the substrate or freely mobile separated from substrate by ultrathin water layer (~1 nm), and their combinations with surface-sensitive analytic techniques enable us to explore both the biological interplay of lock-and-key forces, *e.g.* receptor-ligand binding, and the adhesive behaviors between the cell components such as membrane-membrane [135], membrane–protein [136-138], membrane–DNA [139], and protein-protein [140]. Since fluid membrane where variety of lipids and membrane proteins are self-assembled is dynamic creature in bilayer architecture, the organization and compartmentalization of membrane constituents in the form of domains attracts great interest due to their crucial roles in the membrane-related biological activities including signaling **[38]**, cell deformation **[29]**, and membrane trafficking [44]. As an effort to reconstitute the domains *in vitro*, the supported lipid bilayer membrane (SLBM) has been utilized as robust biomimetic platforms to investigate the physicochemical properties of membrane compartmentalization into domain shape with assistant of surface-sensitive techniques such as secondary ion mass spectrometry [141], epifluorescence microscopy [11], and ellipsometry [142] etc. Recently, surface plasmon resonance (SPR) became one of the most powerful techniques for studying the microscopic interactions by facilitating the high-throughput analysis, label-free, and real-time monitoring. However, major stream of SPR research has been established to measure the intermolecular binding events between immobilized reactant, *e.g.* lipid, on a surface and second components in solution [143] due to the lack of platforms that remodel the cellular membrane where the membrane constituents float and diffuse freely within the membrane itself. Since diverse intermolecular interactions are launched from free rearrangement of membrane constituents within the mobile membranes, constructing ‘fluid’ membrane on the gold surface, which is critical for biomimetic assays for SPR surface, would offer the opportunity for practical biomimicry environments for monitoring reorganizing interactions within a patch of membrane. This will change the paradigm of SPR analysis by redefining of membrane from subsidiary molecules for mimicry ‘environment’ to target molecules to investigate to. In particular, The lipid rafts, massive combinations of sphingolipids (SPMs) and cholesterols (CHOLs) giving the liquid ordered (L_O) domains, are thought to function as sites for the selective assembly of proteins including HIV [144], prion [145], Alzheimer **[39]** disease-associated proteins in two dimensional distributions **[35, 78, 146]**. Even its vital roles in the membrane, however, the reconstitution of L_O domains at SLBM is a laborious task due to nanometer scale of ‘nanoraft’ assembly by nature and unpredictable expressions into aggregates at random position. Therefore, our systematic manipulation technique to phase-separate into L_O domains at predicted regions will help to uncover the interactive kinetics between raft components and consequent formation of raft domains.

Here, we probe the real-time membrane formation and reconstitution of L_O domains within a fluid membrane for the first time by means of time-lapse epifluorescence microscopy coupled to the SPR microscopy. The uniqueness of this combinatorial spectroscopic technique is that it allows to monitor the structural parameters of raft domains such as packing density, refractive index (RI) of raft domains within the lipid bilayer both kinetic state and equilibrium mode. Distinguished from other sensing techniques of membrane bounded SPR devices, our systematic conformations of heterogeneous membrane force the microdomains to aggregate at programmed position which enable the observations of phase-kinetics during raft formations. Author have found the way to reconstitute the heterogeneous membranes that composed of mixtures of SPM-rich and CHOL-rich membranes can be organized within a continuous membrane (**Figure 5.1a**) obtained by alternative introduction of each mixtures through the microfluidic system. The mixing between distinct membrane, between SPM-rich and CHOL-rich, leads well known molecular compaction of SPM with CHOL for raft domains at the boundary between two membranes. Since the penetration depth (P) of the SPR sensing is range of ~100 nm, Lo domains at programmed position

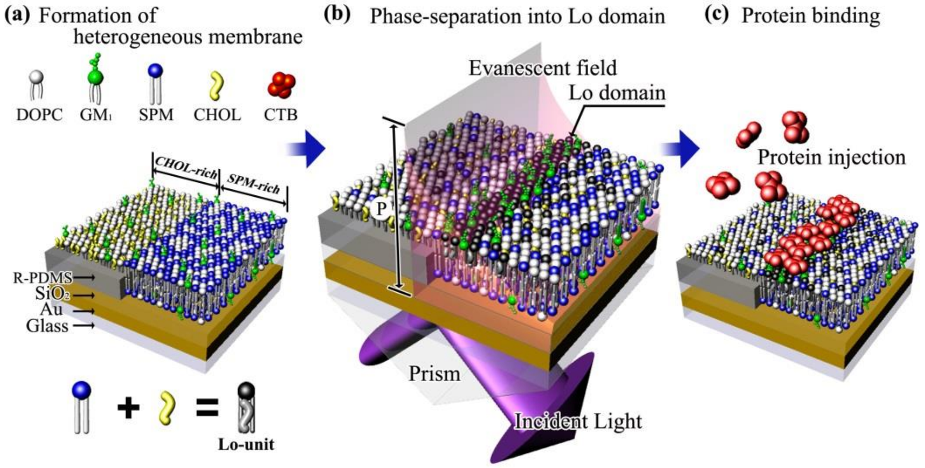

Figure 5.1 : The schematic representation of the experiment. (a) Reconstitution of continuous heterogeneous membrane composed of CHOL-rich and SPM-rich membranes on the prepatterned substrate. Substrate was prepared by deposition of Au (~50 nm), followed by the SiO_2 (~40 nm) for biocompatibility with lipid molecules. Patterned heterogeneous membrane was achieved through the channel-guide fluidic system. (b) The SPR analysis due to membrane phase-separation into L_O domain at the boundary between

two membranes. (c) The L_O domain-marker proteins (CTxB) are injected on the phase-separated membrane to verify the ligand-receptor binding event.

would be directly observed and characterized by SPR device as shown in **Figure 5.1b**. Author also incorporated a GM_1-linked protein (cholera toxin subunit B, CTxB) into our connective membrane and have them to locate at the target L_O domains to see the ligand-receptor binding as shown in **Figure 5.1c.**

5.2 Fluid Membrane for SPR Analysis

5.2.1 Membrane Mixing and Mobility

(a) Membrane Mixing

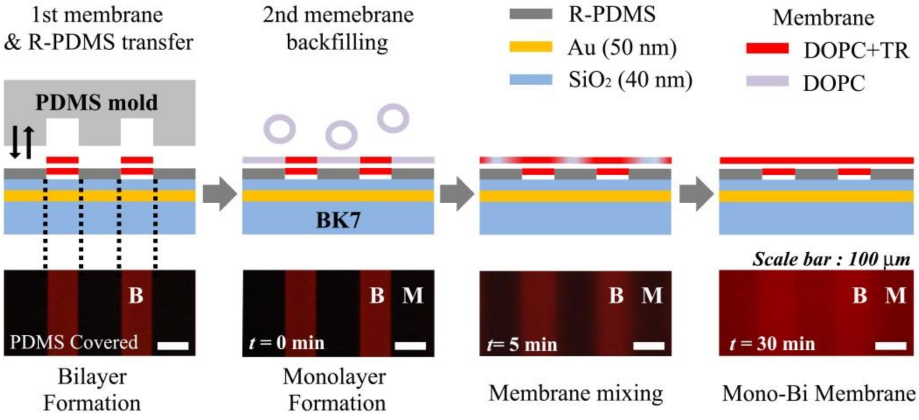

(b) FRAP test

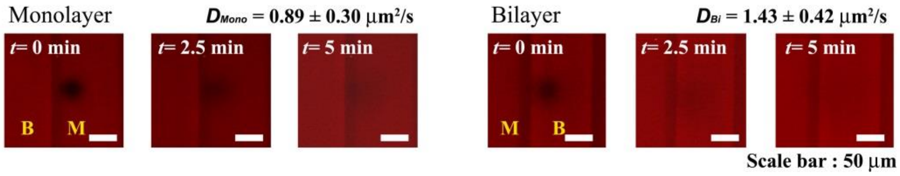

Figure 5.2 : Diffusive characters on heterogeneous membranes. (a) Microfluidic based heterogeneous membrane array and mixing behavior were represented with schematic illustrations (top) and fluorescence micrographs (bottom). The sequential injections of 1st vesicle mixture (DOPC:TR=99:1) along the fluidic channel, and 2nd vesicles (DOPC 100%) lead bilayer (B) and monolayer (M) membranes, respectively. (b) The FRAP test on each monolayer and bilayer membrane is represented.

Our concept majorly starts from the formation of connective heterogeneous membrane which allows mixing between two distinct membranes. The prepared SiO_2 surface must show the hydrophilic properties which is prerequisite which is prerequisite for SLBM formation by spontaneous vesicle rupture process [1]. Author exposes the substrate to UV ozone [31], followed by capping the microchannel-patterned PDMS mold. Microfluidic system enables the successive injections of distinct vesicle mixtures by playing critical roles in two ways. For one thing, it guides vesicle to flow, for another it transfer the R-PDMS which is used for formation of monolayer architecture. Author has already introduced the principle to transfer of R-PDMS to obtain the proper hydrophobicity for lipid monolayer architectures in previous paper **[chap. 3]**. To test our connective heterogeneous membrane conformation with two distinct membranes, we perform the ‘mixing test’. The binary mixture, composed of 1,2-dioleoyl-sn-glycero-3-phoph-ocholine (DOPC) as a base for the formation of the SLBs with 1 mol% negatively charged lipids labeled with red fluorescent dyes, Texas Red 1,2-dihexadecanoyl-sn-glycero-3-phosp-hoethanola-mine (TR), are injected and expressed on the hydrophilic SiO_2 surface as they forms the first (1^{st}) membrane in bilayer (B) architecture. The PDMS mold is removed leaving the R-PDMS at the contacted regions, followed by introducing the secondary (2^{nd}) vesicle for lipid monolayer (M) membranes. The 2^{nd} dye-free mixture (100 mol% DOPC) fills lipid-free region where the R-PDMS regions are expressed. **Figure 5.2a** shows the schematic illustrations and time-lapse microscopic observation after rupturing the 1^{st} and 2^{nd} mixtures in time. The definite difference in fluorescent intensity of TR (t = 0 min) indicate that heterogeneous membranes are achieved across the monolayer and bilayer membranes. The blurring of TR from bilayer to monolayer membrane could be interpreted that the membrane mixing between monolayer and bilayer regions are actively in progress (t = 5 min) and arrived the equilibrium mode (t = 30 min) showing the distinct intensity profiles of TR at each region. The dyes (*e.g.* TR) diffuse down a concentration gradient from where they are more concentrated to where they are less concentrated. This shows that the dye-labeled lipids continue to cross the membrane showing mixing property on the connective membrane. Author also carried out the fluorescence recovery after photo-bleaching (FRAP) studies [4] to measure the diffusion coefficient of TR in each surface. Average values derived from more than 20 independent samples yielded the intensity ratios of ~1.51 (B/M) which is similar with the Howland *et al*. reported [83]. A quantitative analysis of diffusive characters of binary membrane (DOPC:TR=99:1) both at monolayer and bilayer regions reveal that diffusion coefficient is $0.89 \pm 0.3\ \mu m^2/s$, and $1.43 \pm 0.4\ \mu m^2/s$, respectively (**Figure 5.2b**). These data show the great agreement with lipid bilayers on glass [4, 42] and oxidized PDMS substrates [61]. Our FRAP studies indeed confirm that the continuity and fluidity of the binary membrane are completely preserved which is critical prerequisite for our concept.

Evolution of SPR spectra

5.2.2 SPR Spectra at Equilibrium Mode

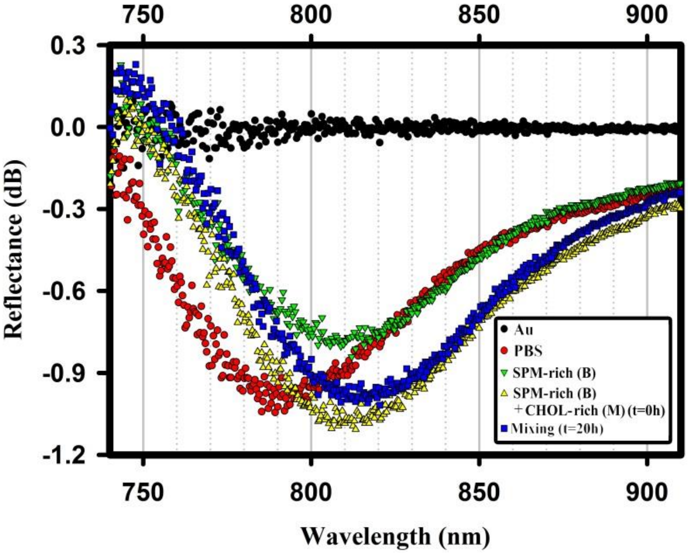

Figure 5.3 : SPR spectra recorded during equilibrium state at a Au-SiO_2 layer without (black ●) and with (red ●) PBS solution. The SPR spectra of 1st SPM-rich membrane (green ▼), followed by 2nd CHOL-rich membrane (yellow ▲) at *t*=0 *h*, and phase-separated membrane (blue ■) at *t*=20 *h* were represented.

Figure 5.3 shows the evolution of wavelength spectra recorded during equilibrium states at sequential injections of raft constituents. In this system, both of 1st (B) and 2nd (M) membranes are generated through the spontaneous vesicle rupture process [1]. Author uses the 1st SPM-rich (SPM:DOPC:GM_1:TR= 33:65:1:1) membrane and 2nd CHOL-rich (CHOL:DOPC:GM_1:TR=33:65:1:1) membrane for bilayer and monolayer conformation, respectively. The SPM-rich membrane on SiO_2 surface cause a peak shift of the resonance wavelength by ~20 nm (green curve ▼) with respect to that (red curve ●) of the sole phosphate buffered saline (PBS) solution at pH 7.4 on the identical substrate, whereas consequent backfilling of 2nd CHOL-rich membrane doesn't show any peak shift (yellow curve ▲) respect to that of 1st membrane. Since we focused our incident laser beam spot at the 1st SPM-rich membrane, these data demonstrate reliability of our SPR analysis. However, the membrane mixing allows advance peak shift of the resonance wavelength by ~5 nm (blue curve ■; t=20 h) compared to peak (yellow curve ▲) of resonance wavelength at t=0 h. This could be interpreted that membrane mixing between SPM-rich (B) and CHOL-rich (M) membrane induce physicochemical alterations of membrane properties (*e.g.* structural parameter such as thickness, packing density of membrane). Unfortunately, information about peak shifts of wavelength at the each equilibrium state couldn't show the molecular interactions occurring within a patch of membrane. Therefore, it is necessary to check real-time peak behaviors of wavelength to understand the membrane dynamics.

5.2.3 Real-time kinetics of Membrane Reorganization

On the basis of concept made above, we observed real-time resonance wavelength variations by SPR microscopy coupled with time-lapse epifluorescence microscopy to monitor the membrane reorganizations for raft domains and incorporated a GM_1-linked protein (CTxB) into our connective membrane to see the ligand-receptor binding. The vesicle mixtures and experimental procedure is identical as explained above. **Figure 5.4a** represents the shifts of the resonance wavelength as function of time during the formation of 1st SPM-rich and 2nd CHOL-rich membrane (I; **Figure 5.4b**), the reorganization of membrane component (II; **Figure 5.4c**), and the protein binding of CTxB to GM_1 assembled regions (III; **Figure 5.4d**), respectively. For general analysis, we indicate the average value of the lowest 30, 40, and 50 wavelengths (represented as unit 30, 40, and 50, respectively) to ignore the noise values. First of all, introduction of PBS solution along the guide channels of fluidic PDMS mold generate peak value at ~790 nm (step ⓐ), followed by injection of SPM-rich (SPM:DOPC:GM_1:TR= 33:65:1:1) vesicle (step ⓑ). Abrupt peak shift to ~860 nm was observed until the 1st SPM-rich vesicle is replaced with PBS (pH. 7.4) solution (step ⓒ) showing the peak value near ~810 nm. The removal of PDMS mold (step ⓓ) shows peak drop about ~10 nm. The 2nd CHOL-rich (CHOL:DOPC: GM_1:TR=33:65:1:1) vesicles (step ⓔ) were injected for filling the R-PDMS region with 2nd membrane showing dramatic peak shift up to ~850 nm. The washing with PBS solution (step ⓕ) was performed again to remove the residual vesicle mixtures floating on the aqueous environment until the SPR signal became stable. Author interprets the drastic peak shifts (step ⓑ and ⓔ) are caused by the range of SPR sensing. As mentioned above, the penetration depth of the evanescent filed is range of ~100 nm. In our system, we have ~40 nm thick SiO_2 layer above the Au layer. Therefore, the residual vesicles which floating on the aqueous surrounding (~60 nm) could be detected including membrane film as well. The washing processes (step ⓒ and ⓕ) remove the residual

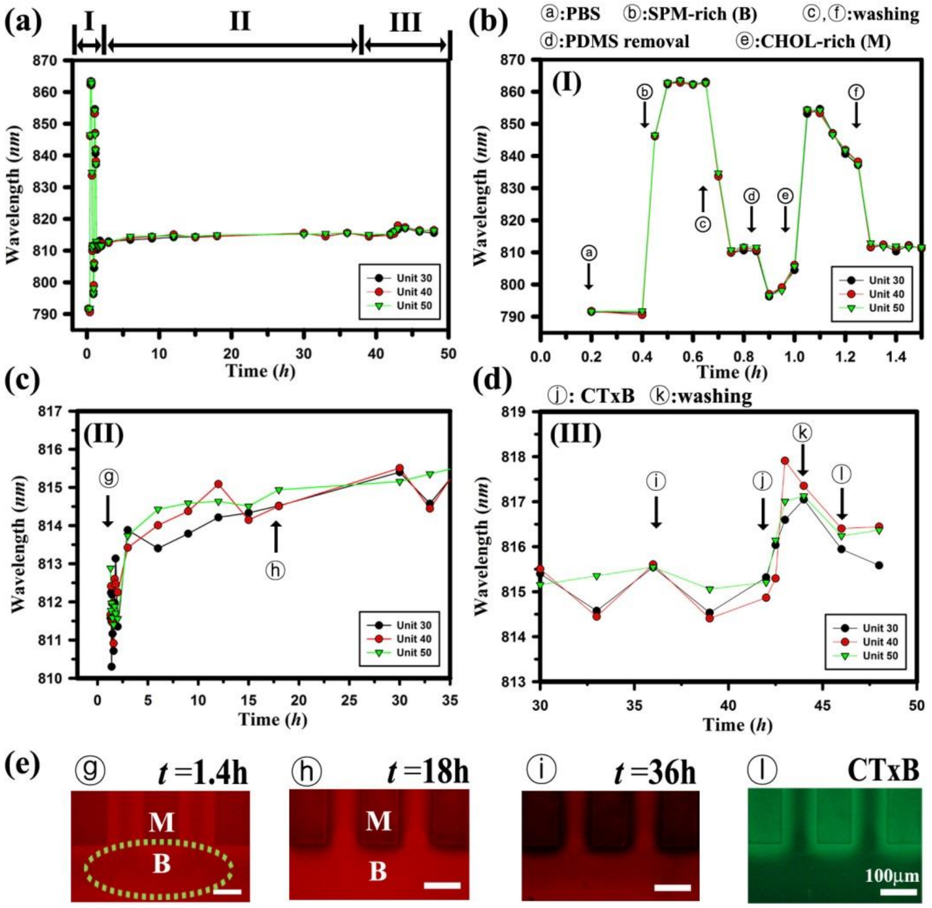

Figure 5.4 : The real-time kinetics of membrane reorganization and protein binding (a) Real time SPR peak behavior as function of time is represented. Magnified peak behavior during (b) the connective heterogeneous membrane, (c) the phase-separation of membrane component, and (d) the protein binding of CTxB are shown with (e) the fluorescent micrographs at each step. Dotted ellipse indicates the position where the incident light was exposed

vesicles and leaving the membrane film showing the peak at ~810 nm. The peak shift of resonance wavelength, $\Delta\omega$, by ~20 nm represent the bilayer lipid film is generated on the substrate. In this way, binary distinct SPM-rich (B) and CHOL-rich (M) membranes are achieved showing patterns of fluorescent intensity across the monolayer and bilayer regions (micrograph ⓖ; **Figure 5.4e**). The rearrangement of membrane constituents within connective membrane is monitored as function of the time. **Figure 5.4c** represents an curvilinear increase of resonance wavelength as function of time showing great accordance with the tendency as function of time with Moore *et al.* reported [147]. It is well known that SPM and CHOL molecules have specific affinity to induce ‘Lo-unit’, called nanorafts. In our system, SPM and CHOL molecules at each domain are forced to diffuse into counterpart-rich membrane. That is, the SPM diffuse toward CHOL-rich membrane, while the CHOL move toward SPM-rich membrane. Author already found that the L_O domains generate at the boundary of each membrane, especially toward the SPM-rich membrane (micrographs ⓗ and ⓘ; **Figure 5.4e**). The principle and detailed explanations are about to submitted. **[chap. 4]** Therefore, the $\Delta\omega$ by ~5*nm* (step ⓗ) respect to that of initial state (step ⓖ) could be caused by membrane reorganization, *e.g.* raft formation. In order to confirm the existence of L_O domain, well known raft-marker protein, alexa fluor 488 labeled *cholera toxin B subunit* (CTxB-488; 5 mg/ml), was additionally incubated (step ⓙ) more than 2 *h*, followed by washing process (step ⓛ) to remove floating CTxBs which fail to bind at GM1 clusters. As shown in Fig. 4d, additional peak shift (step ⓛ) by ~2 nm compared to absent of CTxB (step ⓘ) was monitored. The fluorescent micrographs (**Figure 5.4)** exhibits that the fluorescent intensities of TR at the boundary gets diminished as function of time (from micrographs ⓖ to ⓘ), specially toward SPR-rich region. The localization of CTxB-488 on the dark boundary regions demonstrate the location of L_O domain (micrographs ①; **Figure 5.4e**). Unlike the peak shifts in step II, the SPR responses in step III are ascribed to mass increase due to the ligand-receptor bindings between CTxB-GM_1 [148]. Shifts to larger resonance wavelength are expected when net mass increases occur. The specific binding of relatively small lipid with massive proteins would be major factor that lead peak variations. The combinatorial spectroscopic approaches introduced here highlight the strongpoints of each detection method. That is, the existence of Lo domain at expected region could be observed with fluorescent microscopy, while the kinetic of Lo domain formation could be measured with SPR microscopy. The complementary approach opens the opportunities to determine the structural parameters of raft domains such as packing density, RI of raft domains within the lipid bilayer. The detailed description will be explained later.

5.2.4 ‘Raft Membrane’ vs ‘Component-deficient Membrane’

The question remains to be verified whether or not the curvilinear increase of resonance wavelength definitely comes from the Lo domain within fluid membrane. Thus, we carried out the combinatorial experiments with the individual raft components and compare the results with the wavelength behavior of the membrane where the both of SPM and CHOL are included. At this time, we used the label-free raft mixture (SPM:CHOL:DOPC:GM_1=33:33:33:1) since the wavelength behaviors between label-included and -excluded membrane didn't shows difference (**Figure 5.5**). This data mean that existence of TR doesn't affect the peak

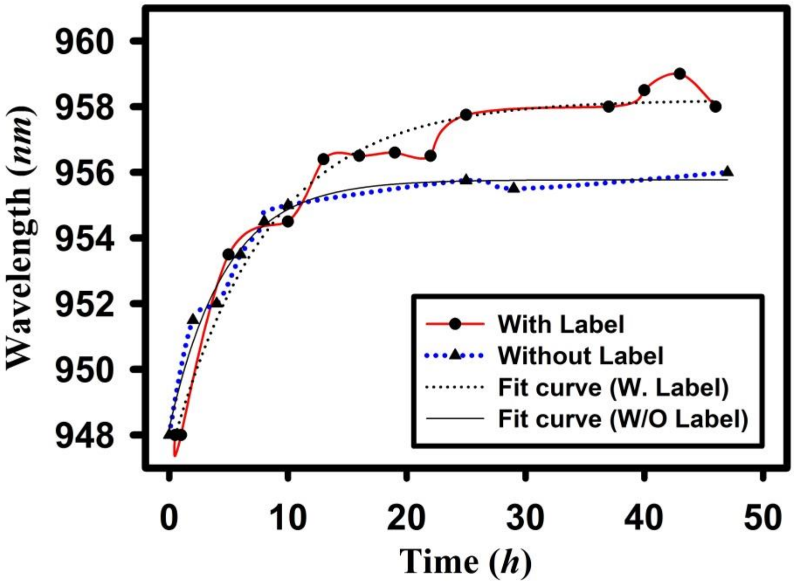

Figure 5.5 : The comparison of real-time SPR signals of labeled membrane (SPM:CHOL:DOPC:GM1:TR=33:33:32:1:1) with label-free membrane (SPM:CHOL:DOPC:GM1=33:33:33:1) both on patterned morphology.

behavior. The label-free raft membrane shows the similar curvilinear increase as function of time until the CTxB (25 μg/ml) was incubated (t = 50 *h*) and washed (t = 52 *h*) as shown in **Figure 5.6**. Whereas, the individual component included membranes didn't show curvilinear increase both at SPM-free (CHOL:DOPC:GM_1=33:66:1) and the CHOL-free (SPM:DOPC:GM_1=33:66: 1) membrane. Although the incident rise and fall at the initial period were detected within both membrane before t = 7 h, the peak shifts settled at the ~950 nm for SPM-free and ~947 nm for CHOL-free membrane, respectively. According to these data, we can conclude that the curvilinear increase indicates the kinetics of L_O domain formation. Author could interpret this as the coarsening of nanorafts and growing from nanometer scale to micrometer scale. Moreover, we also found that the SPM and CHOL couldn't lead phase separation into the L_O domain when they work alone. This could be interpreted that membrane mixing allows the combination between SPM and CHOL for generating 'L_O-unit' at the boundary, and sequential coarsening of L_O-unit into micrometer scale leads the decrease of fluorescent intensity. The curvilinear increase as function of time could be interpreted if we simplify our experiments at the point of first-order reaction model [149]. If we apply the reaction model to our system, the substrate binding between SPM and CHOL molecules forms the 'L_O-unit' complexes due to the affinity between two substrates. This could be expressed as,

$$\text{SPM} + \text{CHOL} \rightarrow \text{L}_\text{O}\text{-unit}$$

The product (*e.g.* 'L_O-unit' complex) as function of time could be expressed by

$$\mathrm{P}(t) = \mathrm{P}_\infty\left(1 - e^{-kt}\right)$$

The preceding expressions, the P_∞ represents the amount of saturated product at equilibrium state, and k represent the association coefficient between two substrates. According to this equation, the amount of Lo-unit complexes increases as function of time until the each substrate is exhausted. This process occurs at the boundary between two membranes. Once the Lo-unit complexes formed, they tend to aggregate each other by escaping from

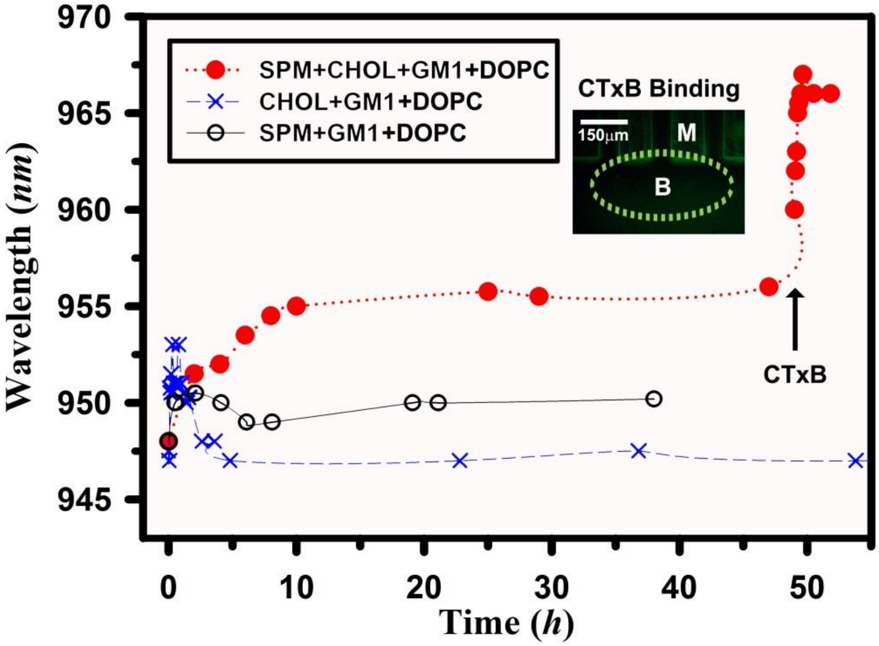

Figure 5.6 : The real-time comparison of raft components involved membrane (SPM:CHOL:DOPC:GM_1=33:33:33:1) reorganization with component-deficient membrane for L_O domain formation. The SPM-free (CHOL:DOPC:GM_1=33:66:1) and the CHOL-free (SPM:DOPC:GM_1=33: 66:1) membrane were used. The CTxB was incubated at t = 50 h for verifying the existence of L_O domain as shown in fluorescent micrograph. Dotted ellipse indicates the position where the incident light was exposed.

energetically unfavorable states that driven by height mismatch between L_O and liquid-disordered (L_d) domain [28]. These aggregations may accelerate the phase-separation into the massive L_O domain formation and induce the alteration of membrane properties from thinner, less ordered, less packed to thicker, more ordered, more packed. Our SPR data shows great agreement with the physical characters of L_O domain which is thicker, more ordered, more packed than surrounding L_d domains [35].

5.2.5 ‘Programmed Raft’ vs ‘Unidomain Raft’

The kinetic of membrane compartmentalization on the course of raft formation remains as central question so far. Although fluid lipid films on the Au surfaces contribute to monitor the kinetics of membrane reorganization on the SLBM, the raft formation at random sites hinders to detect the spontaneous intermolecular packing event between SPM and CHOL. A few of studies [40, 52, 104] already introduced the ways to manipulate the L_O domains by patterning substrate where the SLBM stands. The patterned raft at programmed position could be expected to offer efficient detection of the crucial information in the course of L_O domain formation. To demonstrate our assumption, we carried out the comparative methods for L_O domain generations as shown in **Figure 5.7**. One for ‘programmed raft’ domain that depends on the mixing of two distinct membranes, another for ‘unidomain raft’ that sole depend on the spontaneous aggregates of nanorafts in the shape of isolated and island-type Lo domain at random sites. Author will define this island-type Lo domain as ‘unidomain raft’ due to it generated from sole rupturing raft mixture (SPM:CHOL:DOPC:GM$_1$=33:33:33:1) on the non-patterned SLBM. As shown in real-time resonance wavelength variations as function of time, membrane reorganization for 'patterned raft' shows expected

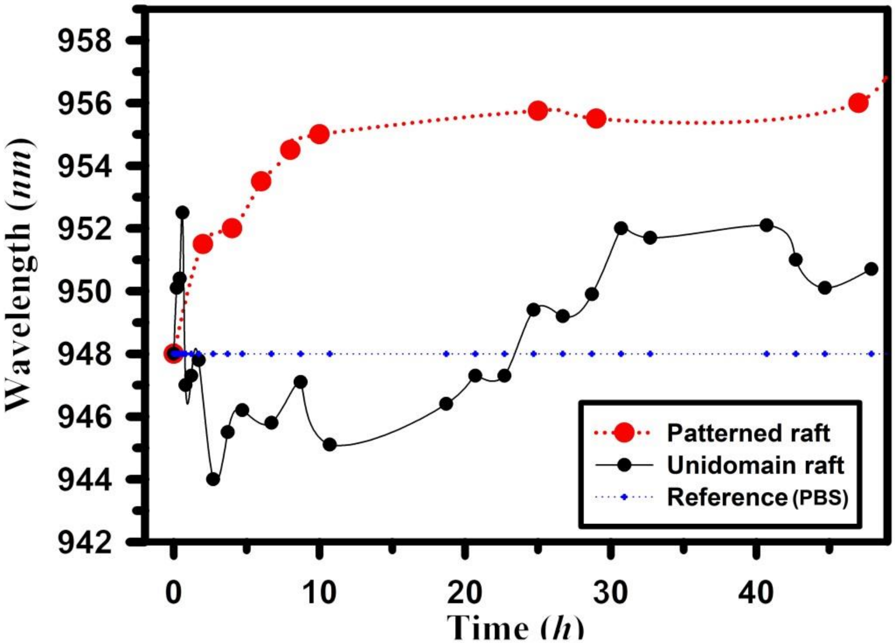

Figure 5.7 : The comparison of real-time SPR signals of patterned heterogeneous membrane (denoted as 'programmed raft') with non-patterned membrane ('unidomain raft') were shown with the reference (PBS with pH. 7.4). The identical membranes (SPM:CHOL:DOPC:GM1=33:33:33:1) were used in both cases.

curvilinear increase (red dots ●), whereas the 'unidomain raft' shows trendless behavior (black dots ●) as function of time. Author represents the reference value (injection of PBS solution) for directive comparison. Author interprets that the trendless data come from the random diffusion of nanorafts. It is well known that coarsening of nanorafts at random sites shows the massive island-type Lo domain. Author also observed the island-type raft aggregates but fail to localize them at the beam focus area. From the results, we could conclude that patterned membrane could offer the opportunity to detect the spontaneous intermolecular packing event in the course of raft formation. The additional uniqueness of our system is that the packing ratio for L_O domain formation could be calculated. The differential value of curvilinear increase at each time (*e.g.* incident slope at each time) represents the ratio for L_O domain formation. Author could not conclude that this index means whether the intermolecular SPM-CHOL packing or the coarsening of L_O-units. However, the programed raft domain gives the information that association ratio for L_O domain tends to decrease and saturated after all which could not be obtained if they formed at random schedule in time and space. Moreover, the programmed raft gave a clue to investigate the RI of the L_O domain. By applying the thickness of L_O domains (~4.6 nm)[35] into our SPR analysis at ~948 nm, we could calculate the RI of SPM-rich membrane ($n_{\text{SPM-rich}}$) is 1.52. These data shows good accordance with data reported by Salamon at el[150]. However, the peak shift by ~8 nm (948→956) lead alteration of RI on programmed raft (n_{prog}) from 1.52 to 1.60, while the peak shift by ~ 3 nm (948→951) alter the RI of unidomain raft (n_{uni}) from 1.52 to 1.55. However, these values don’t indicate the RI of the L_O domain (n_{Lo}) since the RI value of n_{prog}=1.60 represent average value of RI only where the laser beam was exposed. Therefore, by calculating the area fraction (5~7 %) of Lo domain within the beam spot, we could obtained the RI of L_O is $2.26 \leq n_{Lo} \leq 3.12$. The detailed explanation for n_{Lo} is introduced in Fig. S3 in ESI † and summarized in Table 4.

Table 4 : Calculated RI of membrane components

Area	$n_{SPM\text{-}rich}$	n_{uni}	n_{prog}	n_{Lo} (5~7 %)
Peak value (nm)	948	951	956	956
RI	1.52	1.55	1.60	$2.26 \leq n_{Lo} \leq 3.12$

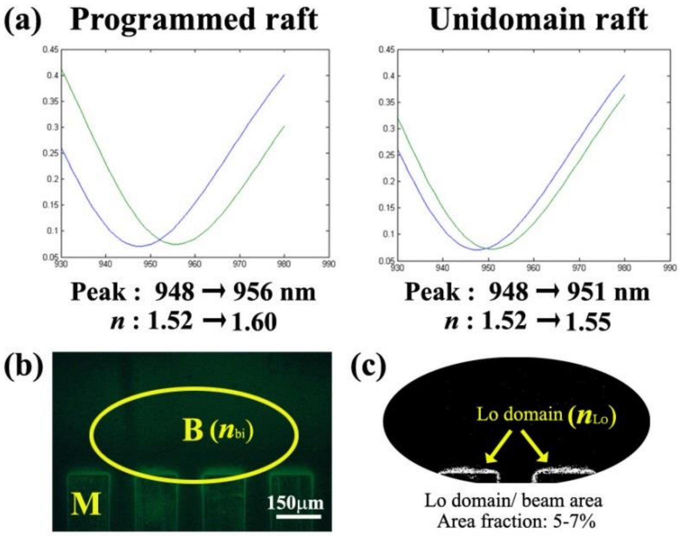

Area	$n_{SPM\text{-}rich}$	n_{uni}	n_{prog}
Peak value (nm)	948	951	956
RI	1.52	1.55	1.60

by assuming the $n_{bi} = n_{SPM}$=1.52 → n_{Lo} = 2.66 ~ 3.12

by assuming the $n_{bi} = n_{uni}$=1.55 → n_{Lo} = 2.26 ~ 2.55

Figure 5.8 : Calculation of RI of Lo domain. (a) Peak shift of programmed and unidomain raft. (b) Fluorescence micrograph showing programmed raft domain by binding a CTxB-488. Location of Lo domains are correspond to the distribution of CTxB. Dotted ellipse indicates the position where the incident light was exposed. (c) Extracted image with image program (Image J) to investigate the area fraction of L_O domain against the beam area.

5.3 Discussion & Conclusion

Author reports the kinetics of L_O domain formation within the fluid heterogeneous membrane by means of the SPR microscopy. In particular, combinatorial observation with time-lapse epifluorescence microscopy allows monitoring the dynamic reorganizations both in kinetic and equilibrium states of Lo domain which have not been reported so far. Systematical, a handful of strategies including channel-assisted composition array [18], membrane stamping [10], and spatial bleaching and backfilling with the secondary membrane [4], tried to reconstruct heterogeneous membrane array due to the importance in numerous biological system. However, lipid-free gap [82-86] or physical barriers made with polymer [56] of proteins [151] have prohibited the mixing properties between heterogeneous membranes systems so far. By overcoming the membrane discrimination across the opposing heterogeneous membranes, the L_O domains are achieved within the fluid bilayer membrane at predicted location. Within the frame work of lipid raft formation, previous studies [148, 150] reported the raft domain sensing through SPR analysis on the solid supports. However, observing through plasmon waveguide resonators [150] has intrinsically limited exploitation of below the cut-off thickness for diverse application in various fields. Moreover, the incomplete reconstruction of raft domain not only by omitting the key raft component [150], *e.g.* CHOLs, but also by detecting the protein-GM_1 complex [148] at random position unable to guarantee the phase-separation into L_O domain within a patch of membrane. However, the fluid membrane based SPR analytic platform associated with patterned heterogeneous membranes enable us to investigate the kinetics and quantitative information of L_O domains for understanding intermolecular events happen on the course of raft formation happen in nanometer scale. By overcoming the immobile membrane which has been major challenges of membrane-involved SPR technique, our analytical tool might provide a promise of a new class of membrane analysis. Incorporation with different classes of membrane constituents such as DNA, virus, other signal proteins would exhibit more functional flexibility for studying cellular activities to understand interactive binding event within/on the membranes as they become the powerful tool in the field of pharmaceutical screening [152], proteomics [153], chemical and biological analysis/detection, and materials engineering.

Materials and methods

PDMS Microfluidic Channels Fabrication. Before coating the photoresist, the glass substrate was immerged in acetone for more than 30 min followed by in deionized (DI) water for 10 min. Cleaning processes were performed in the standard ultra-sonicator at room temperature. After blowing with N_2 gun, standard negative photoresist (SU-8 2050, MICROCHEM) was spun onto the glass substrate according to the vendor's instructions. The coated glass was aligned and exposed through a photo-mask using a mask aligner (MA-6, EVG). After exposure process, SU-8 patterning process was performed giving the film thickness of 50 μm separated by 100/150 μm or 100/100 μm periodically. The elastomeric material, *Sylgard 184* silicone elastomer (Dow Corning Corp.) mixed with curing agent in a 10:1 ratio, was poured onto the mold and subsequently cured for more than 3 h at 80℃ before it was removed from the masters.

Formation of SLBMs and an imaging method. The phospholipids, used as a base for the formation of the SLBs, were 1,2-dioleoyl-sn-glycero-3-phophocholine (DOPC). For imaging the SLBMs, a negatively charged lipids labeled with red fluorescent dyes, texas red 1,2-dihexadecanoyl-sn-glycero-3-phosp-hoethanola-mine (TR, Molecular Probes, Eugene, Oregon) and green flurescent dyes, 4-(4-(didecylamino)styryl)-N-methylpyridinium iodide (D291, Avanti Polar Lipids, Birmingham, Alabama) were mixed with DOPC at 1 mol%, repectively. The cholesterol (CHOL) and *ganglioside* (GM_1; brain, ovine-ammonium salt) were purchase from Avanti Polar Lipids (Birmingham, Alabama). These lipids mixed according to their purpose. All lipid mixtures were dissolved in chloroform. The rapid solvent exchange method [107] was employed to evaporate chloroform and to hydrate with Tris buffer (100*mM* NaCl and 10*mM* Tris at pH 8.0) simultaneously. Small unilamellar vesicles (SUVs) were produced by extruding 20 times through a 50 nm filter. The residual SUVs remained in the tris buffer solution were removed with the DI water after the SLBs was formed after the substrate was exposed to the SUVs solution for 5 min The Texas red lipids were monitored using an epifluorescence microscopy (Eclipse E600-POL, Nikon). Whole processes were performed in room temperature.

Fabrication of substrate for SPR. The sodalime glass was cleaned in piranha solution (H_2O:H_2SO_4=1:3) for 10 min before consecutive deposition with Au and SiO_2. The 50 nm Au layer on the cleaned glass with a 5 nm chromium adhesion layer is prepared with an electron beam evaporator (KVE-3004, Korea Vaccum Corp.), followed by deposition of 40 nm thick SiO_2 layer on Au covered glass with the STS-PECVD equipment.

Formation of binary supported membrane on the R-PDMS surface. The UV ozone treatment [31] was performed on SiO_2 deposited glass to giving hydrophilic surface by formation of hydroxyl (-OH) group. Selective stamping was achieved with photolithographic patterned PDMS mold. The PDMS films thickness of 50μm separated by 100/150 μm or 100/100 μm periodically apart were contacted with hydroxylated glass. Injection of first vesicle mixture along the micro channel results in bilayer membrane, and subsequent peeling process gives a selective patterning of bilayer membrane surrounded by residual PDMS (R-PDMS) [87, 103] regions. Note that the R-PDMS, residual low-molecular-weight oligomers transferred from the PDMS mold, alters the surface property from hydrophilic to hydrophobic. In other word, the regions for lipid bilayer formation changed into that for lipid monolayer. Secondary backfilling of R-PDMS regions with secondary mixture generate connective binary membrane which allows diffusive mixing between heterogeneous membranes.

SPR Analysis of membrane film. SPR signals of samples were measured in Kretshcmann configuration [154, 155]. A sample plate was adhered to a hemi-cylindrical prism (BK7; refractive index is 1.51) with a drop of refractive index matching oil (refractive index is 1.51). Angles of incidence and reflection were kept at a same value between 65° and 70° using two rotational stages (URS150BCC, Newport) which were connected to a white light source and to a detector of optical spectrum analyzer (AQ6317B, Ando), respectively. Author used a relay-optics configuration composed of three lenses and a polarizer so as to have a transverse magnetic polarized light with directionality and to make a beam size as small as possible. Reflectance spectra were measured at wavelength from 700 nm to 1200 nm. Whole processes were performed in room temperature. For the calculation of reflectance spectra and refractive indices on the sample structure under experimental conditions, our own-built rigorous coupled wave analysis (RCWA) tool was used [156, 157] .

Chapter 6. Spatial Manipulations of Charged Lipids into Concentration Gradient

6.1 Introduction

The development of a versatile platform to achieve well-controlled concentration gradients of amphiphilic molecules showing the liquid crystalline order [158, 159], surface-adsorbed species of lipids [36, 160] and proteins [161], and DNA associated adsorbates [162] in micro-patterned arrays has attracted great attention for systematic studies of biological activities [31, 163-165] including cell adhesion, migration, and growth as well as practical applications [166, 167] for axon guidance and chemotaxis. Especially, supported lipid bilayers (SLBs) and model membrane systems reconstituted on solid supports in the charged environment play critical roles on the fundamental studies of membrane-associated activities including cellular deformation [160], vesicle budding [36], signal transduction [162], cell apoptosis [31], and membrane protein trafficking [106].

Recently, microarrays with different concentration profiles of charged lipids in the SLBs have been demonstrated using a number of the fabrication methods, such as a stamping mold [16], the photo-exposure [10], a micropipette [168], and a microfluidic channel [11], that are capable of constructing bilayer arrays with specific composition variations in different corrals. However, many of them tend to deform the lipid components physicochemically in the membrane [16] and they often require quite expensive equipments to manipulate the composition variations [17, 168].

In this work, we develop a viable, cost-effective scheme of constructing a spatially addressed membrane microarray with partitions wherein different concentrations of charged lipids in a supported bilayer are available within the framework of the field-directed diffusion dynamics. In a diffusion cell composed of a patterned substrate with a pore and partition walls distributed in parallel, the concentration of the charged lipids in each partition depends on the pore size, the distance from the pore to the partition, and an external electric field. It is found that a mechanical scratching method [167] produces the stable and permanent confinement of charged lipids within each partition and thus the concentration gradient is accordingly obtained from partition to partition.

6.2 Diffusion Cell with Partition Walls

6.2.1 Preparation of a diffusion cell with partition walls

A glass substrate was first cleaned with a solution of piranha [3:1 (v/v) H_2SO_4:H_2O_2] at 120℃ for 10 min, followed by ultra-sonication in deionized (DI) water for 10 min. Standard negative photoresist (SU-8 2005, MICROCHEM) was then spun onto the substrate at the spinning rate of 3000 rpm for 30 sec and partition walls were produced as shown in **Figure 6.1a** and **b**. **Figure 6.1** shows the schematic diagram of a diffusion cell having partitions with different concentrations of charged lipids in the SLBs in the presence of an external electric field. The thickness of the SU-8 film was 5 μm which corresponds to the height of a partition wall. Based on the photolithographic technique [163] using an ultraviolet (UV) lamp (MA-6, EVG), the partition walls [represented as thick black stripes in **Figure 6.1a**] were fabricated on the glass substrate. A pore of the width *W* and the partition of the distance *L* from the pore were shown in **Figure 6.1b**. The outer side walls of SU-8 were 10 μm thick and the inner partition walls of SU-8 were 4 μm thick. The physical dimensions of the diffusion cell was *Y* = 400 μm and *Z* = 200 μm. The pore width was varies as *W* = 10, 20, 40, 60 μm and the distance from the pore to the inlet of the closest partition was varied as *L* = 40, 60, 80 μm. The gap (*g*) between two adjacent partitions was fixed to be 30 μm. After the fabrication of the partition walls of SU-8, the diffusion cell was exposed to UV ozone for 10 min to have the hydrophilic surface on which the SLB membrane, separated from the glass support cushioned by a thin (10-20

Å) layer of water [31], was spontaneously formed. For the application of an external electric field to our diffusion cell, two platinum (Pt) wires (each 1.5 cm) were placed outermost sides of the cell along the direction longitudinal to the partition walls. The electric field-directed experiment in our study is similar to the electrophoresis experiment [31].

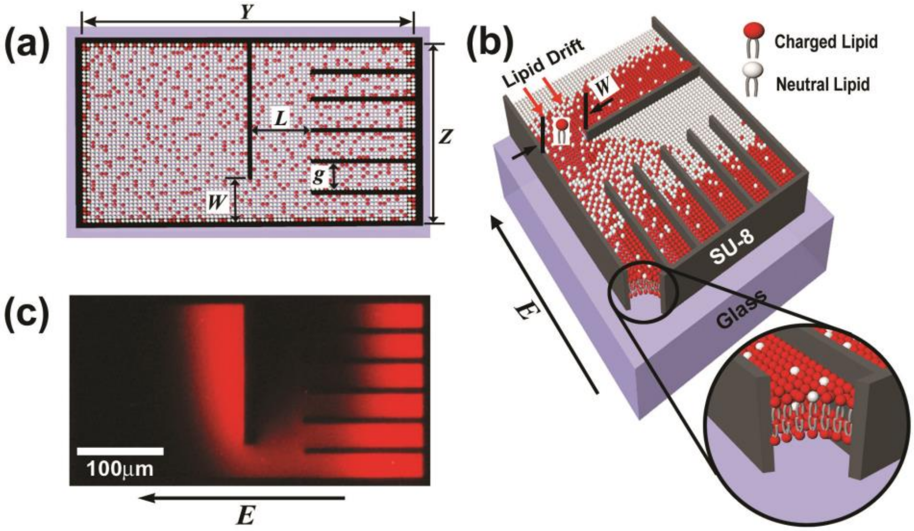

Figure 6.1 : The basic concept of two-dimensional redistribution of charged lipids diffused through a pore (*W*) in the corner of a diffusion cell into a number of partitions fabricated on a solid substrate: (a) the top view of a diffusion cell with charged lipids (represented in red) distributed at random in the membrane under no external field; (b) a schematic diagram of a diffusion cell showing the redistribution of charged lipids in the presence of an electric field; (c) a fluorescence micrograph showing the redistribution of charged lipids, the Texas Red-DHPEs, in a diffusion cell at the electric field of E = 45 V/cm for 20 min.

Across the two Pt wires being used as two electrodes, the direct current electric field of 45 V/cm was applied from a standard power supply. **Figure 6.1**(c) shows a typical fluorescence micrograph of the diffusion cell showing the redistribution of negatively charged lipids (the Texas Red-DHPEs) at the electric field E = 45 V/cm which was applied for 20 min.

6.2.2 Forming and imaging the SLBs

The phospholipids, used as a base for the formation of the SLBs, were 1,2-dioleoyl-sn-glycero-3-phoph-ocholine (DOPC, Avanti Polar Lipids, Birmingham, AL). For imaging the SLBs, negatively charged lipids labeled with red fluorescent dyes, 1,2-dihexadecanoyl-sn-glycero-3-phosp-hoethanola-mine (Texas Red-DHPE, Molecular Probes, Eugene, OR) were mixed with DOPC at 1 mol% (DOPC: Texas Red-DHPE = 99:1). All lipids were dissolved in chloroform. The rapid solvent exchange method [169] was employed to evaporate chloroform and to hydrate with Tris buffer (100 mM NaCl and 10 mM Tris at pH 8.0) simultaneously. Small unilamellar vesicles (SUVs) were produced by extruding 20 times through a 50 nm filter. When the patterned substrate was incubated in the SUV solution, the formation of the SLBs was developed via vesicle adsorption, rupture, and fusion [170]. The residual SUVs remained in the Tris buffer solution were removed with the DI water after the SLBs was fully formed after the substrate was exposed to the SUV solution for 5min. The Texas red lipids were monitored using an epifluorescence microscopy (Eclipse E600-POL, Nikon). The measurements of the fluorescence intensity of fluorescent molecules in SLBs were carried out using an image analyzing program of Image J (National Institute of Mental Health, USA). All the measurements were performed at room temperature

6.2.3 Field-directed Diffusion Dynamics

The direct current electric field moves negatively charged lipids into the partitions through the pore, starting from the upper corner of the first partition. Due to the electric field-directed diffusion, the neutral lipids (DOPC) are expelled by the charged lipids (Texas Red-DHPEs) from their equlibrium position. The diffusion of Texas Red-DHPEs is governed by the field-induced drift motion with a constant velocity (0.13 ± 0.01 μm/s, estimated from the mid-point trajectory method [162]) and the Brownian motion (with the diffusion constant of 1.0 ± 0.1 $\mu m^2/s$, determined from our experimental results of the fluorescence recover after bleaching, which is on the same order of magnitude as in typical lipids [1] as shown in **Figure 6.2**). Moreover, since the redistribution of charged lipids depends on the physical dimensions of *W* and *L* in the presence of the electric field, lipid compositions in the SLBs in the partition varies with the lipid distribution profiles in terms of *W* and *L*.

Author first varies *W* to be 10, 20, 40, and 60 μm for fixed *L* = 60 μm and measure the distribution profiles of charged lipids at the electric field of 45 V/cm for 20 min. Due to the electric field-directed diffusion, the negatively

(a) FRAP Test

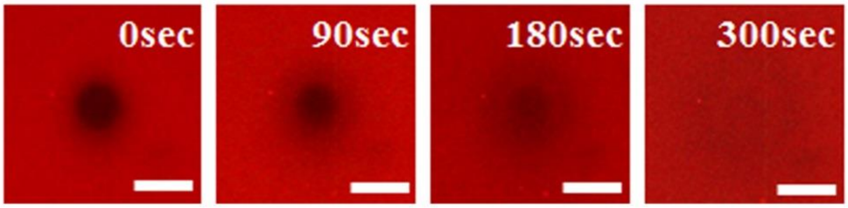

(b) Midpoint Trajectory Method

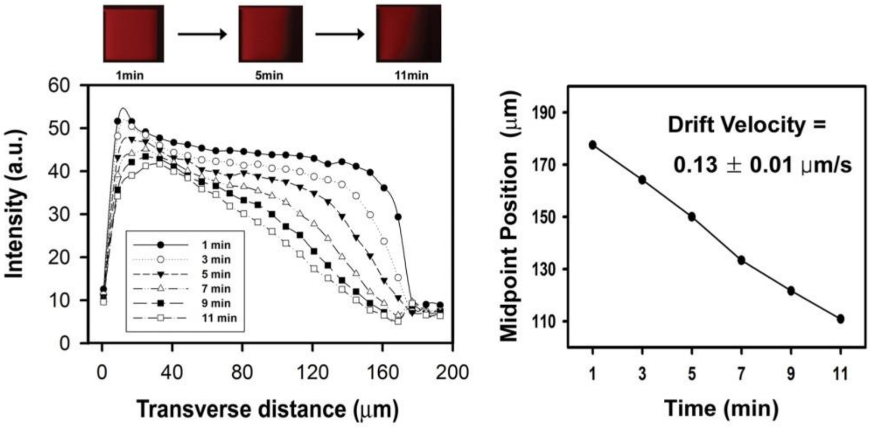

Figure 6.2 : Mobility test of fluorescent dye (Texas-red) by (a) FRAP test and (b) midpoint trajectory method.

charged lipids moved into the partitions of P_1 to P_6 and the concentration gradients across the partitions were produced as shown in **Figure 6.3a-d**. It is clear that the charged lipids were diffused from the pore to the partitions in a continuous manner with different concentration gradients. **Figure 6.3e** shows the fluorescence intensities for several *W*'s as a function of the transverse distance at the partition edges from P_1 to P_6. Defining the diffusion distance (MDD) as the transverse distance at which the parttion fluorescence intensity becomes zero, the MDD of charged lipids experiencing both the thermal diffusion and the electrical drift are different for different *W*'s. The MDD's represented by $I_0(W)$ were shown in **Figure 6.3e**. The MDD values for I_0 (10), I_0 (20), I_0 (40) and I_0 (60) [indicated by black arrows in **Figure 6.3e**] were about 83, 95, 116 and 134 μm, respectively. As shown in **Figure 6.2e**, the number of partitions with non-vanishing fluorescence intensity increases with increasing *W*. For example, the fluorescence intensity becomes nearly zero in P_3 for $W = 10$ μm while it remains in P_6 for $W = 60$ μm. For membrane arrays with different concentrations of the charged lipids, it is desirable to select the physical dimensions of *W* and *L* that produce both the maximum fluorescence intensity in the first partition (P_1) and the MDD in the mid partition (P_3 or P_4) to give uniform concentration gradients of the charged lipids across the partitions when an equlibrium state is reached after the removal of the the electric field. In our case, the above requirements are satified when $W = 40$ μm for given $L = 60$ μm. Author now varies *L* to be 40, 60 and 80 μm for fixed $W = 60$ μm to examine the dependence of the charged lipid distributions in the partitions on the physical dimension of *L*. **Figure 6.4a-c** are the micropraphs and fluorescent images with the iso-contour lines showing the concentration gradients across the partitions for $L = 40$, 60 and 80 μm, respectively. The electric field of 45 V/cm was applied for 20 min. In contrast to **Figure 6.3** where *W* is varied, the maximum fluorescence intensity is quite indepenent of *L* for given $W = 60$ μm. The results for the concentration profiles of the charged lipids in the partions were similar. The values of the MDD for I_0 (40), I_0 (60), and I_0 (80) were about 105, 134 and 185 μm, respectively [indicated by black arrows in **Figure 6.4d**]. As shown in **Figure**

6.4d, the fluorescence intensity for L = 40 μm becomes to zero in P_4 while that for L = 60 μm vanishes in P_5. It is interesting to compare the diffusion in the region without partition walls (free diffusion) and that in the partition (restricted diffusion). The lateral diffusion boundary, above which free diffusion is dominant and below which restricted diffusion occurs, is represented by a blue dotted line in **Figure 6.4a**. **Figure 6.4e** shows the fluorescence intensities measured in the two regions for W = 60 μm and L = 80. Away from the outer side wall of the diffusion cell, the fluorescence intensity for free diffusion decays monotonically as a function of the transverse distance while that for restricted diffusion decreases rapidly from P_1 to P_3 and essentially vanishes from P_4 to P_6. This results from the hindrance of the lateral diffusion of the charged lipids in the presence of the partition walls. we finally demonstrate a spatially adressed membrane arrays with different concentrations of charged lipids in the corrals. The physical dimensions of W = 60 μm and L = 40 μm were taken on the basis of the above resluts. **Figure 6.5a** shows the concentration gradients of charged lipids from one partition to other, obtained at the electric field of 45 V/cm for 25 min. The schematic cross-sectional illustration of the distribution of the charged lipids in the last partition P_6 under an electric field is shown in the right side of **Figure 6.5a**. The concentration gradients measured at the lateral diffusion boundary in the first (P_1) and the last (P_6) partitions as a function the longitudinal distance (denoted as the yellow dotted line from the bottom to the top) are shown in **Figure 6.5b**. Note that P_6 shows two regimes, in one of which the gradual change in the concentration of the charged lipids was observed and in the other, essentially no charged lipids were present at the lateral diffusion boundary.

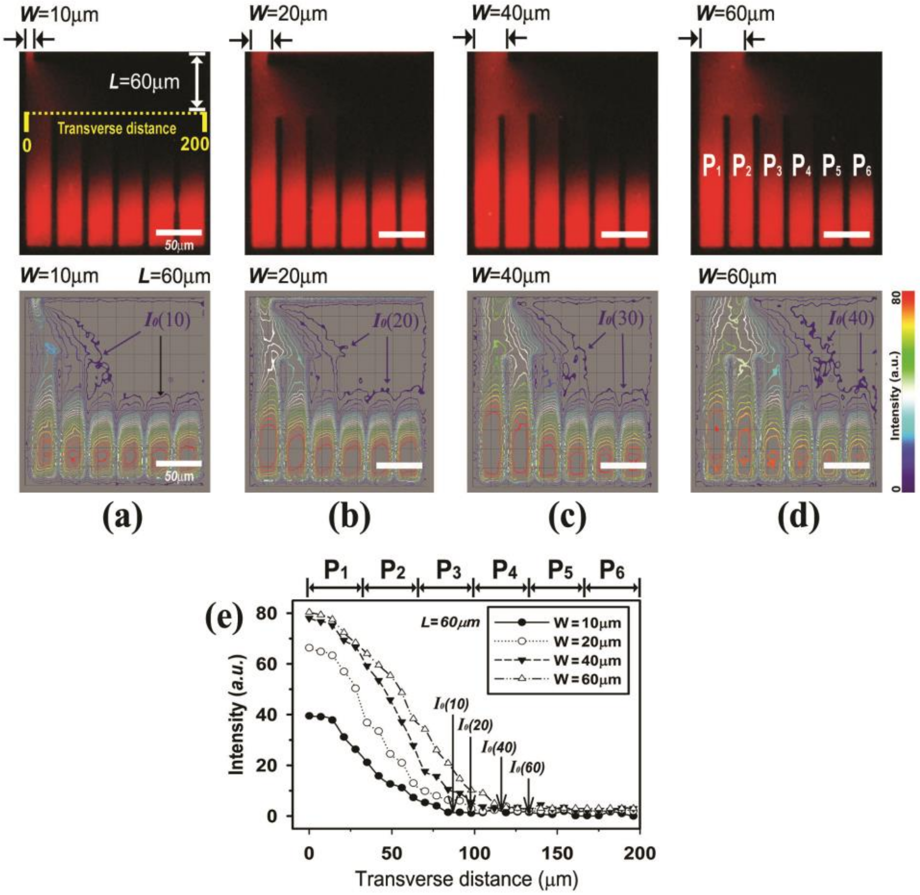

Figure 6.3 : Fluorescence micrographs and fluorescent images with the iso-contour lines showing the distribution of charged lipids across the partitions in the membrane for (a) W = 10 μm, (b) W = 20 μm, (c) W = 40 μm, and (d) W = 60 μm at E = 45 V/cm for 20 min for given L = 60 μm. The fluorescence intensity of Texas Red-DHPEs was shown in (e). The maximum diffusion distance (MDD) was represented by I_0 (W).

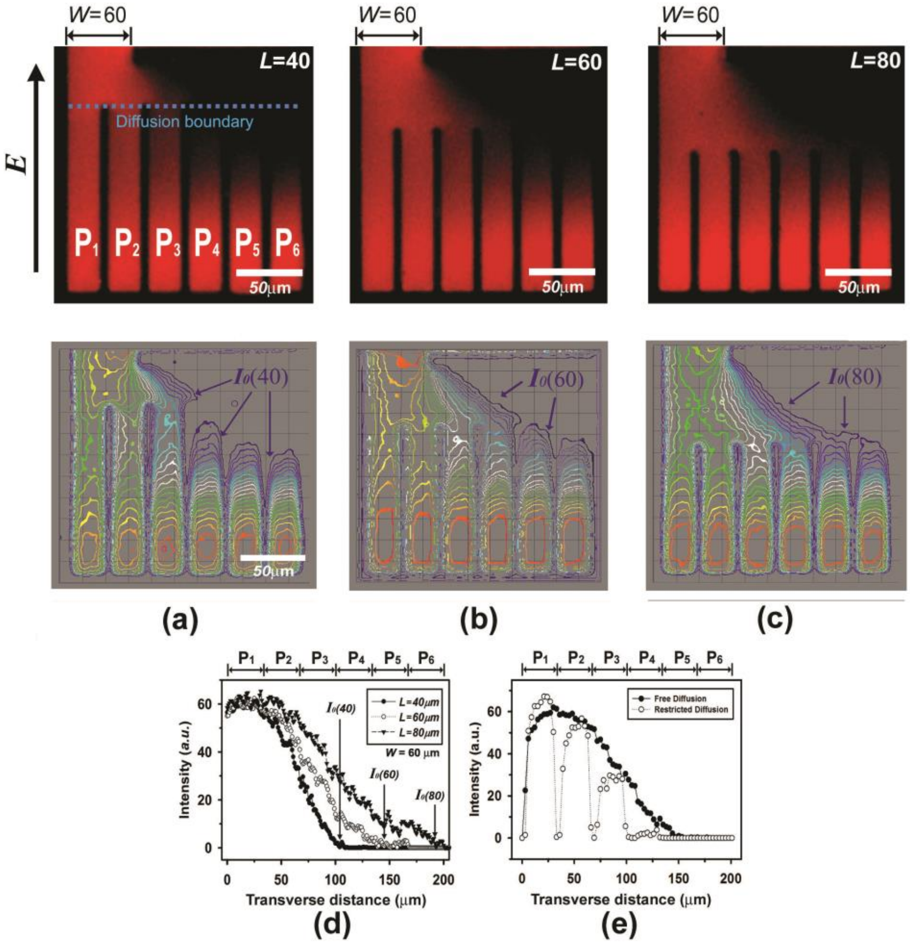

Figure 6.4 : Fluorescence micrographs showing the distribution of charged lipids across the partitions in the membrane for (a) L = 40 µm, (b) L = 60 µm, and (c) L = 80 µm at E = 45 V/cm for 20 min for given W = 60 µm. The fluorescence intensity of Texas Red-DHPEs was shown in (d). The fluorescence intensities measured in two regions (free diffusion and restricted diffusion in the partition) above and below the lateral diffusion boundary for W = 60 µm and L = 80 were shown in (e).

After the removal of the electric field, the lipid concentration in the partition will become to be uniform at equilibrium in time. In P_1, no abrupt change in the concentration of the charged lipids was observed along the longitudinal distance. Applying a mechanical scratching method [1] to **Figure 6.5a** at 1 hr after the removal of the electric field, a spatially addressed membrane array was obtained as shown in **Figure 6.5c** where the charged lipids were permanently confined within the corrals (C_1 to C_6) in the partitions. The scratched lines serve as diffusion barriers for the charged lipids across the corrals. The schematic cross-sectional illustration of the distribution of the charged lipids in the corrals is in the right of **Figure 6.5c**. Figure 6.5d shows both the fluorescence intensities and the concentrations of the charged lipids, Texas Red-DHPE, in the corrals from C_1 to C_6. Based on the geometrical parameters of the corral such as the size and the height (the gap of the partition) together with the initial concentration of the charged lipids in the SLB, The concentration in each corral was calculated from the fluorescence intensity per volume of the membrane. As an example, for C_6, the estimated concentration of Texas Red-DHPE was 1.25 mol%. Effect of self-quenching by frequent exposure to laser source was considered by normalizing the back ground intensity of membrane as shown in **Figure 6.6**. As shown in **Figure 6.5d**, the concentration of the charged lipids can be varied gradually from one corral to the other, being capable of producing a membrane array with different concentrations of the charged lipids. This architecture would be useful for constructing biosensors and developing bioassays for cell culture and growth [163].

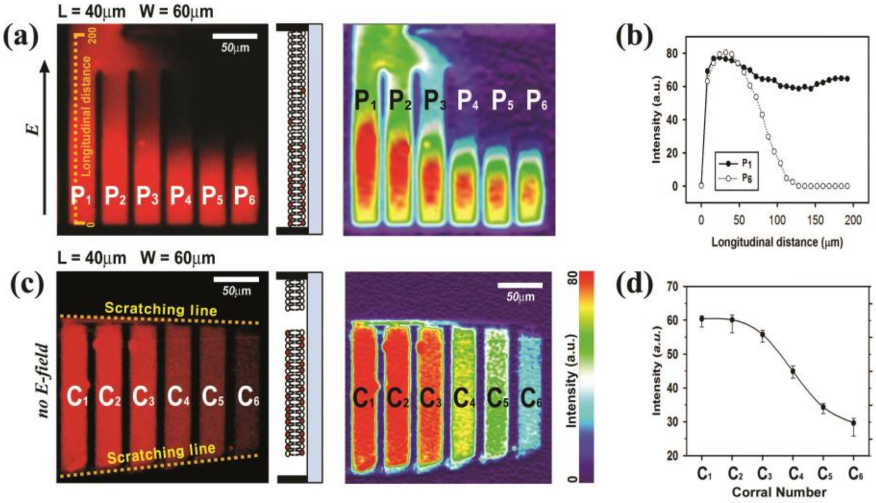

Figure 6.5 : (a) The micrograph showing the concentration gradients of charged lipids from one partition to other for L = 40 μm and W = 60 μm at the electric field of 45 V/cm for 25 min, (b) the concentration gradients measured at the lateral diffusion boundary in the first (P_1) and the last (P_6) partitions as a function the longitudinal distance, (c) the micrograph showing the confinement of the charged lipids in the corrals with different concentrations by mechanical scratching after the removal of the electric field for 1 h, and (d) the fluorescence intensities and the calculated concentrations of the charged lipids in the corrals from C_1 to C_6.

Author developed a viable, cost-effective scheme of constructing a spatially addressed membrane microarray with different concentrations of charged lipids in a supported bilayer from the field-directed diffusion dynamics. In contrast to a direct contact method such as the stamping process [16], our methodology presented here opens a new door to the manipulation of the lipid compositions in the SLB systems and the construction of spatially addressed membrane microarrays with different concentrations of the charged lipids since the field-directed diffusion approach handles the charged lipids in the fluid state in a non-destructive way. Moreover, the partitioning concept presented here can be implemented into microfluidic devices for sorting and positioning colloidal particles [171] and protein molecules [161] using soft lithographic techniques [172, 173].

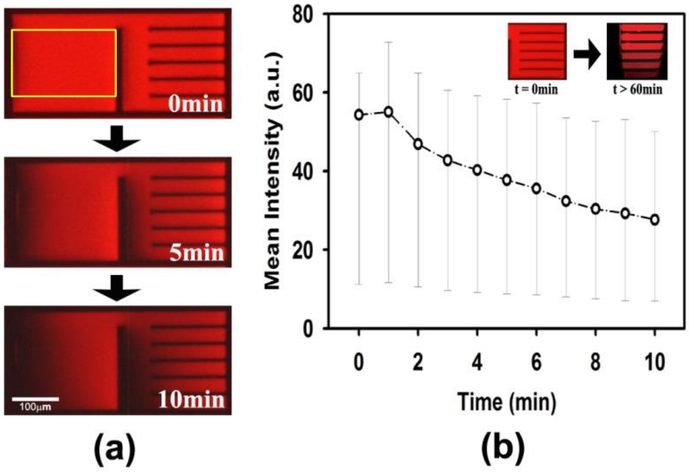

Figure 6.6 : Effect of self-quenching by frequent exposure to laser source. (a) time dependent fluorescent quenching of Texas-red dyes and (b) its representative graphs in time sequence.

6.3 Discussion & Conclusion

In this thesis, viable approaches to spatial manipulation of model membrane components into micro-scaled distinct domains on the solid supports by controlling interfacial interactions, which are investigated from the view point of fundamental physics and potential applications. The intrinsic properties such as adhesion force, interfacial energy, elasticity, spontaneous curvature, electric field, are manipulated by surface micro-templates to organize the membrane components, and colloidal particles in a site selective manner for broad applications of the materials at easy.

In the line with elasticity-based approach to the patterned growth of the raft assembly into spatial regions, geometrically patterned structure induce loop-like raft domain for the first time in model membrane system. Molecular shapes of raft domain prefer to locate at the curved surface for release elastic energy of a patch of membrane which provides lateral diffusions of lipid molecules without any disruption. Another example of approach to organization of patterned assemblies of raft on the solid supports is surface energy-driven construction of raft domains. Author shows binary membrane morphology, appositional formation of lipid monolayer and bilayer maintaining fluidity and continuity within a membrane. Stamping the dry polydimethylsiloxane (S-PDMS) mold on the hydroxylated glass offers sufficient hydrophobicity for generating lipid monolayer morphologies surrounded by unstamped lipid bilayer morphologies without any disruptions and lipid-free regions and consequent introduction of raft component-involved vesicle lead phase separation into liquid ordered domains on stamped regions. This morphological character due to continuity of membrane between monolayer and bilayer regions provides the robust platforms to solve the fundamental question of lipid rafts. That is, how the raft domain generate within the membrane. S-PDMS transfer method and additional injection of secondary vesicle was used for formation of heterogeneous membrane which involves sphingo lipids and cholesterol at each region. Furthermore, by reconstructing heterogeneous membrane which force to phase-separating the L_O domain at expected space, we could observed kinetic of model membrane into raft real-time by surface plasmon resonance on the Au covered glassy substrate.

Another example of approach to the manipulation of lipid molecules is the electric field-directed diffusion of charged lipids in supported membranes for spatially addressed microarrays. Field-directed diffusion of charged phospholipids in supported bilayer membranes into distributed partitions in a diffusion cell is shown. The balance between the field-induced drift and the thermal Brownian motion generates the concentration gradient of the charged lipids from partition to partition under an external electric field applied longitudinal to the partition walls. The concentration gradient across the partitions was found to primarily depend on the pore width and the distance between the pore and the partition wall. This field-directed diffusion approach provides a powerful tool for constructing various spatially addressed membrane arrays.

In conclusion, throughout this thesis, the reorganization of signal molecules on the model membrane has been extensively explored from the viewpoint of physical studies and device applications. The experimental/ theoretical analysis and several device concepts demonstrated here will provide a versatile platform for wide range of future applications by broaden the understandings of the raft domains and by applying as an microarray combined with raft-recognized proteins.

Chapter 7. Concluding Remarks

The **Chapter 1** overview the properties of lipid membrane, especially focused on the supported lipid bilayers as an artificial membrane and micro-patterning of cell components. Among the various characters of lipid membrane, lipid rafts, as one of typical signal molecules that composed of SPMs and CHOLs, and their interaction with solid supports are overviewed in the physicochemical view. As an another typical molecules which deeply related to signaling process, importance and Photolithograpy based membrane patterning of charge lipids introduced as well.

In **Chapter 2**, elasticity-based structural organization of artificial lipid membranes is discussed in the view point of the scientific studies and device application. The concept of competition between elasticity and adhesion of membranes on substrates with bud-pits like template possessing nanoscale curved surface will show the closed loop type raft domain at the corner of bud-neck like regions. Moreover, site selective ligand-receptor binding events on the raft domain with marker proteins are also demonstrated for biosensor applications.

Chapter 3 presents the binary membrane morphology, appositional formation of lipid monolayer and bilayer maintaining fluidity and continuity within a membrane. Stamping the dry polydimethylsiloxane (S-PDMS) mold on the hydroxylated glass offers sufficient hydrophobicity for generating lipid monolayer morphologies surrounded by unstamped lipid bilayer morphologies without any disruptions and lipid-free regions. Author demonstrated that our continuous binary supported membrane (CBSM) shows preferential localization of the signal lipids into ‘weak’ hydrophobic regions, and consequently generation of raft domains demonstrated by additional protein binding.

Chapter 4 deals with the formative hypotheses of raft domain which has not been demonstrated clearly till now. Although it is obvious that combination of signal molecules, SPMs and CHOLs, is essential for generation of raft domain, not any groups directly observe the correlation between SPMs and CHOLs. Especially how the key components combine and how they cluster into micro domains is unclear since 1972. Author will discuss the plausible mechanism of raft generation at the viewpoint of molecular level and demonstrate the hypotheses by experimental observation. Author found the evidences of CHOL intercalation in raft formation for the first time and demonstrate it with our in vitro model membrane system.

In **Chapter 5**, we probed the real-time membrane formation and reconstitution of L_O domains within a fluid membrane for the first time by means of time-lapse epifluorescence microscopy coupled to the SPR microscopy. The uniqueness of this combinatorial spectroscopic technique is that it allows to monitor the structural parameters of raft domains such as packing density, refractive index (RI) of raft domains within the lipid bilayer both kinetic state and equilibrium mode. Distinguished from other sensing techniques of membrane bounded SPR devices, our systematic conformations of heterogeneous membrane force the L_O domains to aggregate at programmed position which enable the observations of phase-kinetics during raft formations.

In **Chapter 6**, we demonstrated the field-directed diffusion of charged phospholipids in supported bilayer membranes into distributed partitions in a diffusion cell. The balance between the field-induced drift and the thermal Brownian motion generates the concentration gradient of the charged lipids from partition to partition under an external electric field applied longitudinal to the partition walls. Our field-directed diffusion approach provides a powerful tool for constructing various spatially addressed membrane arrays.

Through the manipulation of signal molecules, our model membrane based approaches will provide a robust platform not only for understanding biological activities, but for designing highly sensitive patterned membrane arrays which could be applicable to DNA, RNA or proteins for gene therapy or protein arrays.

Bibliography

[1] P. S. Cremer, J. T. Groves, L. A. Kung and S. G. Boxer, "Writing and Erasing Barriers to Lateral Mobility into Fluid Phospholipid Bilayers", *Langmuir*, vol. **15**, no. 11, pp. 3893-3896, (1999).

[2] H. A. Lucero and P. W. Robbins, "Lipid rafts–protein association and the regulation of protein activity", *Archives of Biochemistry and Biophysics*, vol. **426**, no. 2, pp. 208-224, (2004).

[3] P. S. Cremer and S. G. Boxer, "Formation and Spreading of Lipid Bilayers on Planar Glass Supports", *The Journal of Physical Chemistry B*, vol. **103**, no. 13, pp. 2554-2559, (1999).

[4] C. K. Yee, M. L. Amweg and A. N. Parikh, "Membrane Photolithography: Direct Micropatterning and Manipulation of Fluid Phospholipid Membranes in the Aqueous Phase Using Deep-UV Light", *Advanced Materials*, vol. **16**, no. 14, pp. 1184-1189, (2004).

[5] M. Blaxter, "Molecular systematics: Counting angels with DNA", *Nature*, vol. **421**, no. 6919, pp. 122-124, (2003).

[6] C. T. Clelland, V. Risca and C. Bancroft, "Hiding messages in DNA microdots", *Nature*, vol. **399**, no. 6736, pp. 533-534, (1999).

[7] J. P. L. Cox, "Long-term data storage in DNA", *Trends in Biotechnology*, vol. **19**, no. 7, pp. 247-250, (2001).

[8] J. P. L. Cox, "Bar coding objects with DNA", *Analyst*, vol. **126**, no. 5, pp. 545-547, (2001).

[9] N. Winssinger, J. L. Harris, B. J. Backes and P. G. Schultz, "From Split-Pool Libraries to Spatially Addressable Microarrays and Its Application to Functional Proteomic Profiling", *Angewandte Chemie International Edition*, vol. **40**, no. 17, pp. 3152-3155, (2001).

[10] J. S. Hovis and S. G. Boxer, "Patterning Barriers to Lateral Diffusion in Supported Lipid Bilayer Membranes by Blotting and Stamping", *Langmuir*, vol. **16**, no. 3, pp. 894-897, (2000).

[11] J. T. Groves and S. G. Boxer, "Micropattern Formation in Supported Lipid Membranes", *Accounts of Chemical Research*, vol. **35**, no. 3, pp. 149-157, (2002).

[12] L. Kam and S. G. Boxer, "Cell adhesion to protein-micropatterned-supported lipid bilayer membranes", *Journal of Biomedical Materials Research*, vol. **55**, no. 4, pp. 487-495, (2001).

[13] C. Lonez, M. Vandenbranden and J.-M. Ruysschaert, "Cationic liposomal lipids: From gene carriers to cell signaling", *Progress in Lipid Research*, vol. **47**, no. 5, pp. 340-347, (2008).

[14] R. Lill, W. Dowhan and W. Wickner, "The ATPase activity of SecA is regulated by acidic phospholipids, SecY, and the leader and mature domains of precursor proteins", *Cell*, vol. **60**, no. 2, pp. 271-280, (1990).

[15] Z. Fan and J. C. Makielski, "Phosphoinositides Decrease Atp Sensitivity of the Cardiac Atp-Sensitive K+ Channel: A Molecular Probe for the Mechanism of Atp-Sensitive Inhibition", *The Journal of General Physiology*, vol. **114**, no. 2, pp. 251-270, (1999).

[16] L. A. Kung, J. T. Groves, N. Ulman and S. G. Boxer, "Printing via photolithography on micropartitioned fluid lipid membranes", *Advanced materials*, vol. **12**, no. 10, pp. 731-734, (2000).

[17] J. S. Hovis and S. G. Boxer, "Patterning and composition arrays of supported lipid bilayers by microcontact printing", *Langmuir*, vol. **17**, no. 11, pp. 3400-3405, (2001).

[18] L. Kam and S. G. Boxer, "Formation of supported lipid bilayer composition arrays by controlled mixing and surface capture", *JOURNAL-AMERICAN CHEMICAL SOCIETY*, vol. **122**, no. 51, pp. 12901-12902, (2000).

[19] A. Van Oudenaarden and S. G. Boxer, "Brownian ratchets: molecular separations in lipid bilayers supported on patterned arrays", *Science*, vol. **285**, no. 5430, pp. 1046-1048, (1999).

[20] S. J. Singer and G. L. Nicolson, "The Fluid Mosaic Model of the Structure of Cell Membranes", *Science*, vol. **175**, no. 4023, pp. 720-731, (1972).

[21] J. Yu, D. A. Fischman and T. L. Steck, "Selective solubilization of proteins and phospholipids from red blood cell membranes by nonionic detergents", *Journal of Supramolecular Structure*, vol. **1**, no. 3, pp. 233-248, (1973).

[22] G. Van Meer, B. J. H. M. Poorthuis, K. W. A. Wirtz, J. A. F. Op Den Kamp and L. L. M. Van Deenen, "Transbilayer Distribution and Mobility of Phosphatidylcholine in Intact Erythrocyte Membranes", *European Journal of Biochemistry*, vol. **103**, no. 2, pp. 283-288, (1980).

[23] G. van Meer, E. H. Stelzer, R. W. Wijnaendts-van-Resandt and K. Simons, "Sorting of sphingolipids in epithelial (Madin-Darby canine

kidney) cells", *The Journal of Cell Biology*, vol. **105**, no. 4, pp. 1623-1635, (1987).

[24] M. P. Lisanti, M. Sargiacomo, L. Graeve, A. R. Saltiel and E. Rodriguez-Boulan, "Polarized apical distribution of glycosyl-phosphatidylinositol-anchored proteins in a renal epithelial cell line", *Proceedings of the National Academy of Sciences*, vol. **85**, no. 24, pp. 9557-9561, (1988).

[25] D. A. Brown and J. K. Rose, "Sorting of GPI-anchored proteins to glycolipid-enriched membrane subdomains during transport to the apical cell surface", *Cell*, vol. **68**, no. 3, pp. 533-544, (1992).

[26] L. J. Pike, "Rafts defined: a report on the Keystone symposium on lipid rafts and cell function", *Journal of Lipid Research*, vol. **47**, no. 7, pp. 1597-1598, (2006).

[27] S. Mukherjee and F. R. Maxfield, "Role of Membrane Organization and Membrane Domains in Endocytic Lipid Trafficking", *Traffic*, vol. **1**, no. 3, pp. 203-211, (2000).

[28] A. J. García-Sáez, S. Chiantia and P. Schwille, "Effect of Line Tension on the Lateral Organization of Lipid Membranes", *Journal of Biological Chemistry*, vol. **282**, no. 46, pp. 33537-33544, (2007).

[29] Y. Sakuma, T. Taniguchi and M. Imai, "Pore Formation in a Binary Giant Vesicle Induced by Cone-Shaped Lipids", *Biophysical Journal*, vol. **99**, no. 2, pp. 472-479, (2010).

[30] W. B. Huttner and J. Zimmerberg, "Implications of lipid microdomains for membrane curvature, budding and fission: Commentary", *Current Opinion in Cell Biology*, vol. **13**, no. 4, pp. 478-484, (2001).

[31] P. Waring, D. Lambert, A. Sjaarda, A. Hurne and J. Beaver, "Increased cell surface exposure of phosphatidylserine on propidium iodide negative thymocytes undergoing death by necrosis", *Cell death and differentiation*, vol. **6**, no. 7, pp. 624-637, (1999).

[32] A. Filippov, G. Orädd and G. Lindblom, "Sphingomyelin Structure Influences the Lateral Diffusion and Raft Formation in Lipid Bilayers", *Biophysical Journal*, vol. **90**, no. 6, pp. 2086-2092, (2006).

[33] E. London and D. A. Brown, "Insolubility of lipids in Triton X-100: physical origin and relationship to sphingolipid/cholesterol membrane domains (rafts)", *Biochimica et Biophysica Acta (BBA) - Biomembranes*, vol. **1508**, no. 1–2, pp. 182-195, (2000).

[34] C. Möller, D. Fotiadis, K. Suda, A. Engel, M. Kessler and D. J. Müller, "Determining molecular forces that stabilize human aquaporin-1", *Journal of Structural Biology*, vol. **142**, no. 3, pp. 369-378, (2003).

[35] R. M. Henderson, J. M. Edwardson, N. A. Geisse and D. E. Saslowsky, "Lipid Rafts: Feeling is Believing", *Physiology*, vol. **19**, no. 2, pp. 39-43, (2004).

[36] H. Sprong, P. van der Sluijs and G. van Meer, "How proteins move lipids and lipids move proteins", *Nat Rev Mol Cell Biol*, vol. **2**, no. 7, pp. 504-513, (2001).

[37] H. T. McMahon and J. L. Gallop, "Membrane curvature and mechanisms of dynamic cell membrane remodelling", *Nature*, vol. **438**, no. 7068, pp. 590-596, (2005).

[38] K. Simons and M. J. Gerl, "Revitalizing membrane rafts: new tools and insights", *Nature Reviews Molecular Cell Biology*, vol. **11**, no. 10, pp. 688-699, (2010).

[39] V. Michel and M. Bakovic, "Lipid rafts in health and disease", *Biology of the Cell*, vol. **99**, no. 3, pp. 129-140, (2007).

[40] T.-Y. Yoon, C. Jeong, S.-W. Lee, J. H. Kim, M. C. Choi, S.-J. Kim, M. W. Kim and S.-D. Lee, "Topographic control of lipid-raft reconstitution in model membranes", *Nat Mater*, vol. **5**, no. 4, pp. 281-285, (2006).

[41] A. B. Subramaniam, S. Lecuyer, K. S. Ramamurthi, R. Losick and H. A. Stone, "Particle/Fluid Interface Replication as a Means of Producing Topographically Patterned Polydimethylsiloxane Surfaces for Deposition of Lipid Bilayers", *Advanced Materials*, vol. **22**, no. 19, pp. 2142-2147, (2010).

[42] Y. Kaizuka and J. T. Groves, "Bending-mediated superstructural organizations in phase-separated lipid membranes", *New Journal of Physics*, vol. **12**, no. pp. 11, (2010).

[43] G. P. Leser and R. A. Lamb, "Influenza virus assembly and budding in raft-derived microdomains: a quantitative analysis of the surface distribution of HA, NA and M2 proteins", *Virology*, vol. **342**, no. 2, pp. 215, (2005).

[44] E. Ikonen, "Roles of lipid rafts in membrane transport", *Current opinion in cell biology*, vol. **13**, no. 4, pp. 470-477, (2001).

[45] L. J. Pike, "Lipid rafts: bringing order to chaos", *Journal of Lipid Research*, vol. **44**, no. 4, pp. 655-667, (2003).

[46] H. Gao, W. Shi and L. B. Freund, "Mechanics of receptor-mediated endocytosis", *Proceedings of the National Academy of Sciences of the United States of America*, vol. **102**, no. 27, pp. 9469-9474, (2005).

[47] B. J. Reynwar, G. Illya, V. A. Harmandaris, M. M. Müller, K. Kremer and M. Deserno, "Aggregation and vesiculation of membrane proteins by curvature-mediated interactions", *Nature*, vol. **447**, no. 7143, pp. 461-464, (2007).

[48] L. D. Renner and D. B. Weibel, "Cardiolipin microdomains localize to negatively curved regions of Escherichia coli membranes", *Proceedings of the National Academy of Sciences*, vol. **108**, no. 15, pp. 6264-6269, (2011).

[49] B. Windschiegl, A. Orth, W. Römer, L. Berland, B. Stechmann, P. Bassereau, L. Johannes and C. Steinem, "Lipid reorganization induced by Shiga toxin clustering on planar membranes", *PLoS One*, vol. **4**, no. 7, pp. e6238, (2009).

[50] H. Ewers, *et al.*, "GM1 structure determines SV40-induced membrane invagination and infection", *Nat Cell Biol*, vol. **12**, no. 1, pp. 11-18, (2010).

[51] R. Parthasarathy and J. T. Groves, "Curvature and spatial organization in biological membranes", *Soft Matter*, vol. **3**, no. 1, pp. 24-33, (2007).

[52] C. Jeong, S. W. Lee, T. Y. Yoon and S. D. Lee, "Water Meniscus-Directed Organization of Liquid-Ordered Domains in Lipid Monolayer", *Journal of Nanoscience and Nanotechnology*, vol. **11**, no. 5, pp. 4527-4531, (2011).

[53] C. Jeong, T. Y. Yoon, S. D. Lee, Y. G. Park and H. Kwon, "Patterning Process of Membrane-Associated Proteins on a Solid Support with Geometrical Grooves", *Molecular Crystals and Liquid Crystals*, vol. **434**, no. 1, pp. 297-303, (2005).

[54] M. C. Bélanger and Y. Marois, "Hemocompatibility, biocompatibility, inflammatory and in vivo studies of primary reference materials low-density polyethylene and polydimethylsiloxane: A review", *Journal of Biomedical Materials Research*, vol. **58**, no. 5, pp. 467-477, (2001).

[55] J. FÜLLEKRUG and K. Simons, "Lipid rafts and apical membrane traffic", *Annals of the New York Academy of Sciences*, vol. **1014**, no. 1, pp. 164-169, (2006).

[56] Y. S. Ryu, S. W. Lee, B. Lee and S. D. Lee, "Field-Directed Diffusion of Charged Lipids in Supported Membranes for Spatially Addressed

Microarrays", *Molecular Crystals and Liquid Crystals*, vol. **559**, no. 1, pp. 1-8, (2012).

[57] A. S. Dimitrov and K. Nagayama, "Continuous Convective Assembling of Fine Particles into Two-Dimensional Arrays on Solid Surfaces", *Langmuir*, vol. **12**, no. 5, pp. 1303-1311, (1996).

[58] S. C. Park, J. H. Na and S. D. Lee, "stability by thermal fixation for liquid crystal devices", *JOURNAL OF APPLIED PHYSICS*, vol. **112**, no. pp. 023104, (2012).

[59] I. J. Chen and E. Lindner, "The Stability of Radio-Frequency Plasma-Treated Polydimethylsiloxane Surfaces", *Langmuir*, vol. **23**, no. 6, pp. 3118-3122, (2007).

[60] B. T. Ginn and O. Steinbock, "Polymer surface modification using microwave-oven-generated plasma", *Langmuir*, vol. **19**, no. 19, pp. 8117-8118, (2003).

[61] B. Sanii, A. M. Smith, R. Butti, A. M. Brozell and A. N. Parikh, "Bending membranes on demand: Fluid phospholipid bilayers on topographically deformable substrates", *Nano letters*, vol. **8**, no. 3, pp. 866-871, (2008).

[62] G. H. Hansen, L.-L. Niels-Christiansen, E. Thorsen, L. Immerdal and E. M. Danielsen, "Cholesterol Depletion of Enterocytes: EFFECT ON THE GOLGI COMPLEX AND APICAL MEMBRANE TRAFFICKING", *Journal of Biological Chemistry*, vol. **275**, no. 7, pp. 5136-5142, (2000).

[63] S. M. Gruner, R. P. Lenk, A. S. Janoff and N. J. Ostro, "Novel multilayered lipid vesicles: comparison of physical characteristics of multilamellar liposomes and stable plurilamellar vesicles", *Biochemistry*, vol. **24**, no. 12, pp. 2833-2842, (1985).

[64] G. S. Attard, R. H. Templer, W. S. Smith, A. N. Hunt and S. Jackowski, "Modulation of CTP:phosphocholine cytidylyltransferase by membrane curvature elastic stress", *Proceedings of the National Academy of Sciences*, vol. **97**, no. 16, pp. 9032-9036, (2000).

[65] H. M. McConnell and A. Radhakrishnan, "Condensed complexes of cholesterol and phospholipids", *Biochimica et Biophysica Acta (BBA) - Biomembranes*, vol. **1610**, no. 2, pp. 159-173, (2003).

[66] R. G. W. Anderson and K. Jacobson, "A Role for Lipid Shells in Targeting Proteins to Caveolae, Rafts, and Other Lipid Domains", *Science*, vol. **296**, no. 5574, pp. 1821-1825, (2002).

[67] P. Oh, T. Horner, H. Witkiewicz and J. E. Schnitzer, "Endothelin induces rapid, dynamin-mediated budding of endothelial caveolae rich in ET-B", *Journal of Biological Chemistry*, vol. **287**, no. 21, pp. 17353-17362, (2012).

[68] Ü. Coskun and K. Simons, "Membrane rafting: from apical sorting to phase segregation", *FEBS letters*, vol. **584**, no. 9, pp. 1685-1693, (2010).

[69] Hernán E. Grecco, M. Schmick and Philippe I. H. Bastiaens, "Signaling from the Living Plasma Membrane", *Cell*, vol. **144**, no. 6, pp. 897-909, (2011).

[70] J. D. Thatcher, "Intercellular Transport", *Sci. Signal.*, vol. **6**, no. 271, pp. tr4-, (2013).

[71] N. C. Hartman and J. T. Groves, "Signaling clusters in the cell membrane", *Current Opinion in Cell Biology*, vol. **23**, no. 4, pp. 370-376, (2011).

[72] K. Simons and D. Toomre, "Lipid rafts and signal transduction", *Nature Reviews Molecular Cell Biology*, vol. **1**, no. 1, pp. 31-39, (2000).

[73] T. Pawson and J. D. Scott, "Signaling through scaffold, anchoring, and adaptor proteins", *Science*, vol. **278**, no. 5346, pp. 2075-2080, (1997).

[74] D. Brown and E. London, "Functions of lipid rafts in biological membranes", *Annual review of cell and developmental biology*, vol. **14**, no. 1, pp. 111-136, (1998).

[75] P. W. Janes, S. C. Ley, A. I. Magee and P. S. Kabouridis, "The role of lipid rafts in T cell antigen receptor (TCR) signalling", *Seminars in Immunology*, vol. **12**, no. 1, pp. 23-34, (2000).

[76] M. Dykstra, A. Cherukuri, H. W. Sohn, S. J. Tzeng and S. K. Pierce, "LOCATION IS EVERYTHING: Lipid Rafts and Immune Cell Signaling*", *Annual review of immunology*, vol. **21**, no. 1, pp. 457-481, (2003).

[77] E. Sezgin, *et al.*, "Partitioning, diffusion, and ligand binding of raft lipid analogs in model and cellular plasma membranes", *Biochimica et Biophysica Acta (BBA)-Biomembranes*, vol. no. pp. (2012).

[78] K. Jacobson, O. G. Mouritsen and R. G. W. Anderson, "Lipid rafts: at a crossroad between cell biology and physics", *Nature cell biology*, vol. **9**, no. 1, pp. 7-14, (2007).

[79] D. Lingwood and K. Simons, "Lipid Rafts As a Membrane-Organizing Principle", *Science*, vol. **327**, no. 5961, pp. 46-50, (2010).

[80] M. D. Collins and S. L. Keller, "Tuning lipid mixtures to induce or suppress domain formation across leaflets of unsupported asymmetric bilayers", *Proceedings of the National Academy of Sciences of the United States of America*, vol. **105**, no. 1, pp. 124-128, (2008).

[81] V. N. Ngassam, M. C. Howland, A. Sapuri-Butti, N. Rosidi and A. N. Parikh, "A comparison of detergent action on supported lipid monolayers and bilayers", *Soft Matter*, vol. **8**, no. 14, pp. 3734-3738, (2012).

[82] X. J. Han, M. R. Cheetham, K. Sheikh, P. D. Olmsted, R. J. Bushby and S. D. Evans, "Manipulation and charge determination of proteins in photopatterned solid supported bilayers", *Integrative Biology*, vol. **1**, no. 2, pp. 205-211, (2009).

[83] M. C. Howland, A. R. Sapuri-Butti, S. S. Dixit, A. M. Dattelbaum, A. P. Shreve and A. N. Parikh, "Phospholipid morphologies on photochemically patterned silane monolayers", *Journal of the American Chemical Society*, vol. **127**, no. 18, pp. 6752-6765, (2005).

[84] P. Lenz, C. M. Ajo-Franklin and S. G. Boxer, "Patterned supported lipid bilayers and monolayers on poly(dimethylsiloxane)", *Langmuir*, vol. **20**, no. 25, pp. 11092-11099, (2004).

[85] S. E. Feller, Y. H. Zhang and R. W. Pastor, "Computer-Simulation of Liquid/Liquid Interfaces .2. Surface-Tension Area Dependence of a Bilayer and Monolayer", *Journal of Chemical Physics*, vol. **103**, no. 23, pp. 10267-10276, (1995).

[86] K. Glasmastar, J. Gold, A. S. Andersson, D. S. Sutherland and B. Kasemo, "Silicone transfer during microcontact printing", *Langmuir*, vol. **19**, no. 13, pp. 5475-5483, (2003).

[87] L. Yang, *et al.*, "Effect of Surface Free Energy on PDMS Transfer in Microcontact Printing and Its Application to ToF-SIMS to Probe Surface Energies", *Langmuir*, vol. **25**, no. 10, pp. 5674-5683, (2009).

[88] A. L. Briseno, M. Roberts, M. M. Ling, H. Moon, E. J. Nemanick and Z. N. Bao, "Patterning organic semiconductors using "dry" poly(dimethylsiloxane) elastomeric stamps for thin film transistors", *Journal of the American Chemical Society*, vol. **128**, no. 12, pp. 3880-3881, (2006).

[89] S. Kim, Ryu, Y-S, Suh, J-H, Keum, C-M, Sohn, Y, Lee, S-D, "Biocompatible Patterning of Proteins on Wettability Gradient

Surface by Thermo-Transfer Printing", *Journal of Nanoscience and Nanotechnology*, vol. **in press**, no. pp. (2012).

[90] B. Kasemo, "Biological surface science", *Surface Science*, vol. **500**, no. 1-3, pp. 656-677, (2002).

[91] M. Tanaka and E. Sackmann, "Polymer-supported membranes as models of the cell surface", *Nature*, vol. **437**, no. 7059, pp. 656-663, (2005).

[92] L. K. Tamm and H. M. Mcconnell, "Supported Phospholipid-Bilayers", *Biophysical Journal*, vol. **47**, no. 1, pp. 105-113, (1985).

[93] J. W. Park and G. U. Lee, "Properties of mixed lipid monolayers assembled on hydrophobic surfaces through vesicle adsorption", *Langmuir*, vol. **22**, no. 11, pp. 5057-5063, (2006).

[94] N. K. Adam and G. E. P. Elliott, "Contact Angles of Water against Saturated Hydrocarbons", *Journal of the Chemical Society*, vol. no. Jun, pp. 2206-&, (1962).

[95] R. Ziblat, K. Kjaer, L. Leiserowitz and L. Addadi, "Structure of Cholesterol/Lipid Ordered Domains in Monolayers and Single Hydrated Bilayers", *Angewandte Chemie-International Edition*, vol. **48**, no. 47, pp. 8958-8961, (2009).

[96] X. J. Wang, M. Ostblom, T. Johansson and O. Inganas, "PEDOT surface energy pattern controls fluorescent polymer deposition by dewetting", *Thin Solid Films*, vol. **449**, no. 1-2, pp. 125-132, (2004).

[97] A. L. Plant, "Supported hybrid bilayer membranes as rugged cell membrane mimics", *Langmuir*, vol. **15**, no. 15, pp. 5128-5135, (1999).

[98] S. J. Johnson, T. M. Bayerl, D. C. Mcdermott, G. W. Adam, A. R. Rennie, R. K. Thomas and E. Sackmann, "Structure of an Adsorbed Dimyristoylphosphatidylcholine Bilayer Measured with Specular Reflection of Neutrons", *Biophysical Journal*, vol. **59**, no. 2, pp. 289-294, (1991).

[99] H. H. Cao, N. Tokutake and S. L. Regen, "Unraveling the mystery surrounding cholesterol's condensing effect", *Journal of the American Chemical Society*, vol. **125**, no. 52, pp. 16182-16183, (2003).

[100] N. N. Vlasova and L. P. Golovkova, "Effect of bile salts on adsorption of cholesterol on silica adsorbent", *Colloid Journal*, vol. **71**, no. 4, pp. 474-479, (2009).

[101] S. W. Lee, Y. J. Na and S. D. Lee, "Nondisruptive Micropatterning of Fluid Membranes through Selective Vesicular Adsorption and

Rupture by Nanotopography", *Langmuir,* vol. **25**, no. 10, pp. 5421-5425, (2009).

[102] J. A. Wigenius, M. Hamedi and O. Inganas, "Limits to nanopatterning of fluids on surfaces in soft lithography", *Advanced Functional Materials*, vol. **18**, no. 17, pp. 2563-2571, (2008).

[103] K. Liu, Y. Tian, R. Pitchimani, M. Huang, H. Lincoln and D. Pappasa, "Characterization of PDMS-modified glass from cast-and-peel fabrication", *Talanta*, vol. **79**, no. 2, pp. 333-338, (2009).

[104] T. Okazaki, Y. Tatsu and K. Morigaki, "Phase separation of lipid microdomains controlled by polymerized lipid bilayer matrices", *Langmuir,* vol. **26**, no. 6, pp. 4126-4129, (2009).

[105] M. Jung, N. Vogel and I. Köper, "Nanoscale Patterning of Solid-Supported Membranes by Integrated Diffusion Barriers", *Langmuir*, vol. **27**, no. 11, pp. 7008-7015, (2011).

[106] G. J. Vrije, A. Batenburg, J. Killian and B. Kruijff, "Lipid involvement in protein translocation in Escherichia coli", *Molecular microbiology*, vol. **4**, no. 1, pp. 143-150, (2006).

[107] J. T. Buboltz and G. W. Feigenson, "A novel strategy for the preparation of liposomes: rapid solvent exchange", *Biochimica Et Biophysica Acta-Biomembranes*, vol. **1417**, no. 2, pp. 232-245, (1999).

[108] J. H. Kim, B. H. Lee, H. Kang, J. Kim, G. Chae, I. Kang and I. J. Chung, "Self-assembly of Ag nanopowder on OTS-patterned glass", *Applied Surface Science*, vol. **255**, no. 23, pp. 9386-9390, (2009).

[109] A. Pralle, P. Keller, E. L. Florin, K. Simons and J. K. H. Horber, "Sphingolipid-cholesterol rafts diffuse as small entities in the plasma membrane of mammalian cells", *Journal of Cell Biology*, vol. **148**, no. 5, pp. 997-1007, (2000).

[110] T. Harder and K. Simons, "Caveolae, DIGs, and the dynamics of sphingolipid—cholesterol microdomains", *Current opinion in cell biology*, vol. **9**, no. 4, pp. 534-542, (1997).

[111] D. M. Engelman and J. E. Rothman, "The Planar Organization of Lecithin-Cholesterol Bilayers", *Journal of Biological Chemistry*, vol. **247**, no. 11, pp. 3694-3697, (1972).

[112] D. Bach, N. Borochov and E. Wachtel, "Phase separation of cholesterol in dimyristoyl phosphatidylserine cholesterol mixtures", *Chemistry and Physics of Lipids*, vol. **92**, no. 1, pp. 71-77, (1998).

[113] T. N. Tulenko, M. Chen, P. E. Mason and R. P. Mason, "Physical effects of cholesterol on arterial smooth muscle membranes: evidence of immiscible cholesterol domains and alterations in bilayer width during atherogenesis", *Journal of Lipid Research*, vol. **39**, no. 5, pp. 947-956, (1998).

[114] M. D. Houslay and K. K. Stanley, "Dynamics of biological membranes: influence on synthesis, structure, and function", Wiley New York, viii, 330 p., (1982).

[115] R. Preston Mason, T. N. Tulenko and R. F. Jacob, "Direct evidence for cholesterol crystalline domains in biological membranes: role in human pathobiology", *Biochimica et Biophysica Acta (BBA) - Biomembranes*, vol. **1610**, no. 2, pp. 198-207, (2003).

[116] R. E. Brown, "Sphingolipid organization in biomembranes: what physical studies of model membranes reveal", *Journal of Cell Science*, vol. **111**, no. pp. 1-9, (1998).

[117] G. A. Khelashvili and H. L. Scott, "Combined Monte Carlo and molecular dynamics simulation of hydrated 18 : 0 sphingomyelin-cholesterol lipid bilayers", *Journal of Chemical Physics*, vol. **120**, no. 20, pp. 9841-9847, (2004).

[118] R. Bittman, C. R. Kasireddy, P. Mattjus and J. P. Slotte, "Interaction of Cholesterol with Sphingomyelin in Monolayers and Vesicles", *Biochemistry*, vol. **33**, no. 39, pp. 11776-11781, (1994).

[119] F. R. Maxfield and I. Tabas, "Role of cholesterol and lipid organization in disease", *Nature*, vol. **438**, no. 7068, pp. 612-621, (2005).

[120] A. Pandey and M. Mann, "Proteomics to study genes and genomes", *Nature*, vol. **405**, no. 6788, pp. 837-846, (2000).

[121] S. Fodor, R. P. Rava, X. C. Huang, A. C. Pease, C. P. Holmes and C. L. Adams, "Multiplexed biochemical assays with biological chips", *Nature*, vol. **364**, no. pp. 555-556, (1993).

[122] G. A. Michaud and M. Snyder, "Proteomic approaches for the global analysis of proteins", *Biotechniques*, vol. **33**, no. 6, pp. 1308-1317, (2002).

[123] M. R. Wenk, "The emerging field of lipidomics", *Nature Reviews Drug Discovery*, vol. **4**, no. 7, pp. 594-610, (2005).

[124] J. T. Groves, S. G. Boxer and H. M. McConnel, "Electric field-induced reorganization of two-component supported bilayer

membranes", *Proceedings of the National Academy of Sciences of the United States of America*, vol. **94**, no. 25, pp. 13390-13395, (1997).

[125] C. H. Yu, A. N. Parikh and J. T. Groves, "Direct patterning of membrane-derivatized colloids using in-situ UV-ozone photolithography", *Advanced Materials*, vol. **17**, no. 12, pp. 1477-1480, (2005).

[126] Y. S. Ryu, "Insight into cellular signal pathways from ligand-receptor binding across monolayer-bilayer junction in model membrane", *Natue Materials*, vol. **to be submitted**, no. pp. xxx-xxx, (2013).

[127] D. A. Brown and E. London, "Structure and Function of Sphingolipid- and Cholesterol-rich Membrane Rafts", *Journal of Biological Chemistry*, vol. **275**, no. 23, pp. 17221-17224, (2000).

[128] E. Sackmann and H. Trauble, "Studies of Crystalline-Liquid Crystalline Phase-Transition of Lipid Model Membranes .1. Use of Spin Labels and Optical Probes as Indicators of Phase-Transition", *Journal of the American Chemical Society*, vol. **94**, no. 13, pp. 4482-&, (1972).

[129] C. Klein, T. Pillot, J. Chambaz and B. Drouet, "Determination of plasma membrane fluidity with a fluorescent analogue of sphingomyelin by FRAP measurement using a standard confocal microscope", *Brain Research Protocols*, vol. **11**, no. 1, pp. 46-51, (2003).

[130] A. V. Filippov, M. A. Rudakova and B. V. Munavirov, "Lateral diffusion in sphingomyelin bilayers", *Magnetic Resonance in Chemistry*, vol. **48**, no. 12, pp. 945-950, (2010).

[131] C. Hamai, T. Yang, S. Kataoka, P. S. Cremer and S. M. Musser, "Effect of average phospholipid curvature on supported bilayer formation on glass by vesicle fusion", *Biophysical journal*, vol. **90**, no. 4, pp. 1241-1248, (2006).

[132] Y. {McIntosh, 1985 #310;Leonard, 1991 #309;Maxfield, 2005 #308;Maxfield, 2005 #307;Preston Mason, 2003 #305}McIntosh, T.J., "The effect of cholesterol on the structure of phosphatidylcholine bilayers", *Biochimica et biophysica acta*, vol. **513**, no. 1, pp. 43, (1978).

[133] P. L. Yeagle, "Cholesterol and the Cell-Membrane", *Biochimica Et Biophysica Acta*, vol. **822**, no. 3-4, pp. 267-287, (1985).

[134] A. Leonard and E. J. Dufourc, "Interactions of Cholesterol with the Membrane Lipid Matrix - a Solid-State Nmr Approach", *Biochimie*, vol. **73**, no. 10, pp. 1295-1302, (1991).

[135] J. Huang, C. Meyer and C. Zhu, "T cell antigen recognition at the cell membrane", *Molecular Immunology*, vol. **52**, no. 3–4, pp. 155-164, (2012).

[136] S. V. Evans and C. Roger MacKenzie, "Characterization of protein–glycolipid recognition at the membrane bilayer", *Journal of Molecular Recognition*, vol. **12**, no. 3, pp. 155-168, (1999).

[137] S. Scarano, M. Mascini, A. P. F. Turner and M. Minunni, "Surface plasmon resonance imaging for affinity-based biosensors", *Biosensors and Bioelectronics*, vol. **25**, no. 5, pp. 957-966, (2010).

[138] M. Beseničar, P. Maček, J. H. Lakey and G. Anderluh, "Surface plasmon resonance in protein–membrane interactions", *Chemistry and physics of lipids*, vol. **141**, no. 1, pp. 169-178, (2006).

[139] "Real-Time Analysis of Specific Protein-DNA Interactions with Surface Plasmon Resonance", *Journal of Amino Acids*, vol. **2012**, no. pp. (2012).

[140] K. S. Phillips, T. Wilkop, J.-J. Wu, R. O. Al-Kaysi and Q. Cheng, "Surface Plasmon Resonance Imaging Analysis of Protein-Receptor Binding in Supported Membrane Arrays on Gold Substrates with Calcinated Silicate Films", *Journal of the American Chemical Society*, vol. **128**, no. 30, pp. 9590-9591, (2006).

[141] J. T. Groves, "Unveiling the membrane domains", *Science(Washington)*, vol. **313**, no. 5795, pp. 1901-1902, (2006).

[142] M. C. Howland, A. W. Szmodis, B. Sanii and A. N. Parikh, "Characterization of physical properties of supported phospholipid membranes using imaging ellipsometry at optical wavelengths", *Biophysical journal*, vol. **92**, no. 4, pp. 1306-1317, (2007).

[143] R. L. Rich and D. G. Myszka, "Advances in surface plasmon resonance biosensor analysis", *Current Opinion in Biotechnology*, vol. **11**, no. 1, pp. 54-61, (2000).

[144] M. S. Lalonde and W. I. Sundquist, "How HIV finds the door", *Proceedings of the National Academy of Sciences*, vol. **109**, no. 46, pp. 18631-18632, (2012).

[145] P. Critchley, J. Kazlauskaite, R. Eason and T. J. T. Pinheiro, "Binding of prion proteins to lipid membranes", *Biochemical and Biophysical Research Communications*, vol. **313**, no. 3, pp. 559-567, (2004).

[146] P. Lajoie and I. R. Nabi, "Lipid rafts, caveolae, and their endocytosis", *International review of cell and molecular biology*, vol. **282**, no. pp. 135-163, (2010).

[147] D. J. Moore, R. G. Snyder, M. E. Rerek and R. Mendelsohn, "Kinetics of membrane raft formation: fatty acid domains in stratum corneum lipid models", *The Journal of Physical Chemistry B*, vol. **110**, no. 5, pp. 2378-2386, (2006).

[148] G. Margheri, R. D'Agostino, L. Becucci, R. Guidelli, B. Tiribilli and M. Del Rosso, "Surface plasmon resonance as detection tool for lipids lateral mobility in biomimetic membranes", *Biomedical optics express*, vol. **3**, no. 12, pp. 3119, (2012).

[149] R. A. Vijayendran, F. S. Ligler and D. E. Leckband, "A computational reaction-diffusion model for the analysis of transport-limited kinetics", *Analytical Chemistry*, vol. **71**, no. 23, pp. 5405-5412, (1999).

[150] Z. Salamon, S. Devanathan, I. D. Alves and G. Tollin, "Plasmon-waveguide resonance studies of lateral segregation of lipids and proteins into microdomains (rafts) in solid-supported bilayers", *Journal of Biological Chemistry*, vol. **280**, no. 12, pp. 11175-11184, (2005).

[151] L. A. Kung, L. Kam, J. S. Hovis and S. G. Boxer, "Patterning hybrid surfaces of proteins and supported lipid bilayers", *Langmuir*, vol. **16**, no. 17, pp. 6773-6776, (2000).

[152] H. Bayley and P. S. Cremer, "Stochastic sensors inspired by biology", *Nature*, vol. **413**, no. 6852, pp. 226-230, (2001).

[153] N. Winssinger, J. L. Harris, B. J. Backes and P. G. Schultz, "From Split-Pool Libraries to Spatially Addressable Microarrays and Its Application to Functional Proteomic Profiling", *Angewandte Chemie International Edition*, vol. **40**, no. 17, pp. 3152-3155, (2001).

[154] J. S. Yuk and K.-S. Ha, "Proteomic applications of surface plasmon resonance biosensors: analysis of protein arrays", *Exp Mol Med*, vol. **37**, no. pp. 1-10, (0000).

[155] S. Roh, T. Chung and B. Lee, "Overview of the characteristics of micro-and nano-structured surface plasmon resonance sensors", *Sensors*, vol. **11**, no. 2, pp. 1565-1588, (2011).

[156] H. Kim, I.-M. Lee and B. Lee, "Extended scattering-matrix method for efficient full parallel implementation of rigorous coupled-wave analysis", *JOSA A*, vol. **24**, no. 8, pp. 2313-2327, (2007).

[157] H. Kim, B. Lee and J. Park, "Fourier modal method and its applications in computational nanophotonics", CRC PressI Llc, (2012).

[158] Y. Rancon and J. Charvolin, "Epitaxial relationships during phase transformations in a lyotropic liquid crystal", *The Journal of Physical Chemistry*, vol. **92**, no. 9, pp. 2646-2651, (1988).

[159] P. Alexandridis, U. Olsson and B. Lindman, "A record nine different phases (four cubic, two hexagonal, and one lamellar lyotropic liquid crystalline and two micellar solutions) in a ternary isothermal system of an amphiphilic block copolymer and selective solvents (water and oil)", *Langmuir*, vol. **14**, no. 10, pp. 2627-2638, (1998).

[160] A. Grakoui, S. K. Bromley, C. Sumen, M. M. Davis, A. S. Shaw, P. M. Allen and M. L. Dustin, "The Immunological Synapse: A Molecular Machine Controlling T Cell Activation", *Science*, vol. **285**, no. 5425, pp. 221-227, (1999).

[161] K. A. Fosser and R. G. Nuzzo, "Fabrication of patterned multicomponent protein gradients and gradient arrays using microfluidic depletion", *Analytical chemistry*, vol. **75**, no. 21, pp. 5775-5782, (2003).

[162] J. T. Groves, C. Wülfing and S. G. Boxer, "Electrical manipulation of glycan-phosphatidyl inositol-tethered proteins in planar supported bilayers", *Biophysical journal*, vol. **71**, no. 5, pp. 2716-2723, (1996).

[163] J. T. Groves, L. K. Mahal and C. R. Bertozzi, "Control of cell adhesion and growth with micropatterned supported lipid membranes", *Langmuir*, vol. **17**, no. 17, pp. 5129-5133, (2001).

[164] E. W. Barrett, M. V. B. Phelps, R. J. Silva, R. P. Gaumond and H. R. Allcock, "Patterning poly (organophosphazenes) for selective cell adhesion applications", *Biomacromolecules*, vol. **6**, no. 3, pp. 1689-1697, (2005).

[165] J. Nakanishi, Y. Kikuchi, S. Inoue, K. Yamaguchi, T. Takarada and M. Maeda, "Spatiotemporal Control of Migration of Single Cells on a Photoactivatable Cell Microarray", *Journal of the American Chemical Society*, vol. **129**, no. 21, pp. 6694-6695, (2007).

[166] H. Baier and F. Bonhoeffer, "Axon guidance by gradients of a target-derived component", *Science*, vol. **255**, no. 5043, pp. 472-475, (1992).

[167] D. M. Knapp, E. F. Helou and R. T. Tranquillo, "A fibrin or collagen gel assay for tissue cell chemotaxis: assessment of fibroblast chemotaxis to GRGDSP", *Experimental cell research*, vol. **247**, no. 2, pp. 543-553, (1999).

[168] P. S. Cremer and T. Yang, "Creating Spatially Addressed Arrays of Planar Supported Fluid Phospholipid Membranes", *Journal of the American Chemical Society*, vol. **121**, no. 35, pp. 8130-8131, (1999).

[169] S. W. Lee, C. Jeong and S. D. Lee, "Elasticity-Based Patterning of Red Blood Cells on Undulated Lipid Membranes Supported on Porous Topographic Substrates†", *The Journal of Physical Chemistry B*, vol. **113**, no. 12, pp. 3610-3614, (2008).

[170] T. Y. Yoon, C. Jeong, J. H. Kim, M. C. Choi, M. W. Kim and S. D. Lee, "Spontaneous aggregation of lipids in supported membranes with geometrical barriers", *Applied surface science*, vol. **238**, no. 1, pp. 299-303, (2004).

[171] Y.-J. Na, T.-Y. Yoon, S. Park, B. Lee and S.-D. Lee, "Electrically Programmable Nematofluidics with a High Level of Selectivity in a Hierarchically Branched Architecture", *ChemPhysChem*, vol. **11**, no. 1, pp. 101-104, (2010).

[172] S. Haeberle and R. Zengerle, "Microfluidic platforms for lab-on-a-chip applications", *Lab on a Chip*, vol. **7**, no. 9, pp. 1094-1110, (2007).

[173] Y. Xia and G. M. Whitesides, "Soft lithography", *Annual review of materials science*, vol. **28**, no. 1, pp. 153-184, (1998).

Publication

[1] International Journals

1. **Y.-S. Ryu**, S.-W. Lee, B. Lee and S.-D. Lee, "Field-directed diffusion of charged lipids in supported membranes for spatially addressed microarrays", Mol. Cryst. Liq. Cryst. 559, 1-8, (2012)
2. S. Kim, **Y.-S. Ryu**, J.-H. Suh, C.-M. Keum, Y. Sohn and S.-D. Lee, "Biocompatible Patterning of Proteins on Authorttability Gradient Surface by Thermo-Transfer Printing", *J. Nanosci. Nanotechnol*. (in press)
3. **Y.-S. Ryu**, S.-W. Lee, B. Lee, J. Suh, Y. Sohn and S.-D. Lee "Critical reconstitution of lipid rafts and protein-binding in model monolayer-bilayer membranes" to be submitted.
4. **Y.-S. Ryu**, I.-H. Lee, J.-H. Suh, S. Oh, B. Lee, N.L. Jeon, and S.-D. Lee "Curvature-dictated assembly of lipid bilayers into 3-dimensional closed loops for raft formation and protein-binding" to be submitted
5. Y.-S. Ryu, S. Kim, M.-H. Kim, Y. Sohn. and S.-D. Lee " Evidence of the intercalation of cholesterols and lipids for the growth of lipid raft domains and protein binding" to be submitted.
6. **Y.-S. Ryu**, H. Yun, T. Chung, J.-H. Suh, S. Kim, K. Lee, B. Lee, S.-H. Oh, and S.-D. Lee "Kinetic of Model Membrane into Raft Real-time by Surface Plasmon Resonance" to be submitted.
7. S.-W. Lee, **Y.-S. Ryu**, J.-H. Suh, Y. Sohn, and S.-D. Lee "Coarsening nature of liquid-ordered domains in a model membrane probed by the electric field-induced diffusion of phospholipids" to be submitted.

[2] International Conferences

1. C. Jeong, S.-W. Lee, Y.-J. Na, **Y.-S. Ryu**, and S.-D. Lee “Water meniscus directed organization of liquid ordered domains in lipid monolayer” 20th Korean-Japan joint Forum on organic materials for electronics and photonics (Chitose, Japan, 2008) O-12.
2. **Y.-S. Ryu**, S.-W. Lee, J. Shim, and S.-D. Lee “Two dimensional control of charged fluorescence molecules by electric field in lipid bilayer membranes” Proc. KLCC 2009. (Gyeongbuk, Korea, 2009) Vol.11.
3. W. Choi, Y.-J Na, **Y.-S. Ryu**, and S.-D. Lee “Brightness enhancement of organic light emitting displays by periodic in-cell microstructures fabricated using imprinting technique” KJF-ICOMEP (Jeju, Korea, 2009) P160.
4. **Y.-S. Ryu**, S.-W. Lee, J. Shim, and S.-D. Lee “Control of two dimensional distribution of charged molecules by an electric field in lipid bilayer membranes” 10th European Conference on Liquid Crystals (Colmar, France ,2009) P-053.
5. Y.-W. Lim, **Y.-S. Ryu**, K.-M. Koo, and S.-D. Lee “Highly efficient transflective liquid crystal display having in-cell functional optical films” 10th European Conference on Liquid Crystals (Colmar, France ,2009) P-014.
6. **Y.-S. Ryu**, S.-W. Lee, and S.-D. Lee “Diffusion profiles of charged lipids under an electric field in a restricted geometry” 23th International Liquid Crystals Conference (Krakow, Poland, 2010) P-3, 226.

7. S.-D. Lee, S.C. Park, **Y.-S. Ryu**, and S.-W. Lee "Control of structural self-organization of colloids and lipids for optical applications" OLC 2011 (Yerevan, Armenia, 2011) PL-3
8. J. Suh, **Y.-S. Ryu**, and S.-D. Lee " Fabrication of binary liquid crystal grating using thermally assisted transfer printing for surface modification" ISEOFM 2012 (Shanghai, China, 2012) P-43.
9. S. Kim, **Y.-S. Ryu**, J.-H. Suh, C.-M. Keum and S.-D. Lee "Authorttability Gradient Surface Generated by Thermo-Transfer Printing of Poly(dimethylsiloxane)" *23rd ICME&D (Suwon, Korea, 2012) P-78.*
10. **Y.-S. Ryu**, J. Suh, B. Lee and S.-D. Lee "Continuous monolayer-bilayer binary membrane array fabricated by hydrophobicity controlled by PDMS transfer method" Lipid and biomembrane physics, Faraday discussion 161 (London, UK, 2012) P.29

초 록

살아있는 세포의 지질막 상에서, 지질과 단백질과 같은 지질막 구성요소의 재배열 및 분산의 분석 및 조절은 세포 생물학을 포함한 과학적 중요성으로 말미암아 많은 관심을 끌어왔다. 특히 지질의 다이나믹한 본질적 특성은 세포막의 변형, 세포 분획, 신호 전달과 같은 생명현상과 깊게 관련되어있기 때문에, 세포막을 체외에서 재 구성하여 관측하는 시스템은 지질막 연구의 중요한 방법으로 사용되어왔다.

본 논문에서는, 인공지질막을 근거로 하여, 지질 성분의 지엽적 조절을 위한 현실적인 모델 지질막 시스템 내에서, 지질과 맞닿는 계면 특성에 따른 상호작용을 기본적 물리관점과 잠재적 응용의 시야에서 조절함으로써 마이크로 혹은 나노 단위의 지질 도메인 구현을 보였다. 점착힘, 계면 에너지, 탄성, 자발적 곡률, 전기적 필드와 같은 기본적 요소를 마이크로 탬플릿의 조절을 통해 이와 맞닿은 지질 구성성분, 콜로이드 파티클을 선택적으로 조절하였다.

하나의 모델 지질막 시스템으로서, 지지체 기반의 인공 지지막의 경우 마이크로 스케일의 유동적인 인공지질막을, 단순한 베지클의 점착 및 자발적 터짐 과정을 통해 지지체 위에 형성 할 수 있었다. 다양한 기판으로의 인공 지지체 기반 지질막 형성은 지질막 관련된 생명 현상의 연구 및 생체 친화적 장치 개발의 주요한 수단이 되어왔다. 지지 물리학의 흥미로운 주제 중의 하나로, 다른 지질들과 확연히 구분되는 물리학적 특성을 지닌 지질 래프트, 특히 래프트의 체외적 구현은 지질 래프트의 생물학적 중요성으로 말미암아 꾸준히 재현되고자 연구되어 왔다. 지질 래프트는 세포막

상의 스핑고리피드와 콜레스테롤 부유 영역을 지칭하는 것으로, 그 중요성은 알쯔하이머, 파킨슨, 인간 광우병, 심혈관계 질병 심지어 에이즈와 같은 미제의 질병들과 깊게 연관되어있음이 속속히 밝혀지면서 그 중요성이 커지고 있다. 다시말해, 지질 래프트의 경우, 면역 시스템, 세포 사멸, 신경 세포의 질병체로의 변환에 직/간접적으로 관여함으로써 인간 질병연구의 핵심 물질로 여겨지고 있다. 하지만 생명적인 중요성에도 불구하고, 지질 래프트의 명확한 역할 및 발생학적 원리, 질병 형태로의 진화 경로는 명확히 알려져 있지 않다.

탄성체 기반의 접근을 이용한 지질 성분의 특정 영역에서의 집단체로의 성장 및 지형적으로 패턴된 구조체에 의한 특정 지질 래프트의 루프와 같은 도메인의 형성이 최초로 모델 시스템에서 증명되었다. 지질 성분의 각개의 모양에 근거한 지질 성분의 곡률에 따른 선호적 배치는 탄성 에너지를 낮추려는 특성이 유동적 지질체 내에서 구현됨을 이용하여 “링 래프트” 구현을 성공하였다. 또 다른 지질 도메인의 특정 영역으로의 집단체 형성은 기판의 에너지 특성에 따른 지질 성분의 선호적 한정에 따라 재현할 수 있었다. 우리는 이종의 지질 구조체, 즉 단일 지질층과 이중 지질층의 병렬적 배치를 연속적인 하나의 인공지질막에서 구현하였다. 건조한 dry polydimethylsiloxane (S-PDMS) 를 수화된 기판에 찍어냄으로서 S-PDMS 몰드에 있던 올리고머의 전사를 통해, 단일 지질층 형성에 적합한 표면 특성을 지닌 기판을 패터닝함으로써, 연속적이고 병렬적인 단일-이중층 이공 지질막을 구현하였다. 더 나아가, 유동적 특성을 유지하는 이종의 지질막을 골드기판 위에서 제작함으로써, 기대되는 지점의 L_O 도메인 형성을 야기함으로 인해

실시간적인 지질 래프트의 동역학을 SPR 을 통하여 관찰할 수 있었다.

전하를 띤 지질 성문의 외부 전압에 의한 지형적인 장벽이 패턴된 시편 내에서 국지적 제어 또한 나타내었다. 전압에 의한 전하를 띤 지질성분의 준비된 시편에서의 제어는, 전압 의존적인 드리프트 이동과 열에 의한 랜덤한 분산의 균형을 조절함으로써, 기판의 너비와 길이를 변수로하여 준비된 시편 내에서의 횡적, 종적인 분산 정도를 조절할 수 있었다.

결론적으로, 이 박사 논문을 통틀어, 신호전달 지질체의 인공 지질막에서의 재배열은 물리적 관점과 장치 응용 가능성 측면에서 재현되었다. 본 논문에서 증명된 실험적/이론적인 분석과 컨셉의 경우, 생명 현상의 이해 범위 증대 및 질병 관련 단백질 시료로의 응용과 접합되어 강력한 플랫폼으로 사용될 것으로 기대된다.

학 번: 2009-30198